GEOCHEMISTRY AND PETROGENESIS OF LATE CRETACEOUS BENTONITES FROM THE KANGUK FORMATION, AXEL HEIBERG AND ELLESMERE ISLANDS, CANADIAN HIGH ARCTIC

Michael B. Parsons

Submitted in Partial Fulfilment of the Requirements
for the Degree of Bachelor of Science, Combined Honours
Departments of Earth Sciences and Chemistry
Dalhousie University, Halifax, Nova Scotia
March 1994

Distribution License

DalSpace requires agreement to this non-exclusive distribution license before your item can appear on DalSpace.

NON-EXCLUSIVE DISTRIBUTION LICENSE

You (the author(s) or copyright owner) grant to Dalhousie University the non-exclusive right to reproduce and distribute your submission worldwide in any medium.

You agree that Dalhousie University may, without changing the content, reformat the submission for the purpose of preservation.

You also agree that Dalhousie University may keep more than one copy of this submission for purposes of security, back-up and preservation.

You agree that the submission is your original work, and that you have the right to grant the rights contained in this license. You also agree that your submission does not, to the best of your knowledge, infringe upon anyone's copyright.

If the submission contains material for which you do not hold copyright, you agree that you have obtained the unrestricted permission of the copyright owner to grant Dalhousie University the rights required by this license, and that such third-party owned material is clearly identified and acknowledged within the text or content of the submission.

If the submission is based upon work that has been sponsored or supported by an agency or organization other than Dalhousie University, you assert that you have fulfilled any right of review or other obligations required by such contract or agreement.

Dalhousie University will clearly identify your name(s) as the author(s) or owner(s) of the submission, and will not make any alteration to the content of the files that you have submitted.

If you have questions regarding this license please contact the repository manager at dalspace@dal.ca.

Grant the distribution license by signing and dating below.

_____ _____

Name of signatory Date

Dalhousie University

Department of Earth Sciences
Halifax, Nova Scotia
Canada B3H 3J5
(902) 494-2358
FAX (902) 494-6889

DATE April 18, 1994

AUTHOR Michael Benjamin Parsons

TITLE Geochemistry and Petrogenesis of Late Cretaceous Bentonites from the Kanguk Formation, Axel Heiberg and Ellesmere Islands, Canadian High Arctic

Degree B.Sc. Convocation Spring Year 1994

Permission is herewith granted to Dalhousie University to circulate and to have copied for non-commercial purposes, at its discretion, the above title upon the request of individuals or institutions.

Signature of Author

Abstract

Petrographic and geochemical analyses of bulk bentonites, volcanic minerals, and unaltered glass inclusions in quartz phenocrysts reveal the composition and tectonic setting of Late Cretaceous explosive volcanism in the Canadian High Arctic. The bentonitic clays represent altered volcanic ashes intercalated with Kanguk Formation mudstones on Axel Heiberg and Ellesmere Islands. Preliminary $^{40}Ar/^{39}Ar$ dating of sanidine phenocrysts yields a Late Cenomanian to Middle Campanian age for the Kanguk Formation. Grain-size distributions and ash dispersal suggest high energy Plinian-style eruptions. Primary mineral assemblages (quartz, sanidine, ilmenite, zircon, apatite, and acmite) indicate that the parent magmas of the Kanguk bentonites had oversaturated, marginally peralkaline compositions. Microprobe analyses of glass inclusions within quartz phenocrysts confirm such parent melt compositions, and permit evaluations of element mobilities during bentonite formation. Appropriate modelling of elemental fluxes allows recalculation of original ash compositions from bulk bentonite analyses, and indicates a potential for geochemical correlation between individual units or groups of units. Detailed major and trace element geochemistry on both primary phenocrysts and bulk bentonites, in conjunction with discriminant diagrams, reveals a within-plate tectonic setting for the parent volcanism, and a dominance of peralkaline rhyolite compositions. The Kanguk bentonites may represent late-stage magmatic activity along the Sverdrup Rim, or they may be the products of extra-basinal volcanism. Late Cretaceous to Tertiary peralkaline volcanism occurred elsewhere along the north coast of Ellesmere Island and northwestern Greenland; however, no exact match to the age and composition of the bentonites exists to date.

Key Words: bentonite, volcanic ash, Sverdrup Basin, Plinian eruptions, glass inclusions, peralkaline rhyolites, element mobility, tectonomagmatic discrimination, geochemical correlation, Arctic volcanism

TABLE OF CONTENTS

TABLE OF FIGURES

TABLE OF TABLES

Acknowledgements

I am grateful to many people for their guidance and support throughout the entirety of this study. In particular, I wish to thank my supervisor, Dr. Gunter Muecke, for introducing me to the wonders of the Canadian Arctic, and for his enthusiasm and patient guidance. I am indebted to Dr. Barrie Clarke for his numerous editorial revisions, and for his helpful recommendations and discussions. I thank Eric Pearson for many interesting conversations in the field, and for digging extensive trench systems to reveal the Kanguk bentonites. Thanks go to Bob MacKay for his assistance with the electron microprobe, to Sandy Grist for his guidance in the geochemistry lab, to the staff of the Atlantic Regional Geochemical Centre for the XRF and INAA analyses, and to Gordon Brown for his expertise in grain mount preparation. The Polar Continental Shelf Project provided aircraft and logistical support during the 1990 and 1992 field seasons, and the Natural Sciences and Engineering Research Council of Canada helped to finance this study through an operating grant to Dr. Gunter Muecke, and two Undergraduate Student Research Awards to myself. The Northern Scientific Training Program (Department of Indian and Northern Affairs, Government of Canada) also contributed financial support through a Summer Research Fund to myself. Finally, I thank my family and Kim, for their support, patience, and encouragement.

CHAPTER 1: INTRODUCTION

1.1 Opening Statement

Volcanic ash consists of pyroclasts (glass shards, crystals, and lithic fragments) less than 2 mm in diameter (Schmid 1981), generated during explosive volcanic activity. Explosive eruptions occur when volatiles build up, mainly in magmas of intermediate to acid composition, and then exsolve in response to decreasing pressure or temperature to form a free vapor phase. This process results in a rapid volume increase within the magma chamber, which can generate enough energy to project pyroclastic material high into an eruption column. Eruptive plume heights may exceed 30-40 km; therefore, wind currents are effective in distributing ash over large distances (up to 5000 km) in a relatively short period of time (Fisher and Schmincke 1984).

Field mapping of ash layer thicknesses, areal distribution, and grain size analyses (especially maximum clast size) are useful for determining physical parameters associated with an eruption. These data can provide information on paleowind patterns, dynamics of eruption columns, volume and shape of magma chambers, and eruptive energy (Fisher and Schmincke 1984). Chemical analysis of phenocryst minerals, glass shards, and cognate lithic fragments yields important information concerning the parent magma composition, tectonic setting of the eruptive center, and petrogenesis of ash deposits. Geochemical fingerprinting of individual ash layers based on characteristic immobile element ratios is an important tool for stratigraphic correlations over wide areas (e.g., Huff and Kolata 1989). Many ash layers also contain minerals suitable for radiometric dating; this feature, combined with their widespread distribution and short deposition times, has made ash layers invaluable geochronological tools (Baadsgaard and Lerbekmo 1982).

Late Cretaceous explosive volcanism deposited blankets of volcanic ash over much of the Canadian High Arctic (Fig. 1.1). Subaqueous fallout deposits, interbedded with organic-rich mudstones of the Kanguk Formation, occur throughout the eastern Sverdrup Basin region (Fig. 2.1). Axel Heiberg and Ellesmere Islands contain exposures of bentonitic clays within the Kanguk Formation that represent the altered remains of the Late Cretaceous volcanic ashes.

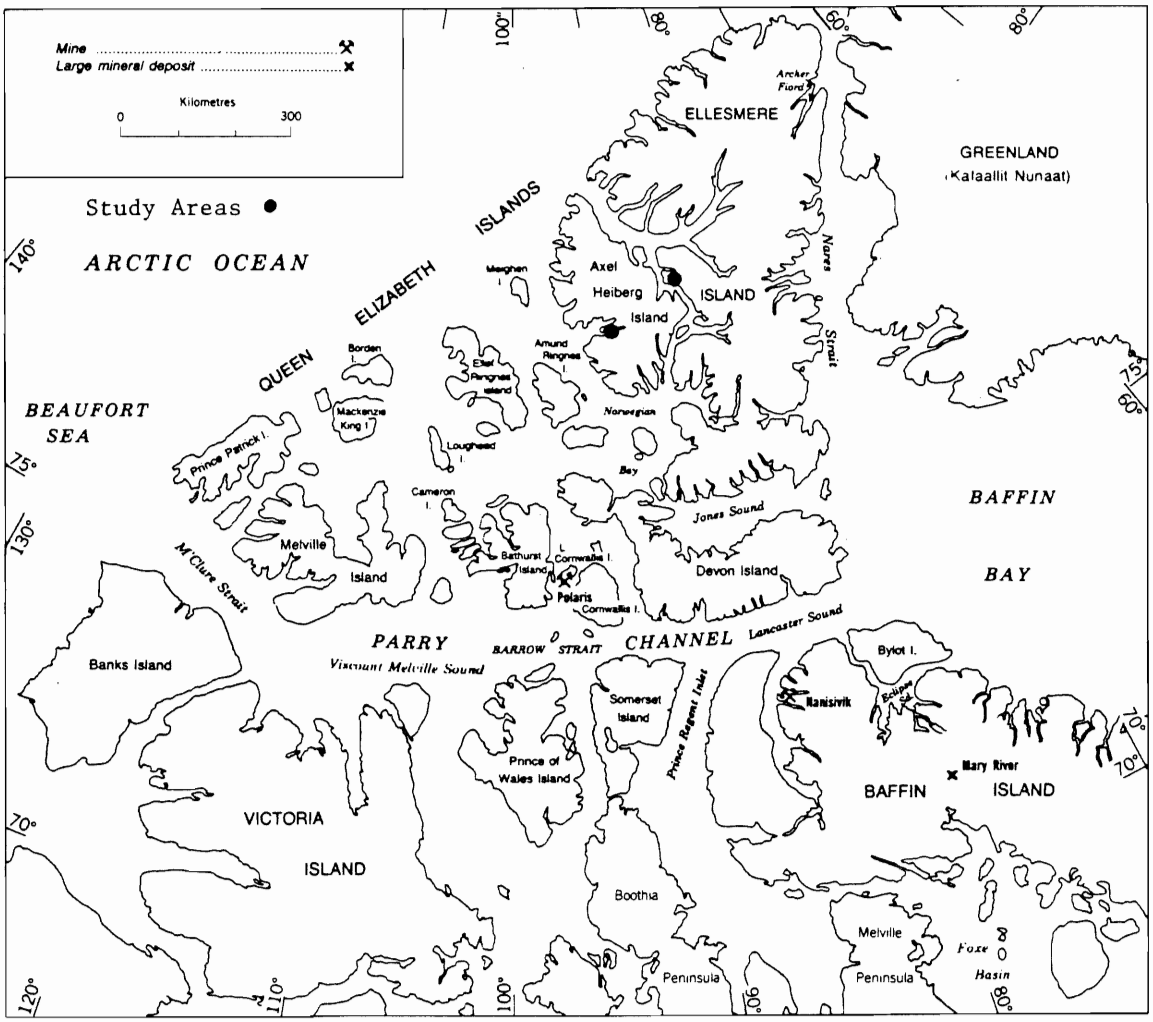

Figure 1.1 Map of the Canadian Arctic Archipelago, showing the locations of Axel Heiberg and Ellesmere Islands, the Queen Elizabeth Islands (those islands north of the Parry Channel), and the location of the Kanguk Formation study areas (modified from Plate 9, Trettin 1989).

1.2 Definitions

Definitions of the term "bentonite" emphasize the origin, clay mineralogy, and industrial uses of this material. Knight (1898) first applied this term to a highly colloidal, plastic clay located in the Cretaceous sediments near Fort Benton, in eastern Wyoming. Original definitions focused on the clay mineralogy of bentonites without any reference to their volcanic origin. Grim and Guven (1978, p 1) defined a bentonite as "Any clay composed dominantly of a smectite clay mineral, whose physical properties are dictated by this clay mineral." Industrial definitions focus on the ability of bentonitic clay to exchange cations, its hydration and swelling capacity, its impermeability and binding behavior, and its rheological properties of viscosity and thixotropy (Christidis and Scott 1993).

In this thesis, the term "bentonite" refers specifically to the alteration products of primary volcaniclastic material. A bentonite is "a soft, plastic, porous, light-colored rock composed essentially of clay minerals of the montmorillonite (smectite) group plus colloidal silica, and produced by devitrification and accompanying chemical alteration of a glassy igneous material, usually a tuff or volcanic ash" (American Geological Institute 1987).

However, not all pyroclastic material undergoes alteration to bentonitic clay following deposition. Bentonite formation occurs predominantly in aqueous environments, where water promotes the devitrification and hydration of volcanic glass to authigenic clay minerals. Sediments associated with bentonitic horizons indicate the wide range of environmental conditions in which bentonites may form. The geological environment may be lacustrine, coal-forming, estuarine, shallow marine, or deep-sea (Person 1982). Wet ash deposited in terrestrial settings may also alter to bentonitic clay. High silica contents (>70%) appear to impede the alteration of volcanic ash, whereas moderate MgO contents (5-10%) (including MgO incorporated from sea water) favor rapid bentonite formation. Bentonitization occurs during early diagenesis, and is probably contemporaneous with the deposition of volcaniclastic material (Grim and Guven 1978).

Most bentonites contain four predominant mineralogical components:

1) primary igneous phenocrysts crystallized within the parent magma and erupted as a component of the original ash (e.g., quartz, plagioclase, sanidine, biotite, zircon, ilmenite, apatite);
2) non-detrital fragments (i.e., xenocrysts, xenoliths) from the walls of the volcanic vent (these may indicate the petrology of the bedrock within the source region);
3) authigenic minerals (mostly clay minerals) formed from the devitrification and hydration of glass shards and associated volcanic minerals; and
4) detrital minerals derived from sedimentary contributions within the local depositional environment.

The geometry and lateral extent of a bentonitized deposit reflect the magnitude of the original eruption, the strength and direction of the prevailing winds prior to deposition, and the reworking of the pyroclastic material within the depositional environment. Deposition of the original volcanic ashes occurs over a wide area in a very short time. Bentonites may also contain minerals suitable for radiometric dating, thus they serve as excellent stratigraphic marker-horizons for geochronological work (Baadsgaard and Lerbekmo 1982; Person 1982). The chemistry of the bulk bentonites and igneous phenocrysts may indicate the nature of the original volcanic ash (provided contamination is minimal), therefore, bentonites are also useful for petrogenetic studies. However, the correct tectonomagmatic interpretation of bentonite compositions must consider the effects of element mobility during the alteration of primary volcaniclastic material.

1.3 Location and Geological Setting

The Kanguk Formation occurs across the entire Sverdrup Basin, from Banks Island in the west to Ellesmere Island in the east (Fig. 1.1). The lower part of the Formation contains bituminous shales and organic-rich mudstones representing starved, offshore shelf deposits. Bentonite beds

are most common within the lower sections of this unit. The shales become siltier, less bituminous, and lighter in color upwards, and the upper sections of the Formation are predominantly prodelta deposits. Intermittent sandstone units occur within the marginal parts of the Formation and represent shallow marine shelf deposits (Embry 1991). Preliminary $^{40}Ar/^{39}Ar$ dates on sanidine phenocrysts separated from the bentonites (approximately 91.5 - 80.7 Ma, GK Muecke, personal communication 1994), combined with micropaleontological work on the interbedded shales (Nunez-Betelu et al, in press), yield a Late Cenomanian to Middle Campanian age for the Kanguk Formation.

1.4 Previous Work

Early researchers from the Geological Survey of Canada (GSC) used ships, dog sleds, and canoes to explore the Canadian Arctic, without the modern conveniences offered by aircraft and weather stations. In 1947, aircraft transported geologists to regions within the High Arctic, with the support of six weather stations (Christie and Dawes 1991). In 1955, the GSC organized Operation Franklin, a combined geological and aerial geophysical reconnaissance project, supported by helicopters and "bush" planes. During this project, land-based geologists documented an extremely thick sequence of sediments in the Canadian Arctic Islands that contained suitable structures for hydrocarbon generation and entrapment (Fortier and Morley 1956). These discoveries prompted widespread petroleum exploration in the 1960's, 1970's, and 1980's involving many exploratory wells and seismic reflection lines throughout the Sverdrup Basin (Thorsteinsson and Tozer 1970; Drummond 1973).

Initial work on Mesozoic strata concentrated on well cuttings from these exploratory boreholes. This work complemented field studies on well-exposed Mesozoic sections in the eastern Sverdrup Basin, and resulted in a large number of summaries of Arctic geology containing sections on Mesozoic stratigraphy. Abundant biostratigraphic data now exists for many Mesozoic

sections (Embry 1991). Many of these reports contain descriptions of Kanguk Formation stratigraphy and paleoenvironmental interpretations based on detailed stratigraphic and sedimentological studies. Embry and Osadetz (1988) provided a comprehensive summary of Cretaceous volcanism throughout the Queen Elizabeth Islands, and noted the existence of thin bentonite beds within the lower Kanguk Formation.

No studies to date have examined the characteristics of the Kanguk Formation bentonites. Nunez-Betelu et al (in press) provide a biostratigraphic framework for the Kanguk shales that will be integrated with radiometric dates from the intercalated bentonites (GK Muecke, personal communication 1994). Several studies on Late Cretaceous Arctic sediments outside the Sverdrup Basin have documented altered volcanic ashes which may be laterally equivalent to bentonites in the Kanguk Formation (Lanphere and Tailleur 1983; Mudie and Blasco 1985; Arctic Summer West Scientific Party 1992).

1.5 Problem and Objectives

The bentonites of the Kanguk Formation originated during a period of explosive volcanism in the Late Cretaceous. The wide areal distribution of bentonites indicates that large volume air fall deposits typical of very powerful eruptions (i.e., plinian or ultraplinian) formed during this period. However, most of the older volcanic rocks within the Cretaceous Sverdrup Basin succession are basaltic flows and localized pyroclastic deposits typical of relatively dry, basic magmatic systems. The only explosive acidic rocks belong to the Hansen Point volcanics (informal stratigraphic unit) of northwestern Ellesmere Island, that erupted after (Late Campanian-Danian) the Late Cenomanian to Middle Campanian Kanguk Formation bentonites (Merrett and Muecke 1989).

This thesis attempts to determine the origin, tectonic setting, and nature of the parent magma(s) that generated the Kanguk Formation bentonites. However, only relatively immobile elements are reliable for classification and tectonic setting discrimination diagrams. The extremely

altered nature of these volcanic ashes, therefore, necessitates an analysis of element mobility during the bentonitization process.

In particular, the research objectives of this thesis include:

1) description of the field relations, physical characteristics, and mineralogical composition of the Kanguk Formation bentonites;
2) determination of the original composition of the parental magma(s) and a description of their chemical evolution over time;
3) assessment of the importance of element mobility during bentonitization, and its implications for geochemical correlation and classification of individual ash layers;
4) comparison of bulk bentonite trace element chemistry with that for primary igneous phenocrysts to determine trace element mobility and element partitioning between crystals and original melt;
5) use of trace element discrimination diagrams to determine the tectonic setting and provenance of the original volcanic ashes; and
6) discussion of the implications for models of Late Cretaceous Arctic volcanism.

1.6 Scope of Study and Thesis Organization

This thesis examines the geochemistry and petrogenesis of the Kanguk Formation bentonites in the framework of the research objectives outlined above. The focus of this study is the petrogenetic aspects of the bentonites; therefore, it provides only a brief description of the sedimentological characteristics. Preliminary radiometric dating of sanidine phenocrysts indicates the duration of explosive volcanic activity represented by the preserved Kanguk bentonites. However, a detailed geochronological study of these ash layers is to be published at a later date (GK Muecke, personal communication 1994) and does not form part of this thesis. The analytical

sections of this study examine only 12 bentonite samples which may not represent the full spectrum of bentonite compositions present within the Kanguk Formation.

Chapter 2 contains a detailed treatment of the regional stratigraphy and bounding units of the Kanguk Formation. A description of the field localities, local stratigraphy, and details of field procedures comprises Chapter 3. Chapter 4 includes a discussion of the textures and mineralogy of the altered volcanic ashes, along with an analysis of the primary igneous phenocryst chemistry. Chapter 5 summarizes the geochemical data for the bulk bentonites, contrasts these data with results obtained from unaltered glass inclusions in quartz phenocrysts, and includes an analysis of element mobility. Chapter 6 includes a discussion of the tectonic setting and provenance of the original ashes, and an interpretation of these results in terms of existing models for Late Cretaceous volcanic activity within the Arctic region. The Appendices contain detailed field descriptions, laboratory techniques and geochemical data.

CHAPTER 2 : GEOLOGICAL SETTING

2.1 Introduction

Axel Heiberg and Ellesmere Islands are part of the Queen Elizabeth Islands, north of the Parry Channel within the Canadian Arctic Archipelago (Fig. 1.1). The Sverdrup Basin, a northeast-southwest trending extensional basin, covers much of the central and eastern regions of the Queen Elizabeth Islands (Fig. 2.1). The Basin is approximately 1300 km long, up to 400 km wide, and served as the major depocentre within the Canadian Arctic Islands from the Early Carboniferous to the Early Tertiary. The Sverdrup Basin contains a succession of marine and nonmarine clastics, carbonates, evaporites, and mafic intrusive and volcanic rocks, with a total thickness of up to 13 km near the axial region. The Sverdrup Rim, a large horst that was the site of active uplift and erosion throughout the Cretaceous Period, separates the Sverdrup Basin from the Canada Basin to the northwest (Balkwill 1978; Trettin 1989).

Active volcanism, associated with a Carboniferous-Early Permian rifting event, took place during the early development of the Sverdrup Basin. Widespread igneous activity also occurred throughout the Cretaceous as a result of minor crustal extension within the Basin, coupled with the main phase of rifting in the adjacent Canada Basin (Williamson 1988). Most magmatism produced basaltic lavas and intrusive rocks interbedded with the basinal sediments. Axel Heiberg and Ellesmere Islands contain excellent exposures of these volcanic rocks. During the Late Cretaceous, most of the Sverdrup Basin underwent thermal subsidence, and volcanic activity took place only in the extreme northeastern parts of the Basin. This volcanism resulted in the extrusion of acid volcanics in addition to basic rocks (Embry and Osadetz 1988; Merrett and Muecke 1989). The bentonites of the Kanguk Formation may represent either a late stage of explosive volcanism along the Sverdrup Rim, or a period of intense extra-basinal volcanic activity.

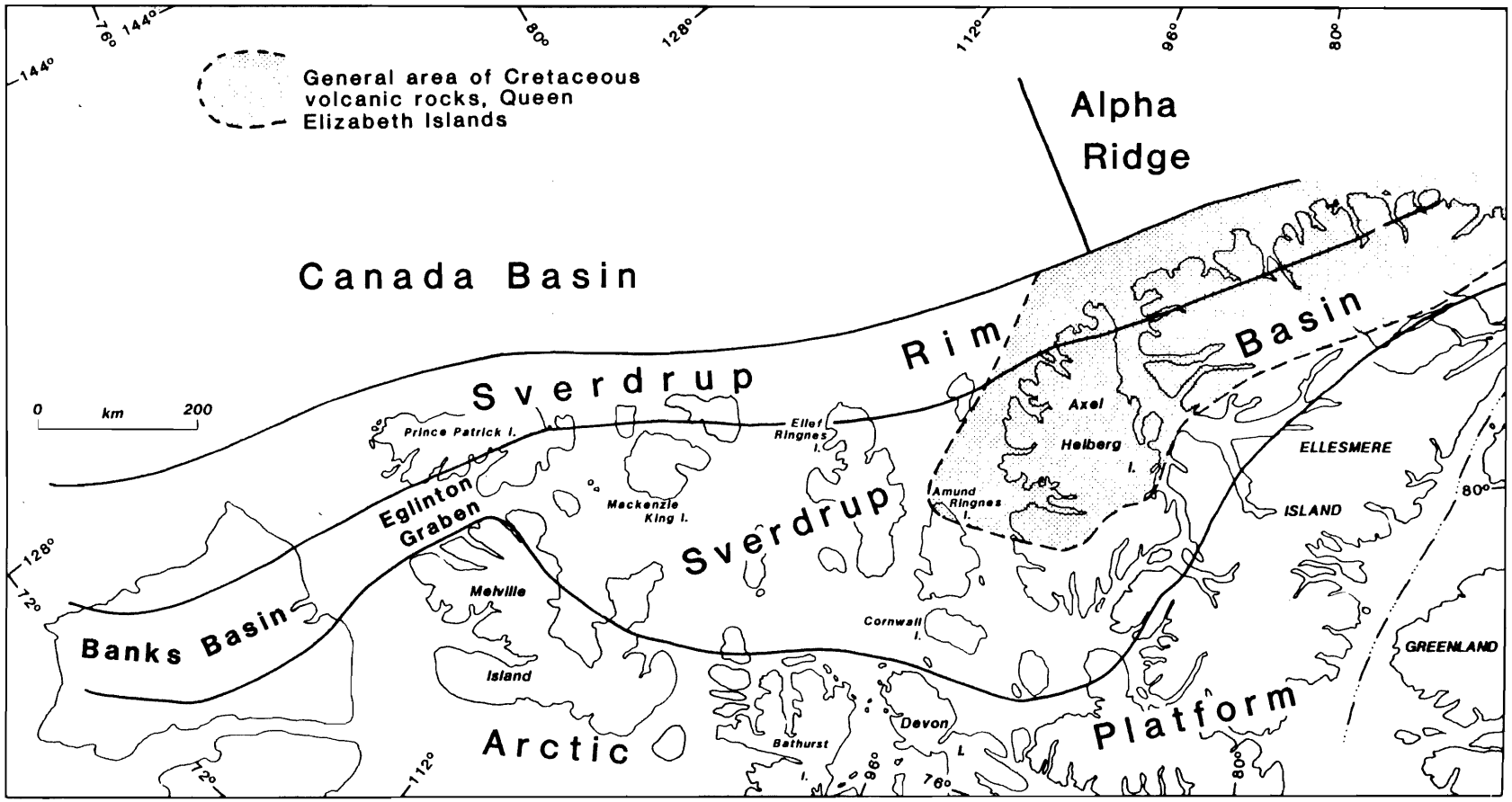

Figure 2.1 Location of the Sverdrup Basin in relation to the major tectonic elements of the Canadian High Arctic during the Cretaceous Period (from Embry and Osadetz 1988).

2.2 The Sverdrup Basin

The Sverdrup Basin originated during Carboniferous to Early Permian rifting of deformed Precambrian to Devonian rocks, and its growth ended with folding and faulting of the Basin strata during the Early Tertiary Eurekan Orogeny (Balkwill 1978). The sedimentary fill of the Sverdrup Basin consists mainly of clastic sediments derived from cratonic areas to the south and east of the Basin. Late Paleozoic sediments include significant volumes of carbonates, evaporites, and chert. Sediment supply to the Basin fluctuated greatly in response to uplift of the craton, thermal subsidence of the Basin, and marine transgressive-regressive cycles. Evaporite diapirism took place from Triassic time onward. Magmatism occurred throughout the history of the Basin, associated with periods of crustal extension (Trettin 1989; Muecke 1990). Figure 2.2 summarizes the tectonomagmatic history of the Sverdrup Basin.

2.2.1 Regional Stratigraphy

The oldest strata within the Sverdrup Basin succession, present along the northern and southern margins of the Basin, are Early Carboniferous (Visean) in age. Diachronous sandstones, conglomerates, and red beds constitute the oldest continuous strata, deposited from the latest Early Carboniferous to Early Permian (Trettin 1989). Volcanic rocks of the Auhild Formation (333-305 Ma) occur within these sediments, and represent the oldest known record of volcanism in the Sverdrup Basin (Ritcey 1989).

Mid-Carboniferous sedimentation involved deposition of mixed clastic and carbonate sediments along the Basin margins, as well as thick accumulations of marine muds, evaporites and carbonate rocks near the axial regions of the Basin. During the Lower Permian, minor folding and faulting associated with the Melvillian Disturbance accompanied the extrusion of the Permian Esayoo Formation basalts (Cameron 1989).

Mesozoic sedimentation in the Sverdrup Basin reflects thirty regional transgressive-regressive cycles resulting from the interplay of subsidence, sediment supply, and eustatic sea level changes. Thermal subsidence of the Basin followed rifting and crustal stretching in the Carboniferous to Early Permian, and continued until the Early Cretaceous. The present Arctic region moved northward throughout the Mesozoic, from 40°N in the early Triassic to 70°N near the end of the Cretaceous (Embry 1991). This movement terminated deposition of carbonates and evaporites, and promoted clastic sedimentation during the Mesozoic Era. A major sea level rise took place in the Early Triassic, and well-defined marginal and axial basin facies developed in the Sverdrup Basin. Up to 4500 m of sediments accumulated near the Basin axis during the Triassic Period. Sediment supply was minimal during the Jurassic, and marine transgression resulted in the deposition of shallow submarine sands (Balkwill 1978).

Renewed rifting from the Early Cretaceous to earliest Late Cretaceous accompanied uplift of cratonic source areas to the south and east. This uplift increased sediment supplies, and generated a coarse-grained fluvial-dominated deltaic system that deposited alluvial sediments of the Isachsen Formation over basinal siltstones and shales (Embry 1991). Extrusion of tholeiitic basalts at Axel Heiberg and northern Ellesmere Islands took place during this main rifting stage. Thermal subsidence throughout the Late Cretaceous accompanied a series of transgressive-regressive cycles, each consisting of a shale-siltstone lower portion and a sandstone-dominant upper portion. The sandstone-dominant Hassel Formation overlies this succession, and consists of a lower unit of delta front, coarsening-upward marine sediments, and an upper unit of interbedded sandstone, shale, siltstone, and minor coal (Embry 1991). The Hassel Formation makes up the topmost portion of the Albian to early Cenomanian interval on the margins of the Sverdrup Basin and in Banks Basin, and is unconformably overlain by the Kanguk Formation. However, the Bastion Ridge (marine shales) and Strand Fiord (volcanic) formations, two stratigraphic units restricted to the central parts of the Sverdrup Basin, are also present within this interval. The uppermost Cenomanian to Maastrichtian cycle contains the Kanguk and Expedition formations. Many

uncertainties exist as to the exact stratigraphic relationships between the Hassel, Bastion Ridge, Strand Fiord, and Kanguk formations, and the base of the Eureka Sound Group (Expedition Formation) (Nunez-Betelu et al, in press).

In the latest Cretaceous and Tertiary, tectonic activity associated with the Eurekan orogeny uplifted the Sverdrup Basin strata, forming the mountain ranges of Axel Heiberg and Ellesmere Islands. Erosion of these arches during the Tertiary Period resulted in thick, sandstone-dominated sequences deposited over Mesozoic sediments in areas of low relief (Balkwill 1978).

2.2.2 Tectonomagmatic History

The initial Carboniferous to Early Permian phase of continental rifting within the Sverdrup Basin involved extension of deformed Precambrian to Devonian rocks. Maximum thinning of continental crust took place in the axial regions of the Basin, where thicknesses decreased by a factor of two or more (Stephenson et al 1987). Evidence for extension also includes listric faults, with associated coarse clastic sediments (Sobczak et al 1986). Theories on the development of rift basins (e.g., McKenzie 1978) suggest that lithospheric extension results in basin subsidence, and upwelling of the underlying asthenosphere to maintain isostatic equilibrium. Decompression of this mantle material may generate partial melts, which can rise to the surface through fractures in the overlying stretched lithosphere. The Carboniferous and Permian volcanic rocks of the Sverdrup Basin represent the igneous products of this initial rifting phase (Cameron 1989; Ritcey 1989). Lithospheric cooling subsequent to this rifting event resulted in thermal subsidence of the Basin from Permian to Early Cretaceous time (Stephenson et al 1987).

The northwestern rim of the Sverdrup Basin contains Carboniferous volcanic rocks of the Audhild Formation, consisting of spilitized basalt flows, with associated pyroclastic material (Ritcey 1989). Minor folding and faulting of Lower Permian rocks along the southern and eastern margins of the Basin took place during the Melvillian Disturbance. Transtensive tectonism during

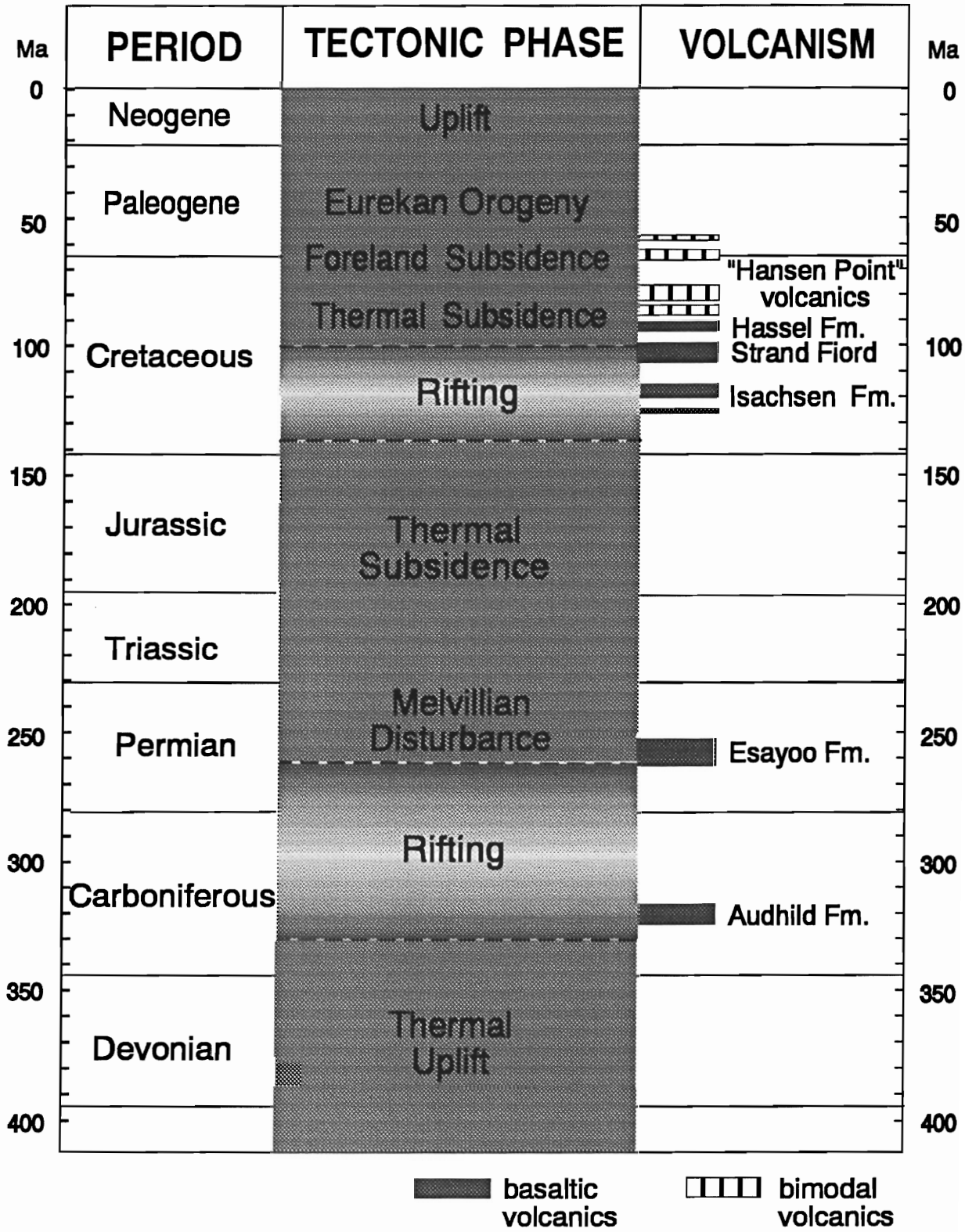

Figure 2.2 Stratigraphic column summarizing the tectonomagmatic history of the Sverdrup Basin.

this period probably relates to extrusion of alkaline to transitional basalts of the Permian Esayoo Formation along the northwestern part of the Basin (Cameron 1989).

Renewed rifting in the eastern part of the Sverdrup Basin during the Early Cretaceous increased subsidence rates, and generated extensive magmatism. Cretaceous volcanic rocks form part of the Sverdrup Basin succession on northern Ellesmere Island, Axel Heiberg Island, and northernmost Amund Ringnes Island (Fig. 2.1). Several different models exist to explain the episodic nature of the resulting intrusive and extrusive magmatism.

The re-activation of continental rifting may reflect the development of the Sverdrup and Canada Basins as conjugate rift systems. The main stage of rifting within the Canada Basin (late Hauterivian to early Cenomanian) corresponds to the peak of volcanic activity within the adjacent Sverdrup Basin. Voluminous subalkaline magmatism occurred along the Sverdrup Basin axis, where maximum thinning of the lithosphere induced partial melting of mantle material. Widespread volcanic activity produced mainly tholeiitic basalt flows and minor pyroclastic rocks, with associated sill and dyke complexes (Williamson 1988; Muecke 1992). "The timing, volume, and composition of melts directly reflects the time, magnitude, and rate of lithospheric thinning. The episodic nature of the magmatism, possibly periodic, suggests that rifting rates were variable and ultimately controlled by processes at the plate margins" (Muecke et al 1990).

Cretaceous dykes trend mainly north-northwest, and appear to radiate from the southern limit of the Alpha Ridge (Fig. 2.1). Based on this observation, Embry and Osadetz (1988) suggested that a mantle plume existed at this apparent center of volcanism, and that it was active throughout the Cretaceous period. The Alpha Ridge thus represents a hot-spot track that developed during seafloor spreading in the Canada Basin through the Late Cretaceous. However, this model incorrectly assumes a northward increase in the number and thickness of volcanic units in the Sverdrup Basin succession. It also does not account for the periodicity of the observed magmatism, the progressive changes in magma composition, and the spatial distribution of compositional types.

By the Late Cretaceous to Early Tertiary, volcanism migrated to the northeastern Sverdrup Rim, and erupted as bimodal suites dominated by strongly alkaline basalts, rhyolites, trachytes, and peralkaline rhyolites (Muecke 1992). Cenomanian to Danian volcanic strata include the Kanguk Formation bentonites (Late Cenomanian to Middle Campanian), and the Hansen Point volcanics on northwestern Ellesmere Island (Late Campanian to Danian). The Hansen Point volcanic sequences near Emma Fiord, Phillips Inlet, and Yelverton Inlet, Ellesmere Island, contain strongly alkaline basalts and substantial amounts of felsic eruptives. These compositions differ from Early Cretaceous to early Late Cretaceous tholeiitic magmatism in the central Sverdrup Basin, and may be a result of thicker crust at the basin rim, and extended crustal residence times of magmas prior to eruption (Merrett and Muecke 1989).

2.3 Late Cretaceous Stratigraphy

The Late Cretaceous stratigraphy of the northeastern Sverdrup Basin involves complex stratigraphic relationships between formations, including several major unconformities (Fig. 2.3). The Kanguk Formation is present across most of the Sverdrup Basin, where it unconformably overlies the Hassel, Bastion Ridge, and the Strand Fiord Formations. Most of the Kanguk Formation consists of organic-rich mudstones with rare to abundant interbeds of bentonites and occasional silty mudstones (Nunez-Betelu et al, in press). The other formations within this interval differ greatly from Axel Heiberg Island to Ellesmere Island; therefore, an analysis of the stratigraphy at each location is necessary.

2.3.1 Western Axel Heiberg Island

The Bastion Ridge Formation, a thin, mudstone and minor siltstone unit, overlies the Hassel Formation on western and southern Axel Heiberg Island. A sideritic sandstone, containing plant

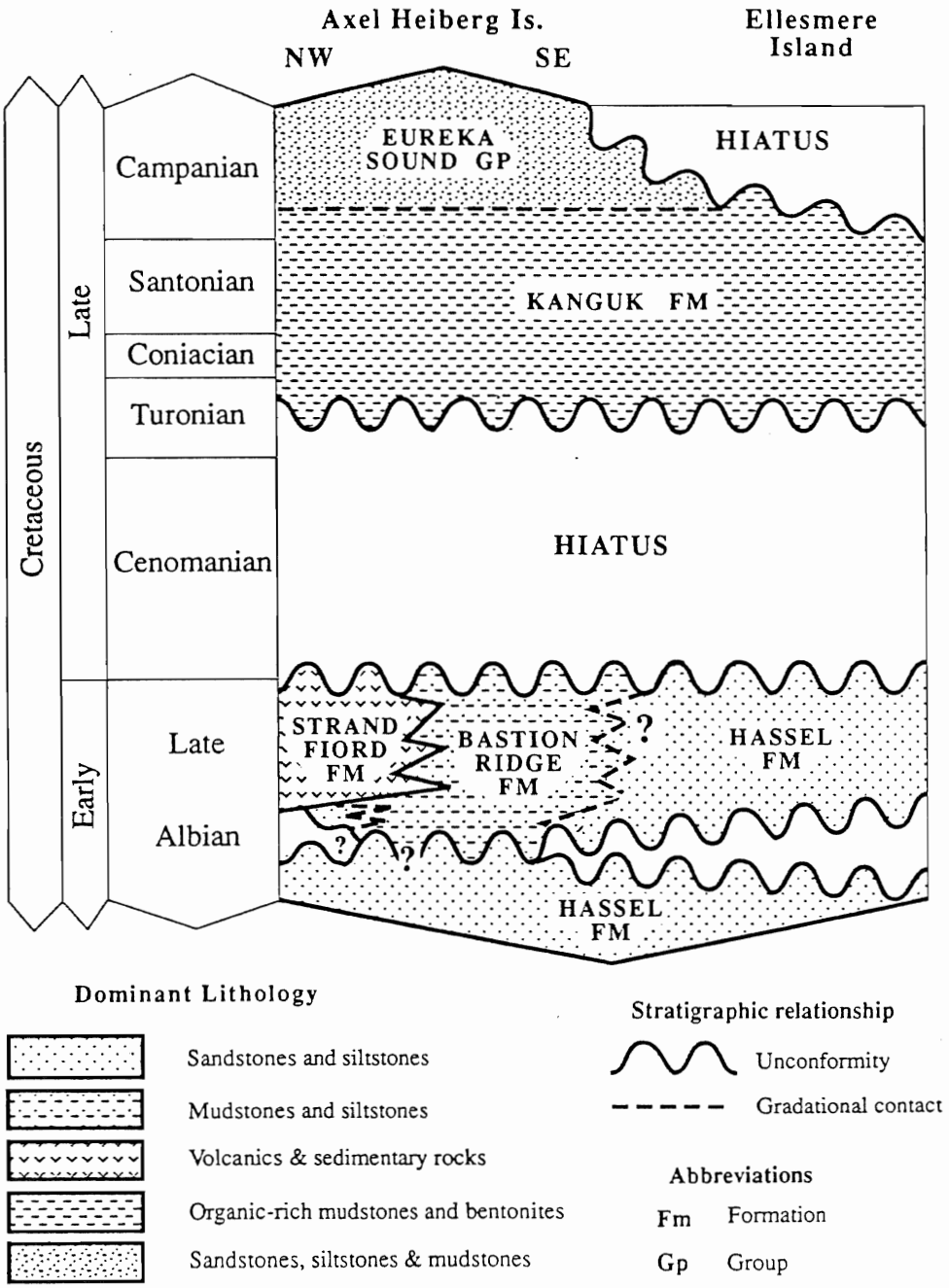

Figure 2.3 Time-stratigraphic relationships within the Upper Albian to Lower Campanian interval. A minor unconformity may occur between the Hassel and Bastion Ridge formations in areas where the Strand Fiord Formation is present. In other areas, where the Strand Fiord Formation is absent, sedimentological evidence supports the presence of this unconformity. Sandstones intercalated with the Bastion Ridge Formation could represent lateral equivalents of this formation and unconformably rest on the Hassel Formation. The hiatus defined on top of the Kanguk Formation and lower part of the Eureka Sound Group extends into the Paleocene (from Nunez-Betelu et al, in press)

macrofossils and an undulose contact, represents an unconformity between these two units in the south (Nunez-Betelu et al, in press). The Bastion Ridge Formation underlies and interfingers with the Strand Fiord Formation, a volcanic succession consisting mainly of subaerial flood basalts, at several locations on western Axel Heiberg Island. The contact between these two units constitutes a mixing zone of pyroclastic breccia and epiclastic volcanic strata (Ricketts et al 1985). Basal flows near the margins of the basalt plateau display characteristics diagnostic of invasive flows that burrowed into weakly consolidated sediments. These features include large basalt rafts, rootless dykelets, and irregular pillow-like structures in the mixing zones, which show chilled margins and vesicle zonation indicating rapid quenching against wet sediments (Muecke et al 1991).

The Kanguk Formation directly overlies the Bastion Ridge Formation, where the Strand Fiord volcanics are absent. A very fine- to fine-grained, bioturbated to hummocky-crossbedded sandstone caps the Bastion Ridge Formation on southern Axel Heiberg Island (Embry 1991). In this region, the Bastion Ridge is uncomformably overlain by the Kanguk, with a well-developed paleosol separating the two formations (Nunez-Betelu et al, in press).

The Strand Fiord Formation is in direct, unconformable contact with the underlying Hassel Formation, on northwestern Axel Heiberg Island. The Strand Fiord volcanics range in thickness from 40 m to approximately 1000 m, and contain minor clastic interbeds composed mainly of carbonaceous mudstones and siltstones. The most continuous section consists of 38 basalt flows, with scoriaceous flow tops, and minor pyroclastic units. The Kanguk Formation unconformably overlies the Strand Fiord Formation, with boulder conglomerates and altered flow tops marking the contact (Embry and Osadetz 1988; Nunez-Betelu et al, in press).

The sandstone-dominated Expedition Formation of the Eureka Sound Group conformably overlies the Kanguk Formation. The contact is transitional, with the Kanguk Formation shales becoming siltier upwards, and grading into the coarsening-upward delta front sediments of the Eureka Sound Group (Embry 1991).

The Bastion Ridge Formation may be time-equivalent to the Strand Fiord Formation in some localities, and both may be time equivalent to the upper Hassel Formation. The Bastion Ridge and Strand Fiord formations may also represent a hiatus, elsewhere in the Sverdrup Basin, between the Hassel and Kanguk Formations. "The gap in age, determined by palynology, between the Bastion Ridge and Strand Fiord formations (late Albian), and the overlying Kanguk Formation (late Turonian) spans the Cenomanian, and represents an extensive unconformity that is recognized over the entire study area" (Nunez-Betelu et al, in press p 8).

2.3.2 Fosheim Peninsula, Ellesmere Island

The Kanguk Formation is in direct, unconformable contact with the underlying Hassel Formation on the Fosheim Peninsula, Ellesmere Island (Fig. 3.1). Thick, massive sandstones of the Hassel Formation pass abruptly into the organic-rich mudstones of the Kanguk Formation (Fig. 2.3). The absence of thick sedimentary and volcanic sequences between the Hassel and Kanguk Formations on Ellesmere Island reflects the marginal position of this region, relative to western Axel Heiberg Island. The Eureka Sound Group unconformably overlies the Kanguk Formation sediments, with a sudden transition from dark grey, marine shale into light-colored fluvial-deltaic sandstone.

2.4 Summary

The Sverdrup Basin, located within the Canadian Arctic Archipelago, contains a thick sequence of sediments deposited from the Early Carboniferous to the Early Tertiary. Erosion of cratonic source areas to the south and east of the Basin occurred during periods of active tectonism in the Arctic region. Continental rifting, associated with the development of the Canada Basin, resulted in thermal subsidence of the Sverdrup Basin, and widespread volcanic activity.

Most volcanism resulted in extrusion of basaltic flows and pyroclastic material. Major intrusive activity also took place during the Cretaceous. Late Cretaceous to Early Tertiary volcanism along the Sverdrup Rim generated bimodal compositions, including felsic volcanics. The distribution of these rocks reflects their positions relative to the Basin axis, and a possible mantle plume to the north of Ellesmere Island. The Kanguk Formation bentonites may represent late-stage magmatic activity along the Sverdrup Rim, or they may be the products of extra-basinal volcanism.

CHAPTER 3 : FIELD RELATIONS AND MACROSCOPIC DESCRIPTIONS

3.1 Introduction

Exposures of Kanguk Formation bentonites exist on Kanguk Peninsula, Axel Heiberg Island, and Fosheim Peninsula, Ellesmere Island. Measurement and sampling of bentonites for this study took place during two field seasons, at three different stratigraphic sections of the Kanguk Formation (Fig. 3.1). In July 1990, G.K. Muecke, R.A. MacRae, and G. Fisher collected five bentonites from the Kanguk Peninsula (Section 90-05) and two bentonites from an exposure along the Kanguk River (Section 90-01). During the 1992 field season, G.K. Muecke, E.W. Pearson, and M.B. Parsons documented 27 individual bentonites from a stream exposure in the Fosheim Anticline, Ellesmere Island. This section (92-01) contains the most numerous and lithologically diverse bentonites and is, therefore, the main focus of the field descriptions in this chapter. Appendix A contains detailed field descriptions for all bentonite and shale samples collected from each location.

During the 1992 and 1993 field seasons, L.V. Hills, L.K. Nunez-Betelu, and R.A. MacRae also collected bentonites from 12 different locations around Fosheim and Raanes Peninsulas, Ellesmere Island, and two locations on Axel Heiberg Island. These bentonites do not form part of this thesis, but may soon form part of a regional stratigraphic study of the Kanguk Formation (GK Muecke, personal communication 1994).

3.2 Kanguk Formation Stratigraphy

The Kanguk Formation consists mainly of bituminous shales and organic-rich mudstones, with intercalated sandstone units near the marginal parts of the Sverdrup Basin. Embry (1991) and Balkwill (1978) provided detailed summaries of the stratigraphy and sedimentological

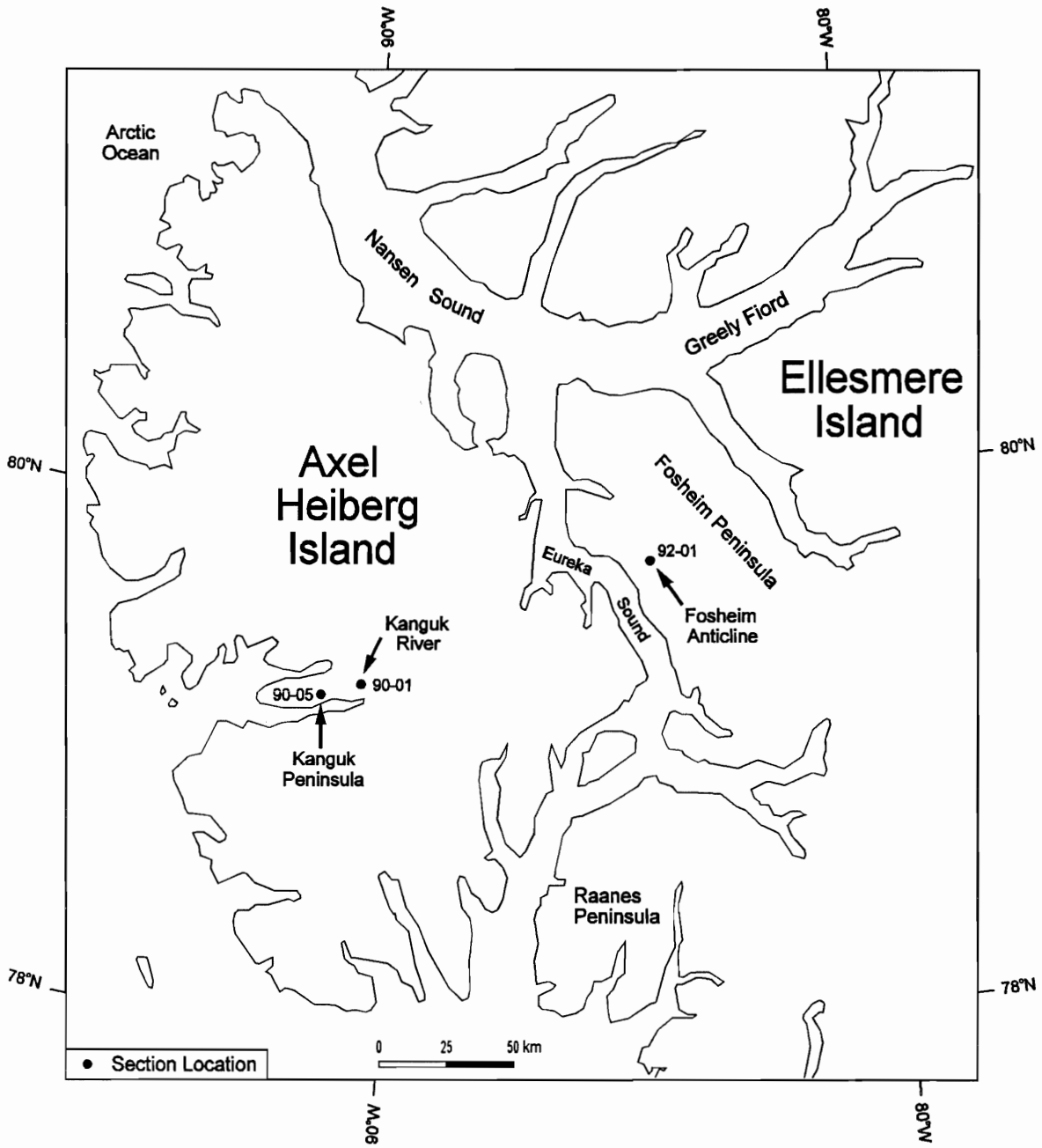

Figure 3.1 Location map showing measured sections on the Kanguk Peninsula, western Axel Heiberg Island, and on Fosheim Peninsula, western Ellesmere Island. Appendix A includes exact geographical coordinates for each of the section locations.

characteristics of this formation. Nunez-Betelu (1991) presented palynological data on the shales and mudstones of the Kanguk Formation. The present study focuses exclusively on the volcaniclastic units interbedded with these basinal sediments, with reference only to the relative stratigraphic positions of individual shale, mudstone, and sandstone units.

3.2.1 Kanguk Peninsula

On Kanguk Peninsula, the Kanguk Formation unconformably overlies subaerial basalt flows of the volcanic Strand Fiord Formation. "In this area, Mesozoic strata are broadly folded in the form of doubly plunging anticlines and synclines, and are locally cut by diapiric anhydrite of the Otto Fiord Formation" (Williamson 1988, p 42). Sampling of bentonites occurred at two separate stream exposures of the Kanguk Formation. Section 90-01, located at 79°18' N latitude and 90°37' W longitude, contains two individual bentonites exposed along the east side of the Kanguk River. Section 90-05, located at 79°15' N latitude and 91°31' W longitude, contains at least 16 individual bentonites exposed near a small creek on the south side of Kanguk Peninsula. The poor exposure of bentonites in these sections may greatly influence the number of individual units documented. Figure 3.2 shows the measured stratigraphy at both locations.

In the Kanguk River section, the Kanguk Formation is in direct, unconformable contact with the underlying Strand Fiord volcanics. The first bentonite occurs 48.2 m above the base of the Kanguk strata, separated from the second bentonite at 118.4 m by greenish to grey Kanguk shales. The lowest bentonite (sample AX90-004) is approximately 15 cm thick, yellowish-green to yellow in color, contains a sharp base against dark grey-black shale, and has a poorly defined top. Orange-rusty oxidation colors increase towards the top, and veinlets of pure white clay material are common. The upper bentonite (sample AX90-003) is approximately 20 cm thick, greenish-yellow in color, has a sharp basal contact against 40 cm of black, highly bituminous

shales, and underlies a thin (15 cm) sandy bed. Light-colored, siliceous concretions are common throughout this bentonite. The exact location of the contact between the Kanguk Formation and the overlying Eureka Sound Group is a matter of considerable debate. The contact is gradational from shales into sandstones, however, the thickness of individual units is variable, and strongly controlled by facies (Ricketts 1991). If the boundary is taken as the base of the first major sandstone unit, the total thickness of the Kanguk Formation strata in this section is approximately 145 m.

Poor outcrop quality, and thinness of units (often < 1 cm), prevented collection of many bentonite horizons from Section 90-05, on Kanguk Peninsula. The stratigraphically lowest sample (AX90-020) occurs 48.2 m above the contact with the Strand Fiord Formation, and overlies at least six very thin bentonitic layers intercalated with the Kanguk shales. Subsequent laboratory work revealed that even this sample, obtained from a bentonite 2-3 cm thick, contains significant shale contamination and is, therefore, unsuitable for geochemical work. At least one bentonite horizon, less than 2 cm thick, separates AX90-020 from the next sampled unit (AX90-021), a 2-4 cm bentonite located at 99.7 m. This bentonite is yellowish-green, locally up to 20 cm as a result of slumping, and overlies a 10 cm thick ironstone bed. Two thin bentonites occur between this sample and a 20 cm thick unit (sample AX90-022) at 141.0 m, which is in sharp contact with the underlying shales. This bentonite is light grey, with rusty brown weathering in its upper portion, and contains pockets of pure white clay similar to those in the lowermost bentonite of the Kanguk River section. Two more bentonite horizons (> 2 cm thick) occur before the first sandstone unit of the overlying Eureka Sound Group, one at 151.0 m (20 cm thick, sample AX90-023), and one at 233.0 m (10 cm thick, sample AX90-024). Each of these units is yellowish-green to rusty brown as a result of weathering near the surface, and changes to a grey color at depth. The total thickness of the Kanguk Formation in this section is approximately 253 m, if the base of the first major Eureka Sound sandstone defines the contact.

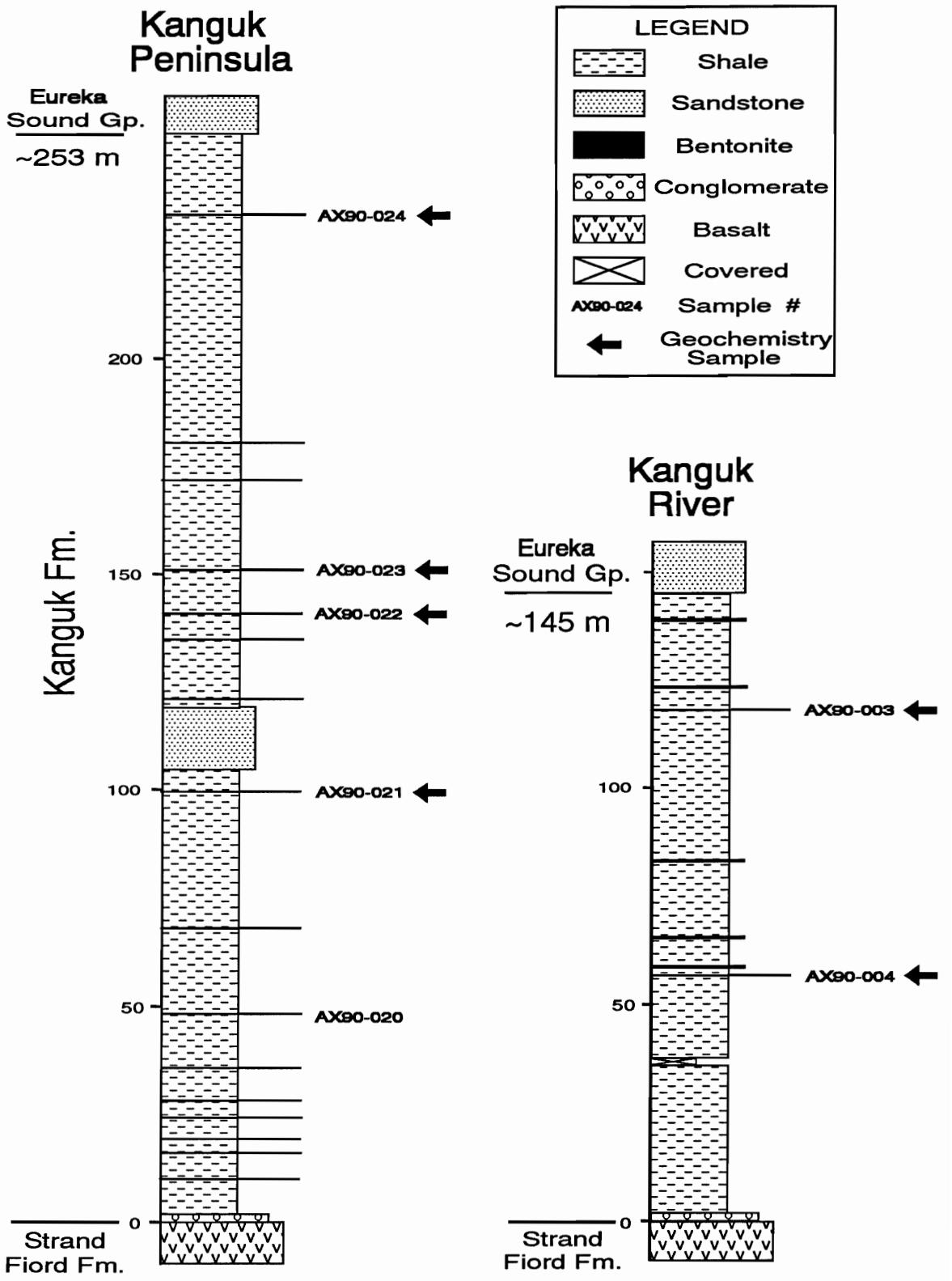

Figure 3.2 Stratigraphy at Section 90-01 (Kanguk River), and Section 90-05 (Kanguk Peninsula), showing the position and thicknesses of individual bentonites, and the upper and lower contacts of the Kanguk Formation. The horizontal width of the bentonite horizons in this diagram emphasizes the stratigraphic position of individual units, and is not a measure of their relative competence. Bentonites are much softer, and more easily eroded, than the interbedded sandstone and shale horizons.

3.2.2 Fosheim Peninsula

Good exposures of Kanguk Formation strata exist in stream-cut sections through the Fosheim Anticline, Ellesmere Island. This anticline is part of the Eureka Sound Fold Belt, formed during the Early Tertiary Eurekan Orogeny. Throughout Fosheim Peninsula, the Kanguk Formation unconformably overlies the sandstone-dominated Hassel Formation. Sampling of bentonites took place at a location where good exposure of this contact allowed accurate measurement of stratigraphic distances from the base of the Kanguk Formation. Section 92-01, located at 79°43' N latitude and 84°47' W longitude, contains 27 individual bentonites, with a cumulative thickness of 911 cm. A complete section of gently dipping Kanguk strata is present at this location, including well-exposed upper and lower bounding unconformities.

Section 92-01 includes 266 m of Kanguk Formation strata, exposed in an easily accessible hillside bordering a braided meltwater stream. Figure 3.3 illustrates the complete measured stratigraphy at this location, including two short covered intervals. Sampling of bentonites took place midway up the hillside, where localized slumping and faulting of the strata were minimal (Fig. 3.4).

The last Hassel Formation sandstone, containing coalified plant debris, defines the base of the Kanguk Formation in this section. Several sandstone units, and many thin ironstone beds, also occur within the Kanguk shales at this location. The first bentonite (Unit A1, sample EL92-001) is present 2.0 m above the basal unconformity, and is intercalated with organic-rich, platy mudstones. Most of the bentonites (Units A3 - A23) occur between 35.0 m and 120.0 m, and range in thickness from 2 - 100 cm. The thickest bentonite is Unit A22 (at 116.3 m), which displays well-developed color layering and internal zonation. Bentonites A14 to A19 are all less than 15 cm thick, and comprise two distinct sets of triplets (Fig. 3.5). No more bentonites are present until 207 m (note that this interval includes a covered section), where four bentonites (Units A24 - A27) occur between 207 m and 223 m. Several disaggregated blebs of yellowish-

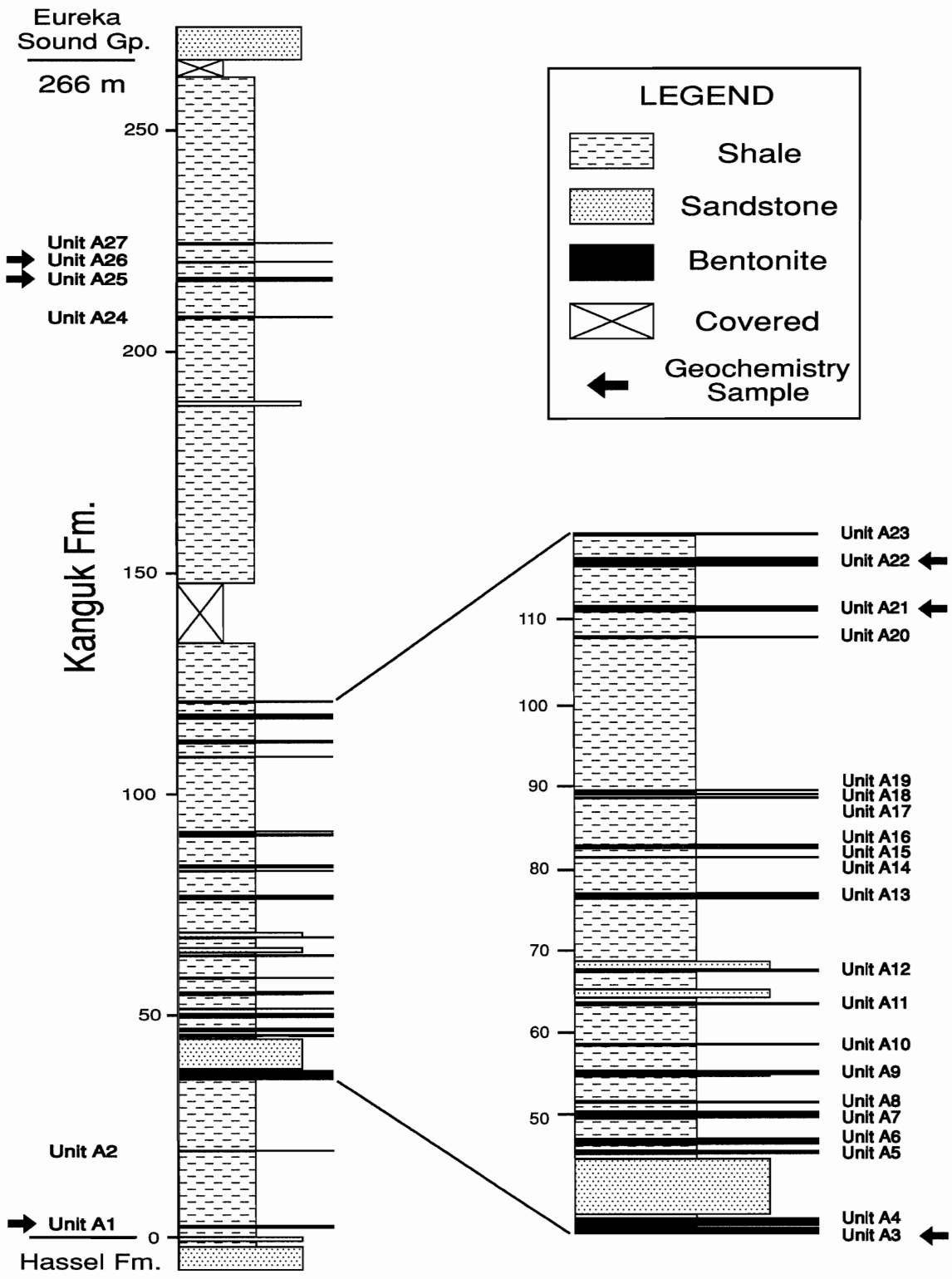

Figure 3.3 Stratigraphy at Section 92-01, on the Fosheim Anticline, showing the position and thicknesses of individual bentonites, and the bounding unconformities of the Kanguk Formation. The horizontal width of the bentonite horizons in this diagram emphasizes the stratigraphic position of individual units, and is not a measure of their relative competence.

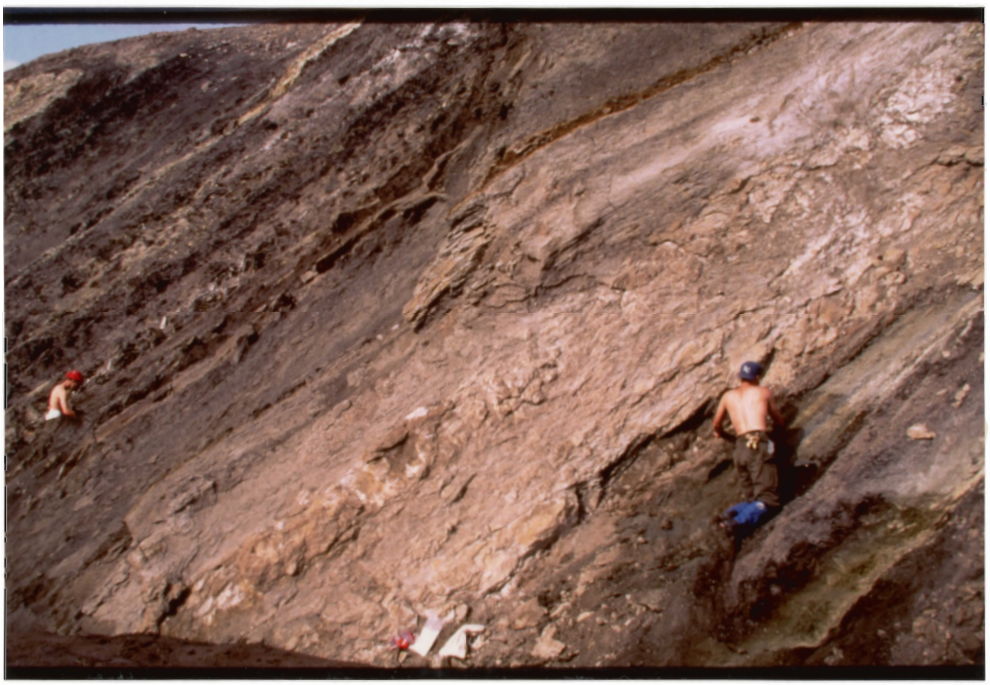

Figure 3.4 Photograph of gently dipping Kanguk Formation strata, exposed in the lower part of Section 92-01 on the Fosheim Anticline. Several recessive bentonite horizons are visible, interbedded with more competent sandstone and mudstone units.

Figure 3.5 View of the upper triplet of bentonites (from right, Units A17, A18, and A19). Each bentonite is thin and uniform in character, and intercalated with black Kanguk shales.

green bentonite above 223 m may represent another unit, or slumped material from lower in the outcrop. Section 3.3 includes a more thorough discussion of the lithologic properties of individual bentonites from the Fosheim Anticline.

3.3 Bentonite Field Characteristics

The lithology of individual bentonite horizons within each section is extremely variable. Field descriptions focused on many different characteristics, including color, thickness variations, contacts and bounding units, internal layering, weathering profiles, degree of lithification, contamination, quality of exposure, and continuity along strike. The field characteristics of bentonites from Kanguk Peninsula differ only slightly from those on Fosheim Peninsula. In general, poorer exposures exist on Kanguk Peninsula, fewer bentonites are visible, total bentonite thickness is much less, and individual bentonites do not reach the same thicknesses as those from the Fosheim Anticline. Several bentonites from Kanguk Peninsula contain small pockets of white clay or concretions that are not present in other Kanguk Formation bentonites, however, none exhibits internal layering.

Bentonite colors range from light yellow to dark green in outcrop. Many different shades of green, grey, and brown exist in unweathered bentonites, with colors gradually becoming more orange to rusty brown in surface weathering profiles. Several "layered" bentonites in Section 92-01 (Units A4, A7, A9(?), A22) exhibit well-developed internal color zonation, which roughly parallels the upper and lower contacts (Fig. 3.6). All of these bentonites are greater than 35 cm thick, and have a sharp basal contact overlain by light greenish-grey bentonitic clay. In general, this basal portion grades upward into a dark grey-brown, plastic clay (lighter than Kanguk shales), in contact with the overlying shales. However, surface oxidation of these layered bentonites may also result in significant color changes along strike (Figs. 3.7, 3.11). This stratified color zonation

may reflect compositional heterogeneities resulting from diagenetic, or original magmatic processes. Thomas et al (1990) report similar compositional zonation in the Plateau Tuff, a 25 cm (average) bentonite from the Upper Cretaceous Judith River Formation, in Dinosaur Provincial Park, southern Alberta. Bentonites less than 35 cm thick do not display this distinctive zonation, but may include rusty-brown weathering horizons, diffuse contacts (possibly caused by bioturbation), and oxidation along partings (Figs. 3.8, 3.5).

Many bentonites pinch and swell along strike, and may exhibit thickness variations of up to 25 cm over distances of several meters (Fig. 3.9). Incorporation of fragments of the surrounding sediments can accompany this plastic deformation, leading to contamination of the bentonite (Figs. 3.10, 3.11). Small-scale soft-sediment deformation structures, such as load casts and ball-and- pillow structures, are visible along the irregular margins of some bentonites.

Several bentonites (Units A7, A9, A13) are very blocky and strongly lithified. Lithification is common in bentonites that contain an additional clastic component (i.e., incorporated detrital material); however, lithification also occurs within individual horizons in layered bentonites. This partial induration may lead to the development of a blocky, fracture-controlled texture (Figs. 3.9, 3.12).

Thin calcareous layers also occur throughout the sediments in Section 92-01 (Fig. 3.10). These veins are up to 1 m long and consist of shell material from the mollusc *Inoceramus lundbreckensis.* These large bivalves are common throughout the upper Kanguk Formation, and provide an age range of mid-late Santonian to early Campanian. Inoceramids are more tolerant of oxygen-deficient water than are most other bivalves, and may have thrived in euxinic conditions within the depths of the Kanguk Sea (Ricketts 1991).

Figure 3.6 Photo of a layered, 80 cm thick bentonite (Unit A-4) in Section 92-01. Above a sharp basal contact with the underlying Kanguk shales, five distinct color zones are visible: olive green, light grey, bluish grey, greenish grey, and light grey (highly plastic clay). The upper contact is transitional into fissile shales, possibly as a result of bioturbation, or other mixing processes.

Figure 3.7 Photo of a layered, 80 cm thick bentonite (Unit A-4) in Section 92-01. Above a slightly deformed basal contact with the underlying Kanguk shales, four distinct color zones are visible: yellow, orange-brown, light grey, and greyish-brown. Note the significant color changes of this bentonite along strike (compare Figure 3.6), resulting from surface oxidation.

Figure 3.8 Photograph of bentonite A-5, a 35 cm thick unit in Section 92-01. Note the sharp basal contact with the Kanguk shales (on right), oxidation along partings, and the gradual darkening of the unit upward.

Figure 3.9 Photograph of bentonite A-3, a 75 cm bentonite that pinches and swells along strike. Note the highly deformed lower contact (on right), slight lithification, and diffuse upper contact (possibly reflecting bioturbation) of this bentonite.

Figure 3.10 Closeup view of contact between bentonite A24 in Section 92-01, and black Kanguk shales. Unit A24 is 20 cm thick, but pinches and swells along strike. Note plastic deformation, incorporated lithic fragments, and giant *Inoceramus lundbreckensis* shells above and below the bentonite.

Figure 3.11 View of bentonite A10 in Section 92-01, showing variable thickness from 4 - 8 cm resulting from plastic deformation during slumping. Note injection and incorporation of fragments of Kanguk shale into the bentonite, and color changes resulting from surface oxidation.

Figure 3.12 Photograph of bentonite A9, a layered unit 45 cm thick in Section 92-01. Light grey base (at right) consists of a 3-6 cm layer of quartz grit, split by a 1 cm layer of shale. This grades upwards into a light greenish grey bentonite, overlain by a lithified layer containing a high proportion of clastic material.

3.4 Measurement and Sampling Methods

Many factors complicate the measurement and sampling of bentonite horizons. Bentonitic clays are very soft and easily deformed, therefore, they erode quickly, and are susceptible to localized slumping, faulting, and solifluction processes. In the Arctic region, permafrost limits sampling to shallow depths (usually less than 30 cm), and contributes to bentonite deformation through repeated freezing and thawing of sediments above the permafrost table. Individual bentonites commonly pinch and swell along strike, and can have very irregular or diffuse margins, making thickness estimates difficult. Incorporation of clastic material with bentonite deposits can occur during slumping and deformation of the sediments, rendering the bentonites unsuitable for geochemical work. Contamination prevented sampling of bentonitic layers less than 2 cm thick.

The Jacob staff method (Compton 1985) allowed measurement of the true stratigraphic positions and thicknesses of the Kanguk Formation strata. In this study, the Jacob staff was a 3 m graduated collapsible aluminum survey pole, and a Brunton compass served as a clinometer. Use of this method involves measurement errors of 5-10 % (Cameron 1989), resulting from difficulties in positioning the pole at right angles to bedding, and advancing downdip to the exact point sighted from the survey pole. Thickness measurements obtained during this study agree closely with similar measurements of the Fosheim Anticline section made by L.V. Hills and L.K. Nunez-Betelu in July 1991, except for the interval from 35 - 65 m (remeasured).

Poor exposure of many bentonites on Kanguk Peninsula necessitated careful sampling. Removal of bentonitic clay from the center of individual horizons, and immediate transfer to a sealed plastic bag, minimized sample contamination. Documentation and collection of bentonites from the Fosheim Anticline followed continuous trenching of the hillside using a collapsible shovel. Small trowels allowed complete exposure of individual bentonite cross sections, and careful collection of uncontaminated samples. Collection of blocky, indurated bentonites followed removal of strongly weathered material by hand.

3.5 Summary

Both the Kanguk and Fosheim peninsulas contain bentonites interbedded with the organic-rich shales and mudstones of the Kanguk Formation. The quality of exposure ranges from poor to excellent, but is generally much better in the Fosheim Anticline section. Measurement and collection of bentonites produced mainly contamination-free samples, with associated stratigraphic positions accurate to within 5-10 %. Fewer bentonites are present on Kanguk Peninsula, and total bentonite thicknesses are much less than the Fosheim Anticline section. The lithology of individual bentonite horizons varies greatly within each section, and field descriptions focused on many different characteristics. Section 92-01 contains the most numerous and lithologically diverse bentonites.

CHAPTER 4 : BENTONITE PETROGRAPHY

4.1 Introduction

The vitric-crystal ashes deposited within the Kanguk Formation on Axel Heiberg and Ellesmere Islands contained two main types of subaqueous fallout tephra. Most of the ash probably consisted of fragmental glassy material, produced by rapid quenching of vesiculated magma during explosive volcanic eruptions. Devitrification and hydrolysis of these glass shards have generated the clay matrix of the Kanguk bentonites. Primary igneous phenocrysts, including quartz, sanidine, ilmenite, zircon, apatite, and acmite, comprised a minor crystal component. The relative proportions of individual phenocryst phases now in the bentonites may reflect pre-eruptive magmatic fractionation processes, eolian and hydrodynamic fractionation during transport, and the relative stability of phenocryst minerals within the diagenetic environment.

Some of the Kanguk Formation bentonites also contain significant quantities of authigenic and detrital minerals. In addition to clay minerals, dominant authigenic phases include gypsum, pyrite, and siderite. Detrital material consists mainly of sandstone and mudstone clasts, as well as grains of quartz and altered feldspar. The authigenic and detrital mineral assemblages reflect conditions within the local sedimentary environments, and do not form part of this study. However, the presence of these inherited components required careful sample processing to ensure pure mineral separates for geochemical and geochronological work. Appendix B contains detailed descriptions of laboratory techniques used for mineral separation and purification.

Time constraints allowed detailed petrological and geochemical analyses of only twelve Kanguk Formation bentonites. This study examines six bentonites from the Kanguk River and Kanguk Peninsula, Axel Heiberg Island (AX90-003, -004, -021, -022, -023, -024), and six bentonites from the Fosheim Anticline, Ellesmere Island (EL92-001, -002, -032, -034, -038, -039). The Fosheim Anticline samples represent the lower, middle, and upper stratigraphic positions of bentonites within Section 92-01 (Units A1, A2, A21, A22, A25, and A26 in Figure 3.3).

4.2 Petrographic Description

Petrographic analysis of the Kanguk bentonites reveals the diagenetically stable, primary phenocryst mineralogy of the original volcanic ashes. The diameters of pyroclastic fragments reflect the original magmatic crystal size distribution, vent proximity, relative volcanic energy, and paleowind directions. However, complete replacement of vitric fragments, and contamination by detrital material, complicate an accurate determination of the original modal mineralogical composition. Previous studies illustrate the difficulty of using modal analyses of bentonites to identify original melt compositions. For example, Thomas et al (1990) obtained three separate rock names (rhyolite, dacite, and andesite) for the same bentonite using quartz-alkali feldspar-plagioclase (QAP) point count values plotted on the ternary diagram of Streckeisen (1979). This range of classifications may reflect distortion of the original modal ash compositions as a result of sample processing (individual rock names represent whole-rock, bulk-, and "lights"-grain mounts, respectively). Therefore, this study focuses on establishing the identity of all major pyrogenic minerals (i.e., those minerals crystallized within the parent melt), and uses mineral compositions to characterize the nature of the parent magma(s).

4.2.1 Primary Phenocryst Mineralogy

The predominant phenocryst phases within the Kanguk bentonites are, in general order of decreasing abundance, sanidine, quartz, ilmenite, zircon, apatite, and acmite. Thorough examination using a petrographic microscope showed no evidence of any surviving glassy fragments.

Sanidine. Sanidine comprises approximately 50-60% of the pyrogenic crystal fraction in all Kanguk bentonites. Most crystals occur as angular to subangular, subhedral fragments. Crystals are generally colorless and translucent, but may be white and virtually opaque if altered (Fig. 4.1).

Some crystals show microperthitic exsolution textures, present as Na-rich feldspar lamellae aligned parallel to (100) crystallographic planes in the K-rich hosts. Small (< 50 μm) glass and mineral inclusions occur in many crystals, and composite grains with ilmenite are present in all samples.

Quartz. In most bentonites, quartz phenocrysts account for approximately 30-40% of the pyrogenic crystal fraction. Quartz crystals are generally angular to subangular, subhedral fragments, but do occur as euhedral hexagonal bipyramids in some samples. Most crystals are grey and translucent, and some have a slightly pitted surface texture. Mineral inclusions (e.g., acicular rutile) and unaltered glass inclusions (up to 100 μm wide) occur in many crystals (Fig.4.2).

Ilmenite. Ilmenite constitutes up to 15% of the primary phenocrysts in many Kanguk Formation bentonites. Grains of ilmenite are black, opaque, magnetic, and have a shiny metallic luster. Crystals are generally euhedral to subhedral, with thick tabular or prismatic shapes, and are characteristically angular to subangular. Many crystal faces display a pitted surface texture, and composite grains with quartz, zircon, and rutile occur in some samples (Fig. 4.3).

Zircon. Zircon phenocrysts form a volumetrically minor component (< 2%) of all Kanguk bentonites. Crystals are typically less than 180 μm long, angular to subrounded, euhedral to subhedral, and form tetragonal prisms with pyramidal terminations. Most grains are translucent, and pinkish-orange in color. Mineral, fluid, and glass inclusions occur in many crystals, and composite grains with ilmenite are present in several bentonites. Some zircons have rounded to subhedral cores with euhedral overgrowths, suggesting possible inheritance (Fig. 4.4).

Apatite. Trace amounts of apatite occur in most samples as colorless to white, translucent crystals, less than 150 μm long. Most crystals are angular to subrounded, euhedral to subhedral, and form elongate hexagonal prisms. Euhedral inclusions of apatite occur in some ilmenite grains.

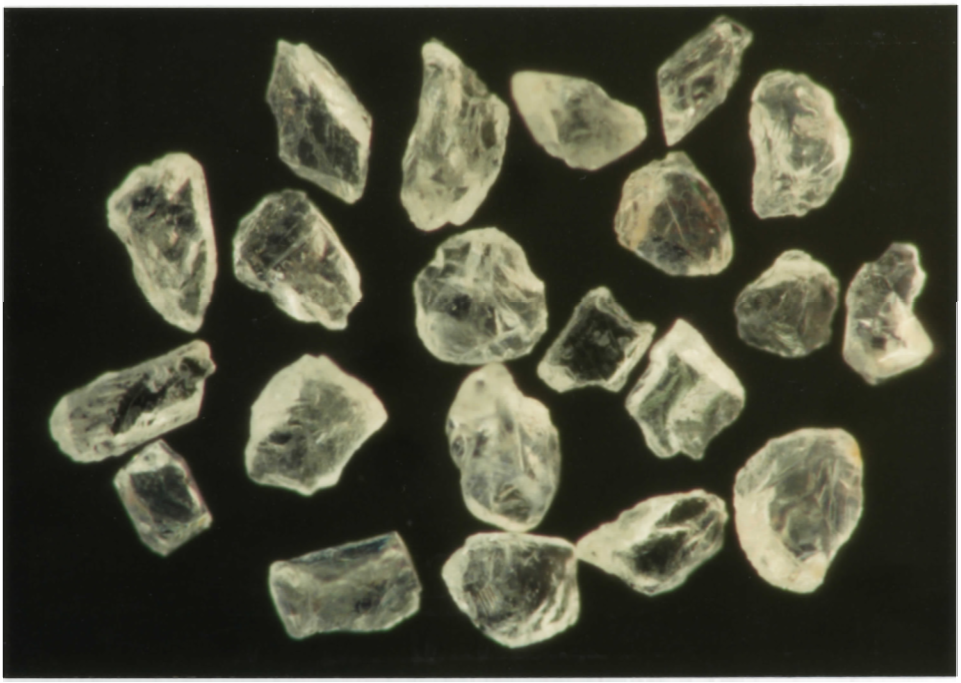

Figure 4.1 Photomicrograph of sanidine crystals from bentonite AX90-024. Most crystals are angular to subangular, and subhedral in form. Field of view = 7.5 mm.

Figure 4.2 Photomicrograph of quartz phenocrysts from bentonite AX90-004. Crystals are angular to subangular, with subhedral forms. A distorted bipyramid containing a green mineral inclusion is visible near the upper left corner. Note that many crystals contain mineral and glass inclusions. Field of view = 7.5 mm.

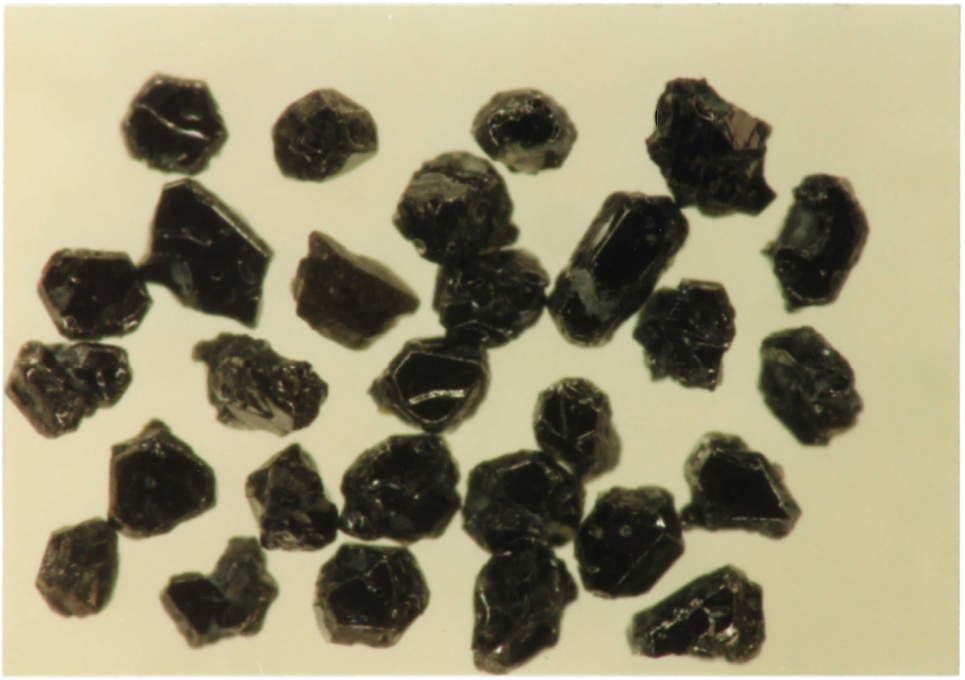

Figure 4.3 Photomicrograph of ilmenite crystals from bentonite AX90-003. Most phenocrysts are angular to subangular, and have euhedral to subhedral, thick tabular or prismatic habits. Note that many crystal faces display a pitted surface texture, and several grains have attached zircon and quartz fragments. Field of view = 7.5 mm.

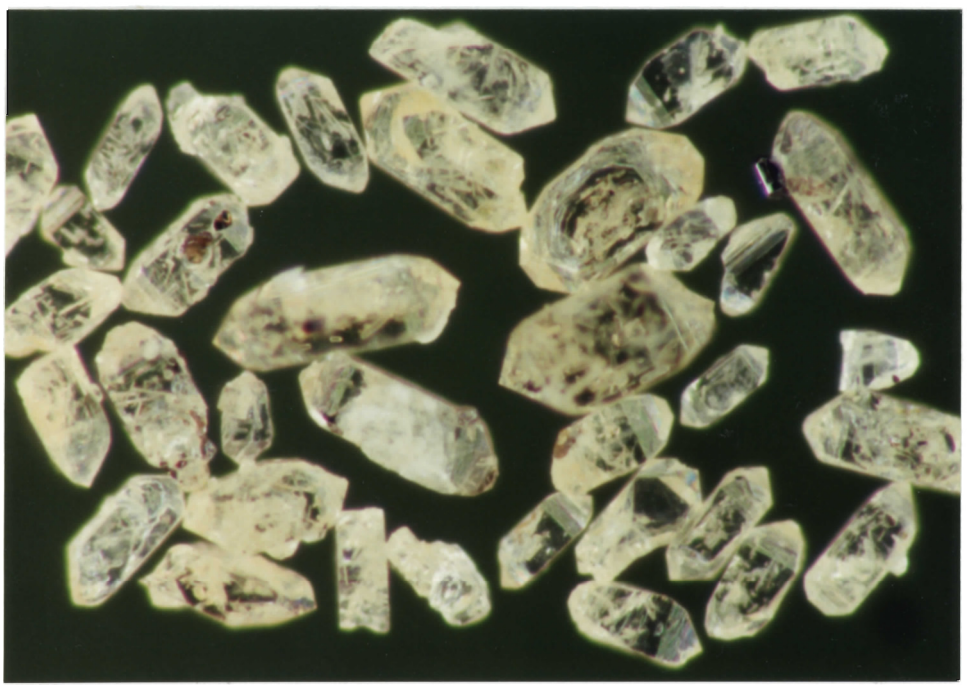

Figure 4.4 Photomicrograph of zircon phenocrysts from bentonite AX90-023 Crystals are angular to subrounded, and form tetragonal prisms with pyramidal terminations. Some phenocrysts contain mineral and fluid inclusions, and composite fragments of ilmenite. One zircon near the lower right corner contains a rounded core bounded by a euhedral overgrowth. Field of view = 4.5 mm.

Acmite. Acmite ($NaFe^{3+}Si_2O_6$) is present in some bentonites as brown, elongate (< 180 μm), prismatic crystals, with sharply pointed terminations. Most crystals display two well-developed cleavages, and are slightly translucent along edges.

4.2.1 Texture

Size distributions of pyrogenic crystals from the Kanguk Formation bentonites provide some constraints on eruption dynamics, location of the volcanic vent, and the style and duration of pyroclast transport. Previous studies of bentonite grain-size distributions (e.g., Zhang and Huff 1992) assume that primary phenocrysts represent original air-fall particles and, therefore, their regional distribution reflects dynamic eruption parameters, and the prevailing atmospheric conditions of wind velocity and temperature. Detailed grain-size analysis of recent volcanic ashes indicate that primary minerals occur as free crystals, as aggregates of crystals and glass, and as microlites in glass shards (e.g., Sigurdsson and Carey 1989). The absence of relict glass textures within the Kanguk bentonites precludes estimates of size relationships between free crystals and vitric pyroclasts. Therefore, the following discussion assumes that most pyrogenic minerals in the bentonites represent free crystals (i.e., not microlites or aggregates) that may provide rough estimates of vent proximity. However, measurements of maximum grain diameters and sorting parameters from only three sections have limited utility for constructing isopach maps. Hand-sieving and measurements of individual grains yield approximate grain-size distributions for the Kanguk bentonites.

Bulk grain-size distributions are similar for bentonites collected from each section; however, distributions are very different between the Axel Heiberg and Ellesmere sections. More than 80% of crystals from the Kanguk Peninsula and Kanguk River samples fall within the coarse ash (2 mm to 1/16 mm) size range (Schmid 1981). Approximately 60-70% of the crystals are between 1/4

mm and 1/16 mm, corresponding to the fine-very fine sand (2-4 phi) size range of the Udden-Wentworth sediment classification scheme (Pettijohn et al 1972). In contrast, most bentonites from the Fosheim Anticline section contain up to 40-50% of primary phenocrysts in the fine ash (less than 1/16 mm) size range. Dry-sieving of the coarse ash fraction reveals that greater than 80% of the crystals are between 1/8 mm and 1/16 mm, equivalent to the very-fine sand size range. In general, phenocrysts of sanidine and quartz form the largest and most abundant crystals in all Kanguk bentonites. Measurements of these phenocrysts yield maximum grain diameters of approximately 1.2 mm for the Kanguk Peninsula and Kanguk River samples, and up to 0.4 mm for the Fosheim Anticline samples.

Grain-size parameters within the Kanguk bentonites suggest that the volcanic source of the original ashes was closer to Kanguk Peninsula than to Fosheim Peninsula. Bentonites from the same location contain similar grain-size distributions, and do not display systematic variations in grain-size over time. However, significant differences in the average grain-size of primary phenocrysts exist between the Axel Heiberg and Ellesmere sections. These observations suggest that free-crystal grain-sizes within the Kanguk bentonites reflect mainly eolian fractionation, rather than differences in pre-eruption crystallization histories.

The widespread ash dispersal, and relatively well-sorted, fine-grained crystals in most bentonites coincide with theoretical considerations of large-magnitude (i.e., Plinian) explosive eruptions. Plinian-style volcanic eruptions can project ash to heights of 30-40 km, where stratospheric winds control the ash dispersal (Walker 1981). Under these conditions, eruptive plume heights, and the prevailing paleowind patterns following eruption are the dominant controls on ash distribution (Fisher and Schmincke 1984). Therefore, grain-size parameters do not provide reliable estimates of proximity of the Kanguk sections to the volcanic vent(s) without the support of additional data.

4.3 Mineral Chemistry

The primary mineral assemblages of the Kanguk Formation bentonites help to characterize the nature of the original parent magma(s). Chemical analyses of individual phenocryst phases also supply additional petrogenetic information. The compositions of primary phenocrysts indicate chemical conditions within the parent magma(s) at the time of eruption, under conditions of equilibrium crystallization. These data can provide estimates on the degree of crystal-liquid fractionation, the activities of various chemical species, and the temperature of the magma(s) at the time of eruption (McBirney 1984).

Use of the JEOL 733 Superprobe at Dalhousie University yielded compositional data for all phenocrysts separated from the Kanguk bentonites. Electron microprobe analyses of all minerals employed an Oxford Link eXL energy dispersive system and a standard ZAF matrix correction program. This software accounts for the effect of atomic number (Z), X-ray absorption (A), and secondary fluorescence (F) on each analysis. Resolution of the energy dispersive detector is 137 eV at 5.9 keV. Each spectrum was acquired for 40 s using an accelerating voltage of 15 kV, a beam current of 15 nA, and a spot size of 1-2 microns. Cobalt metal served as a calibration standard, yielding instrument precision of approximately 0.5% for 10 replicate analyses. Accuracy for all major elements is about 1.5 to 2.0% relative to standard values. Unpolished grains mounted on conducting tape allowed qualitative phenocryst identification. Polished grain mounts provided quantitative mineral chemistry data. Appendix C includes tabulated electron microprobe analyses of feldspar and Fe-Ti oxide phenocrysts.

4.3.1 Feldspar compositions

Microprobe analyses of primary feldspar phenocrysts in six bentonites from the Kanguk Peninsula and Kanguk River sections reveal a narrow range of alkali feldspar compositions (Fig.

4.5). The only primary feldspar present is a sodic-potassic sanidine, with a compositional range from Or_{41} to Or_{52} (molecular percent orthoclase). Table C1 contains average weight percent Or values for all six samples, ranging from Or_{43} to Or_{49}. No primary plagioclase occurs in any of the samples, in contrast to bentonites from many other studies in which plagioclase is generally the most abundant igneous mineral (Baadsgaard and Lerbekmo 1982; Thomas et al 1990). Minor euhedral to subhedral intergrowths of ilmenite, rutile, and apatite exist in some grains. Compositional zonation is insignificant in all phenocrysts analyzed, suggesting that most crystals are probably close to equilibrium compositions. Time constraints prevented microprobe analysis of feldspar phenocrysts from the Fosheim Anticline bentonites.

4.3.2 Oxide minerals

Ilmenite is the dominant oxide mineral in all Kanguk Formation bentonites. However, small inclusions of rutile also occur within phenocrysts of ilmenite and quartz. Tables C2 and C3 contain average microprobe analyses of ilmenite and rutile, respectively, from three Axel Heiberg bentonites. Phenocrysts of ilmenite have FeO_t contents from approximately 43-47 wt%, and TiO_2 contents from about 50-55 wt%. In general, Al_2O_3, MgO, Cr_2O_3, and CaO are all less than 0.5 wt%, and MnO contents range from about 0.1 to 2.5 wt%. Recalculation of total iron from the microprobe to FeO and Fe_2O_3 (Carmichael 1967) illustrates limited solid solution between ilmenite and hematite (Fig. 4.6). Rutile inclusions contain approximately 95-99% TiO_2, with traces of FeO and SiO_2.

4.5 Petrogenetic Interpretation

One of the main research objectives of this thesis is to determine the original composition of the parent magma(s) of the Kanguk bentonites, and to describe their chemical evolution over time.

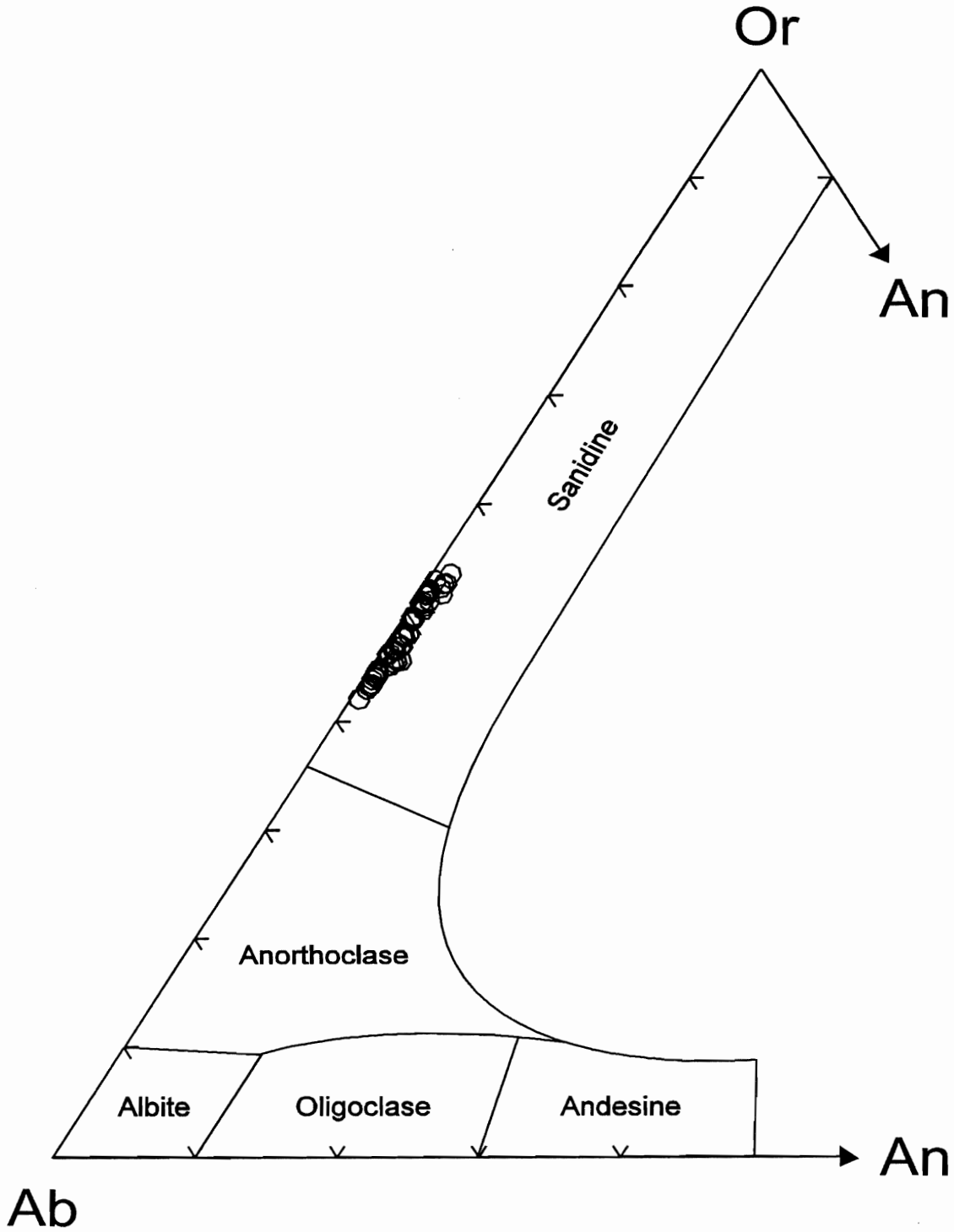

Figure 4.5 Modified ternary plot of Kanguk bentonite feldspar compositions in the system $KAlSi_3O_8$ (orthoclase: Or) - $NaAlSi_3O_8$ (albite: Ab) - $CaAl_2Si_2O_8$ (anorthite: An). The cluster of data points near the midpoint of the Ab-Or join reflects the narrow compositional range of the sanidine phenocrysts. Note the low molecular proportion of the anorthite component.

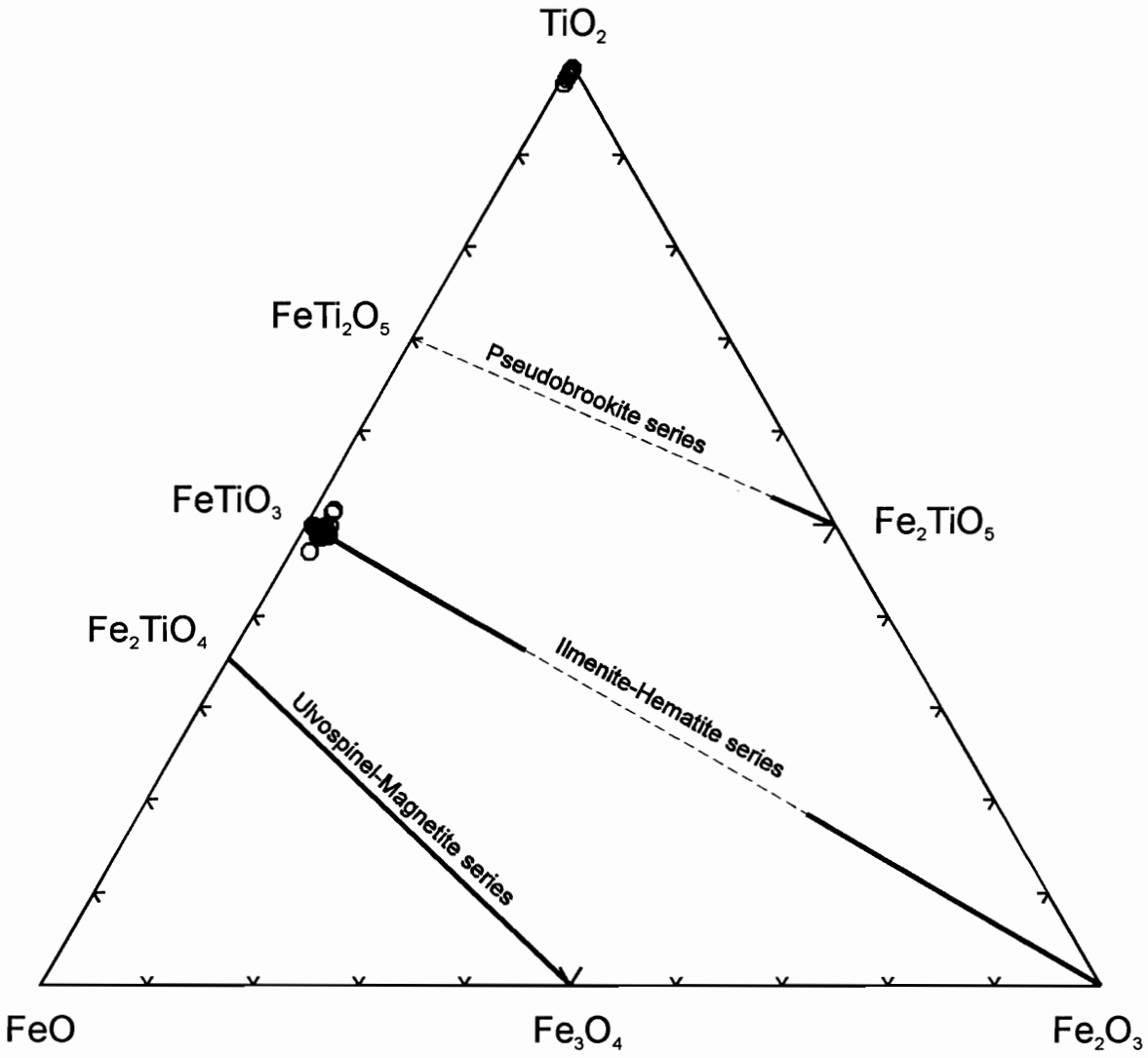

Figure 4.6 Ternary plot of Kanguk bentonite Fe-Ti oxide compositions in the system FeO-Fe_2O_3-TiO_2. Solid bars indicate the extent of solid solution between end member compositions. Note the limited solid solution of oxide minerals from the Kanguk bentonites within the ilmenite-hematite solid solution series, and the coexistence of rutile inclusions in some samples.

Therefore, the bentonites selected for this study represent early, middle, and late stages of volcaniclastic deposition within each section. Petrographic analysis of the twelve chosen samples indicates no major differences, apart from grain-size parameters, between the Axel Heiberg and Ellesmere bentonites. The identities and relative proportions of major phenocryst minerals are similar for all bentonites analyzed. These initial observations suggest that the Kanguk bentonites may represent deposits from a single volcanic source region, however, thorough characterization of the source requires additional geochemical information.

The primary mineral assemblage and phenocryst compositions of the Kanguk Formation bentonites provide some important constraints on the nature of the original parent magma(s). Abundant primary quartz phenocrysts in all samples indicate oversaturation of the magmatic source with respect to silica. The presence of acmite in at least three samples (AX90-024, EL92-034, EL92-038) is diagnostic of a peralkaline bulk composition, in which molecular $(Na_2O + K_2O) > Al_2O_3$, and the excess Na_2O enters acmite (Nicholls and Carmichael 1969). These parameters indicate that the parent magmas of the Kanguk bentonites have peralkaline rhyolite compositions (Macdonald 1974a). The peralkaline nature of these melts precludes the use of silica as a reliable measure of differentiation, for it may increase non-linearly or even reverse its trend to decline in the final stages of differentiation of highly alkaline series (McBirney 1984).

Compositions of feldspar phenocrysts from the Axel Heiberg bentonites also suggest that peralkaline conditions prevailed during the eruption of these volcanic ashes. The complete absence of primary plagioclase may indicate that feldspar fractionation was a major controlling factor in the compositional evolution of the parent melts. Fractionation of relatively anorthitic plagioclase from an anorthite-poor magma rapidly depletes the residual melt in Ca and Al, generating an alumina undersaturated, peralkaline melt. This "plagioclase effect" also leads to relative enrichment of Na, K, and Si in the residual liquid. As the melt becomes more peralkaline, alkali feldspar replaces plagioclase. Fractionation of alkali feldspar produces increasingly sodic peralkaline melts, because K is more compatible than Na in the crystallizing feldspar (Roux and Varet 1975). However, these differentiation trends hold true only if feldspar is the dominant crystallizing mineral. If Al-poor

ferromagnesian minerals are also fractionating, their separation from the original melt may impede the depletion of Al through plagioclase crystallization (McBirney 1984).

The restricted range of sanidine compositions within the Kanguk bentonites is consistent with reported analyses of sodic sanidines (Or_{40-46}) in oversaturated peralkaline rhyolites from the Kenya Rift Valley (Macdonald et al 1987). Yet, the values are slightly more potassic than several peralkaline suites (average: Or_{30-40}) studied by Nicholls and Carmichael (1969). Higher Or values in the Kanguk sanidines may be the result of extended fractionation of sodic ferromagnesian minerals within the parent magma(s), leading to progressively more potassic feldspars (Roux and Varet 1975).

Iron, and many high-field strength cations, including Ti and Zr, have a high solubility in strongly peralkaline, rhyolitic (pantelleritic) magmas. High concentrations of these elements occur in late crystallizing accessory phases, including sodic pyroxenes (e.g., acmite), sodic amphiboles, and aenigmatite, which replace Fe-Ti oxide minerals through reactions such as:

$$2\,Fe_2SiO_4 + FeTiO_3 + 2\,SiO_2 + Na_2Si_2O_5 = Na_2Fe_5TiSi_6O_{20} \qquad (4.1)$$

fayalite ilmenite quartz melt aenigmatite

(Nicholls and Carmichael 1969; Gwinn and Hess 1989). The ubiquitous nature of ilmenite in the Kanguk samples, coupled with the low abundance of acmite and apparent absence of aenigmatite, suggest that the parent magma compositions were only mildly peralkaline. The presence of primary zircon phenocrysts within most Kanguk bentonites also provides constraints on the degree of melt peralkalinity. In peralkaline, felsic magmas, zircon solubility shows pronounced linear dependence upon the molecular ratio $(Na_2O + K_2O)/Al_2O_3$. Extreme Zr enrichment in strongly peralkaline magmas is possible because the feldspar fractionation that produces these melts does not cause zircon saturation in the residual liquid (Watson 1979). Therefore, saturation of the Kanguk parent magmas with respect to zircon (promoting zircon crystallization) indicates that these melts were not strongly peralkaline.

The lack of coexisting Fe-Ti oxides in the Kanguk bentonites precludes estimates of crystal-liquid equilibration temperatures, and associated oxygen fugacities. However, the relative proportions of FeO and Fe_2O_3 within the oxide minerals indicate general redox conditions within the parent magmas. As shown in Figure 4.6, ilmenite phenocrysts contain very little of the hematite component, and no coexisting magnetite phenocrysts are present. These observations indicate that most iron within the parent magmas existed in the ferrous oxidation state (Fe^{2+}), suggesting highly reducing conditions. The low abundance of acmite in all samples may, therefore, result from buffering reactions within the parent melts which stabilize minerals containing ferrous iron (e.g., ilmenite - $Fe^{2+}TiO_3$).

The presence of rutile inclusions in some ilmenite crystals may indicate high Ti/Fe ratios in the parent magmas. However, the absence of free rutile phenocrysts coincides with experimental studies which show that rutile is not a primary accessory mineral in igneous rocks, because rutile saturation requires TiO_2 concentrations far above those of natural silicate liquids (Ryerson and Watson 1987; Bacon 1989). Further petrographic work may help to confirm a primary, or secondary origin for these rutile inclusions.

4.6 Summary

The Kanguk bentonites represent the altered remains of vitric-crystal ashes generated during explosive volcanic eruptions of peralkaline rhyolite magmas. Primary mineral assemblages, and phenocryst compositions, indicate that the parent magmas of the Kanguk bentonites were only mildly peralkaline. Grain-size distributions and ash dispersal suggest high-energy eruptions typical of Plinian systems. All bentonites analyzed from the Axel Heiberg and Ellesmere sections contain similar proportions of major phenocryst phases, suggesting that the Kanguk bentonites may represent deposits from a single volcanic source region. Slightly coarser grain sizes in the Kanguk Peninsula and Kanguk River sections, relative to the Fosheim Anticline section, may reveal their greater proximity to the original volcanic vent.

CHAPTER 5 : BENTONITE GEOCHEMISTRY

5.1 Introduction

Geochemical studies of bentonites can provide information on parent magma compositions, tectonic settings, and the post-depositional alteration of original volcanic ashes. However, the correct tectonomagmatic interpretation of bentonite compositions must consider the effects of element mobility during the devitrification and hydration of glassy volcaniclastic material. Many elements, including Si, Na, K, Ca, Ba, Rb, Sr, and several of the light rare earth elements (REE), are very mobile during alteration. Gains or losses of these elements through chemical weathering result in apparent changes in the concentrations of all other elements within the bulk sample (Faure 1991). Appropriate modelling of these chemical fluxes is necessary to reconstruct the original ash compositions.

The geochemical characteristics of the Kanguk Formation bentonites provide further evidence for the petrographic interpretation, and classification, presented in Chapter 4. Microprobe analyses of unaltered glass inclusions preserved in quartz phenocrysts characterize the major element composition and pre-eruptive volatile content of the original parent magmas. These inclusions represent small portions of melt trapped within phenocrysts during rapid crystal growth in the magma chamber (Roedder 1984). The compositions of these glass inclusions permit evaluations of element mobilities within six of the bulk ashes, based on a number of assumptions. The corrected trace element and REE concentrations in these bentonites permit a further classification of the original volcanic ashes, and reveal distinct compositional trends within the parent magmas. Therefore, classification of the Kanguk bentonites integrates petrographic characteristics, the major element compositions of unaltered melt inclusions, and corrected bulk bentonite trace element distributions. This classification scheme, combined with analyses of mineral compositions, and distinct major and trace element compositional trends, outlines the petrogenetic history of the Kanguk bentonite parent magmas.

5.2 Analytical Methods

Careful preparation of twelve bentonite samples preceded chemical analyses for major, minor, trace, and rare earth elements. Samples of bentonitic clay were manually disaggregated and dried in covered pans for several weeks, prior to crushing using an agate mortar and pestle. The binding properties of these clays prevented the use of swing-mills and other automated crushing mechanisms. Dry-sieving of approximately 50-60 g of pulverized material using 100 μm nylon sieves, followed by thorough mixing of the powders, ensured homogeneous samples for geochemical work.

Wavelength-dispersive X-ray fluorescence spectrometry (XRF) analyses, performed at the Atlantic Regional Geochemical Centre, Saint Mary's University, provide concentrations for 10 major and minor element oxides, and 14 trace elements. Table D1 in Appendix D contains tabulated XRF analyses for 12 Kanguk Formation bentonites. Results for duplicate bentonite samples, and two USGS standards, MAG-1 (Marine Mud), and SCo-1 (Cody Shale), provide an indication of the accuracy and reproducibility of the analytical data. Precision and accuracy are better than 5% for the major and minor oxides, and between 5-10 % for the trace elements. Loss on ignition (LOI) values represent the mass lost by heating the bentonite samples in an electric furnace for 1.5 hours at 1050 °C. The extremely hydrated nature of these clays yields LOI values from 9.30-19.0 weight percent.

Three bentonites (AX90-003, AX90-024, EL92-001) and two sanidine samples (AX90-003, AX90-024) received further analysis for selected REE (La, Ce, Nd, Sm, Eu, Tb, Yb, Lu) and trace elements (Hf, Ta, Th, U, Sc, Co) using instrumental neutron activation analysis (INAA) at the Atlantic Regional Geochemical Centre. Table D2 in Appendix D includes tabulated INAA data for these bentonite and sanidine samples. Gibson and Jagam (1980) provided a summary of the analytical procedures. Hand-picking of 100 mg of sanidine from each sample for INAA followed the separation and purification procedures outlined in Appendix B. Time constraints precluded the preparation of additional sanidine samples.

The JEOL 733 electron microprobe, described in Section 4.3, provided major element analyses of glass inclusions in quartz phenocrysts. Table D3 in Appendix D contains average microprobe analyses of melt inclusions from six Kanguk Formation bentonites. The use of a defocused beam (10 μm spot size) reduced Na volatilization from these glasses. Cobalt metal was used to calibrate the instrument, and CAM66, a glass standard, provided a measure of accuracy and precision. Instrument precision for 10 analyses of cobalt metal was approximately 0.5%. Relative accuracy for major elements is between 1.5 and 2.0%. In order to generate a suitable number of inclusion analyses for each sample, additional polishing of the grain mounts followed each microprobe session. Multiple analyses of large inclusions, exposed at various depths within the quartz crystals, were collected by carefully noting the stage coordinates for all melt inclusions. Replicate analyses of several large glass inclusions indicated absolute analytical precision of 0.2-0.5% for all major elements.

5.3 Bulk Bentonite Geochemistry

Uncorrected XRF analyses of bulk bentonites are of limited use for petrogenetic studies. Element mobility during bentonite formation obscures the original ash compositions by changing the relative concentrations of all constituents. For example, if a significant amount of one major element leaves during bentonitization, the relative concentrations of all other elements will increase. Conversely, if the original ashes gain a significant amount of an element, the relative concentrations of all other elements must decrease (Faure 1991). Modelling of these chemical fluxes, based on a number of simplifying assumptions, allows the recalculation of selected elemental concentrations within the bulk bentonites. Section 5.5 illustrates this technique, and includes an interpretation of the corrected elemental distributions.

However, the ratios of certain relatively immobile minor and trace elements, including Ti, Zr, Y, and Nb, provide a means of classifying the Kanguk bentonites using uncorrected geochemical data. Each of these elements, because of its very large or very small ionic radius, or high ionic

charge, is not easily transported by fluids which accompany secondary alteration processes (Winchester and Floyd 1977). Therefore, the relative abundances of these "immobile" elements in the original volcanic ashes should not change during bentonite formation.

The concentrations and ratios of many immobile elements also vary systematically with progressive magmatic differentiation. These HFS (high field strength) or "incompatible" elements, including Zr^{4+}, Hf^{4+}, Ta^{5+}, Nb^{5+}, and Th^{4+}, have ionic radii or ionic charges not easily accommodated by common igneous minerals. Therefore, these elements are the last to form, or enter, minerals during fractional crystallization, and are first to enter the liquid phase during partial melting. Partial melting of a source rock having a particular ratio of two incompatible elements produces a magma that preserves this initial ratio, provided that subsequent differentiation does not separate the two elements. The ratio of these elements may distinguish rocks derived from magmas with differing ratios, and may indicate a cogenetic relation for all rocks with similar ratios (McBirney 1984).

Figure 5.1 shows a plot of the incompatible, immobile element ratios Zr/TiO_2 against Nb/Y. With progressive differentiation of a basic magma, the ratio Zr/TiO_2 increases as the TiO_2 content of non-basaltic differentiated rocks decreases. Therefore, this ratio represents a differentiation index, in contrast to the Nb/Y ratio, which increases only slightly with progressive differentiation. With increasing alkalinity, the ratio Nb/Y increases steadily, reflecting the higher Nb contents that characterize alkaline rocks. The ratio Zr/TiO_2 also increases rapidly, indicating the strong concentration of Zr in alkaline rocks (Winchester and Floyd 1977). Figure 5.1 illustrates that most of the Kanguk Formation bentonites are alkaline differentiates, with characteristically high Zr/TiO_2 and Nb/Y ratios. This classification diagram indicates several different parent magma compositions for the Kanguk bentonites, including comendite-pantellerite, rhyolite, trachyte, and trachyandesite. Table 5.1 summarizes the classification of individual samples. This classification assumes preservation of the primary Zr/TiO_2 and Nb/Y ratios within the Kanguk bentonites, and a direct correlation between trace element geochemistry and petrography in the "type" suite used to construct this diagram.

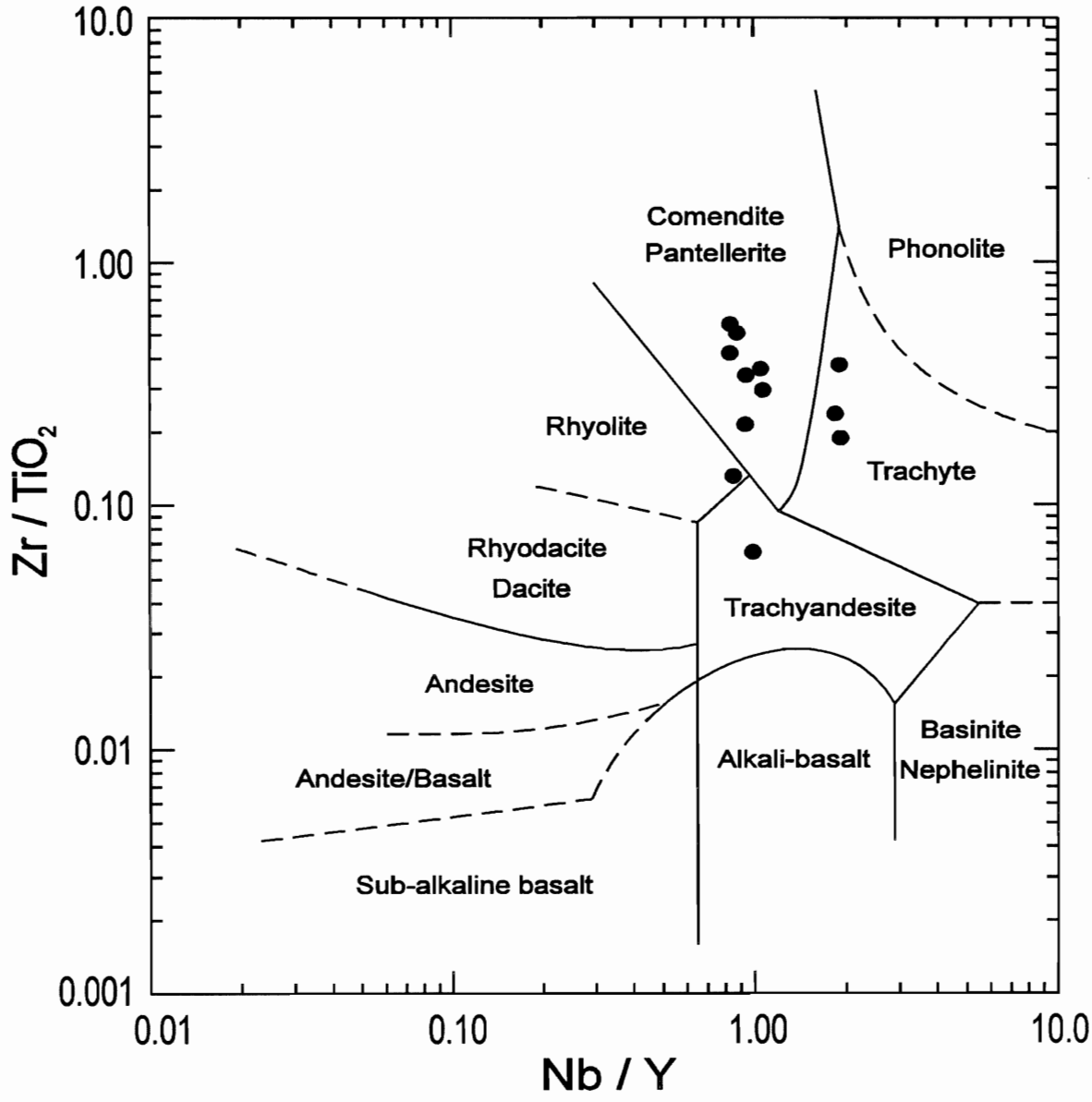

Figure 5.1 Zr/TiO_2 vs Nb/Y discrimination diagram showing the delimited fields for common volcanic rocks. The Kanguk bentonites demonstrate strongly alkaline and differentiated compositions based upon the ratios of these immobile, incompatible elements (after Winchester and Floyd 1977).

Western Ellesmere Island		Western Axel Heiberg Island	
Sample	**Classification**	**Sample**	**Classification**
EL92-001	Trachyandesite	AX90-003	Comendite-Pantellerite
EL92-002	Comendite-Pantellerite	AX90-004	Comendite-Pantellerite
EL92-032	Comendite-Pantellerite	AX90-021	Rhyolite
EL92-034	Comendite-Pantellerite	AX90-022	Comendite-Pantellerite
EL92-038	Trachyte	AX90-023	Comendite-Pantellerite
EL92-039	Trachyte	AX90-024	Trachyte

Table 5.1 Classification of the Kanguk Formation bentonites based on Zr/TiO_2 and Nb/Y delimited fields from Figure 5.1. Note that samples from each section are listed in stratigraphic order, as shown on Figures 3.2 and 3.3.

These results confirm the petrographic classification (Section 4.5) of some of the Kanguk bentonites as peralkaline rhyolites. Both comendites and pantellerites are peralkaline rhyolites, differing only in their FeO and Al_2O_3 contents (Macdonald 1974a). The high Zr/TiO_2 ratios are consistent with experimental studies on zircon saturation in felsic liquids (Watson 1979). However, the presence of zircon phenocrysts in many of the Kanguk bentonites indicates that some of the parent magmas were only mildly peralkaline (Section 4.5).

The Zr/TiO_2 versus Nb/Y plot also permits some preliminary consideration of the evolution of the parent magmas. Within the Fosheim Anticline section, the stratigraphically lowest bentonite has a trachyandesitic composition. The following three samples, in stratigraphic order, display peralkaline rhyolitic compositions. The uppermost two bentonites studied in this section have trachytic parent magmas. Similar compositional variations occur in the bentonites from western Axel Heiberg Island. The stratigraphically lowest unit in the Kanguk Peninsula section displays a rhyolitic composition, and is overlain by two bentonites with peralkaline rhyolitic compositions. The uppermost unit has a trachytic composition. Both bentonites from the Kanguk River section have peralkaline rhyolitic parent magmas.

If the Kanguk bentonites originated from a single, evolving magma chamber, these results suggest that the melt initially became more differentiated (increasing Zr/TiO_2), without much

change in alkalinity, and then became more alkaline (increasing Nb/Y), without much change in the degree of differentiation. However, given the range in compositions, and the total time span represented by these volcanic events (approximately 91.5 - 80.7 Ma, GK Muecke, personal communication 1994), eruption of all the volcanic ashes from a single, evolving magma chamber seems extremely unlikely. Instead, the Kanguk bentonites probably represent ashes from several magmatic sources, within the same volcanic province, each in a different stage of evolution. Additional geochemical evidence reveals distinct compositional trends in the Kanguk bentonites, and helps to constrain the petrogenetic history of the parent magmas.

5.4 Glass Inclusion Analysis

Glass inclusions occur within quartz phenocrysts separated from all Axel Heiberg bentonite samples. Inclusions also exist in quartz crystals from the Ellesmere bentonites, but are difficult to identify as a result of the fine grain size of these ashes. Most melt inclusions are between 10 and 100 μm in diameter, have subrounded to negative-crystal shapes, and are generally clear and undevitrified (Figs. 5.2, 5.3). None of the inclusions studied contains separate vapor phases, and none shows evidence of breaching by cracks or fractures. However, several glass inclusions include brown to opaque blebs of material attached to the walls of the inclusion (Fig. 5.4). These isolated blebs may represent immiscible sulfide or silicate melt globules, or they may be small anhedral daughter crystals nucleated on the inclusion walls (Roedder 1984). Several quartz phenocrysts contain acicular rutile crystals that form radiating clusters near the glass inclusions (Fig. 5.5).

Most quartz crystals contain only one or two melt inclusions, but up to 15 individual inclusions are present in some phenocrysts (Fig. 5.7). The distribution of inclusions in most phenocrysts is essentially random; however, some crystals contain groups of elongate inclusions aligned parallel to the crystal faces (Fig. 5.6). These linear groups may indicate entrapment of the

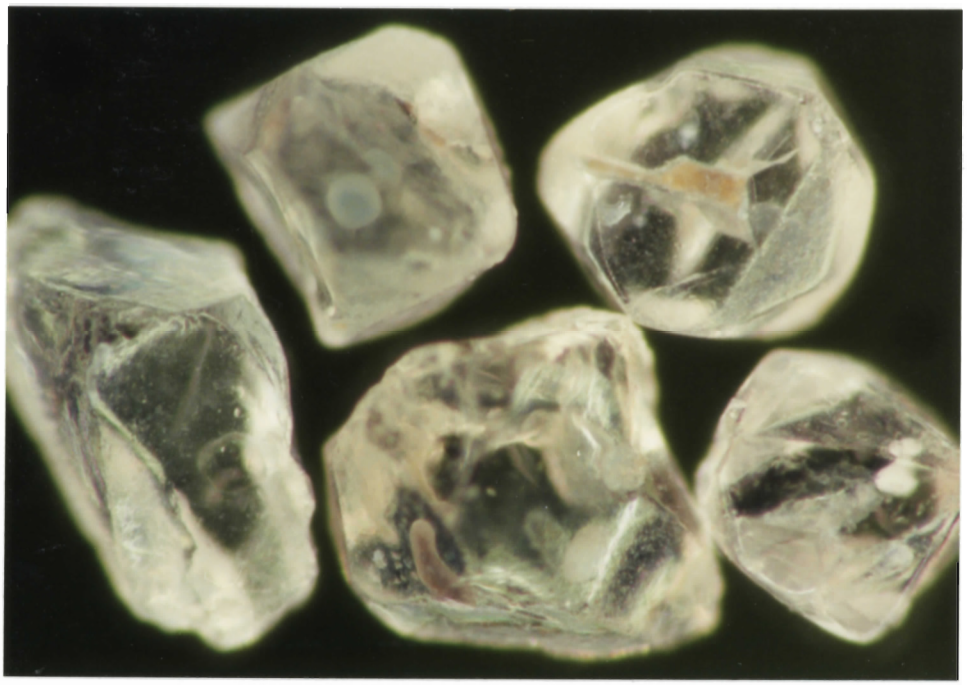

Figure 5.2 Photomicrograph of quartz phenocrysts from bentonite AX90-004. Both glass and mineral inclusions occur in these crystals. The phenocryst on the left contains a clear, subrounded, 80 μm wide melt inclusion. Field of view = 1.2 mm.

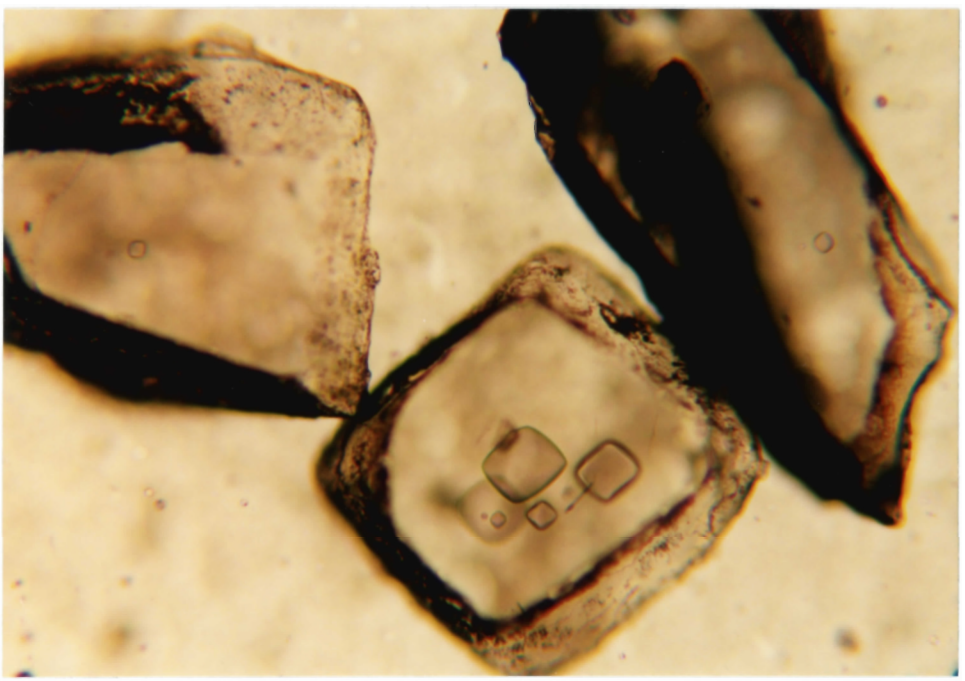

Figure 5.3 Photomicrograph of polished quartz phenocrysts from bentonite AX90-004. Glass inclusions show subrounded to negative crystal shapes, and all are clear and undevitrified. The lower phenocryst contains nine individual inclusions at various depths within the crystal, however, only 6 occur in the focal plane of the picture. Field of view = 1.2 mm.

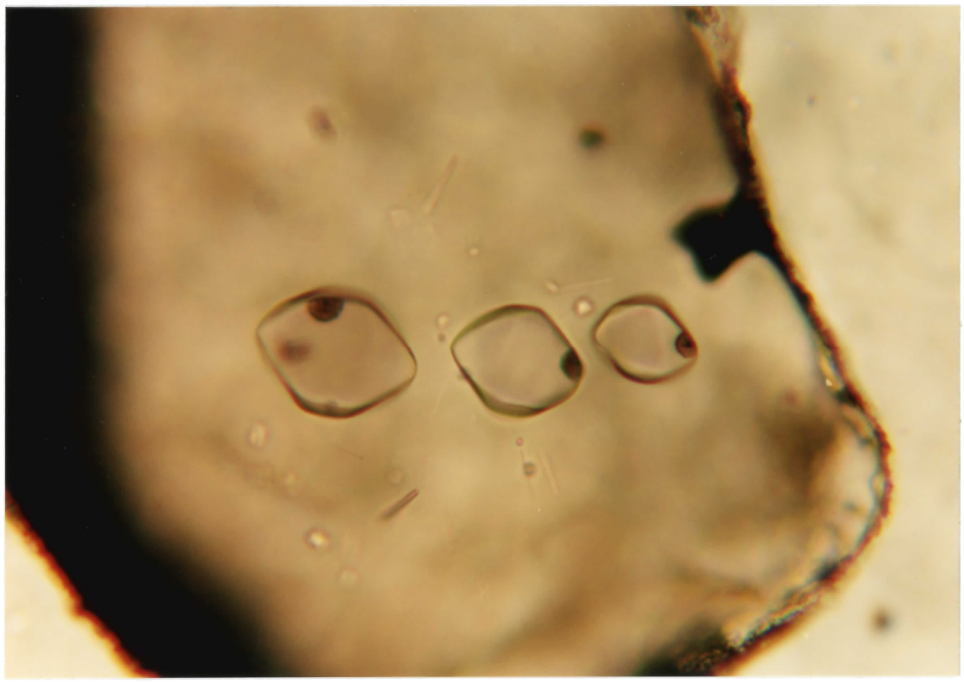

Figure 5.4 Photomicrograph of three negative-crystal shaped melt inclusions in a quartz phenocryst from bentonite AX90-003. Each inclusion contains a small bleb of darker material attached to the inclusion boundary. These blebs may represent immiscible sulfide or silicate melt globules, or they may be small anhedral daughter crystals nucleated on the inclusion walls. Field of view = 0.5 mm.

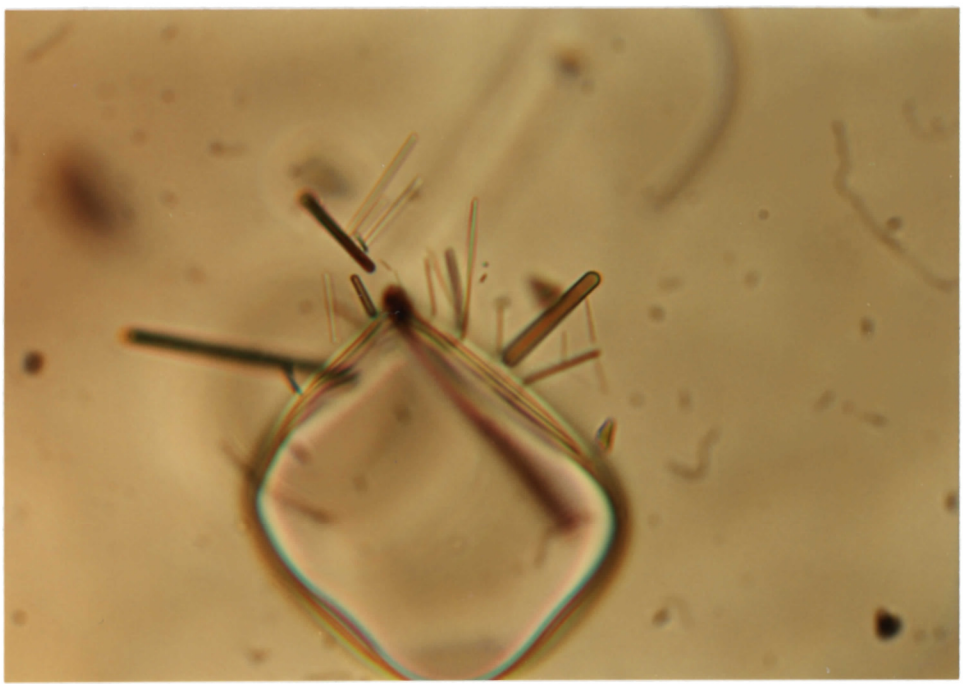

Figure 5.5 Photomicrograph of acicular rutile crystals located near a subrounded 60 μm glass inclusion. (quartz host from bentonite AX90-004). Note that the largest rutile crystal occurs below, not within, the melt inclusion. Field of view = 0.2 mm.

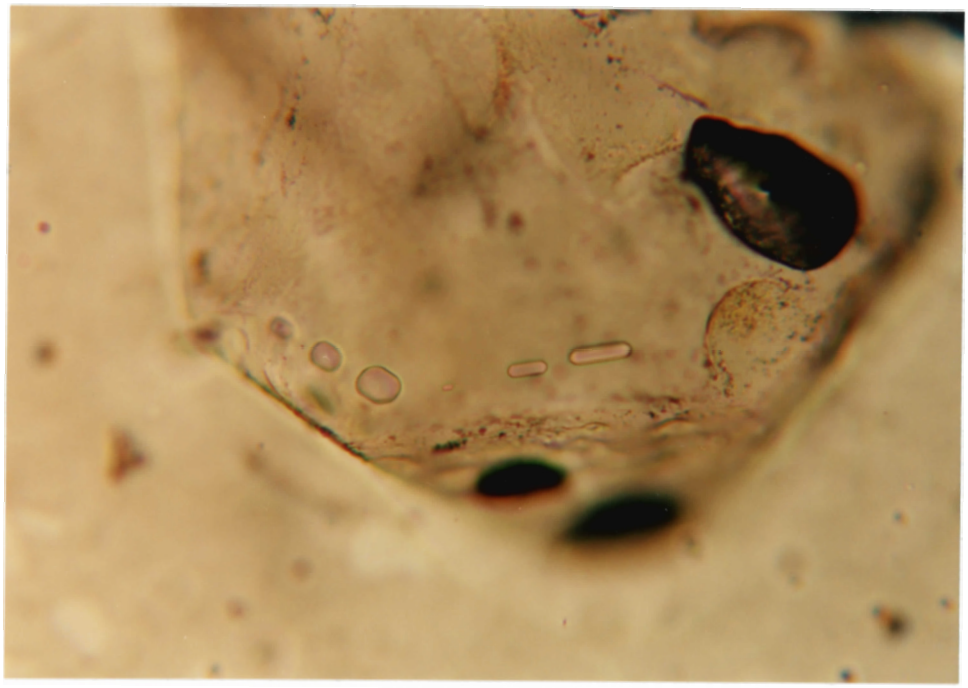

Figure 5.6 Photomicrograph of elongate glass inclusions aligned parallel to the crystal faces of a quartz phenocryst from sample AX90-022. Trapping of these melt inclusions probably occurred during a rapid phase of crystal growth. Field of view = 0.8 mm.

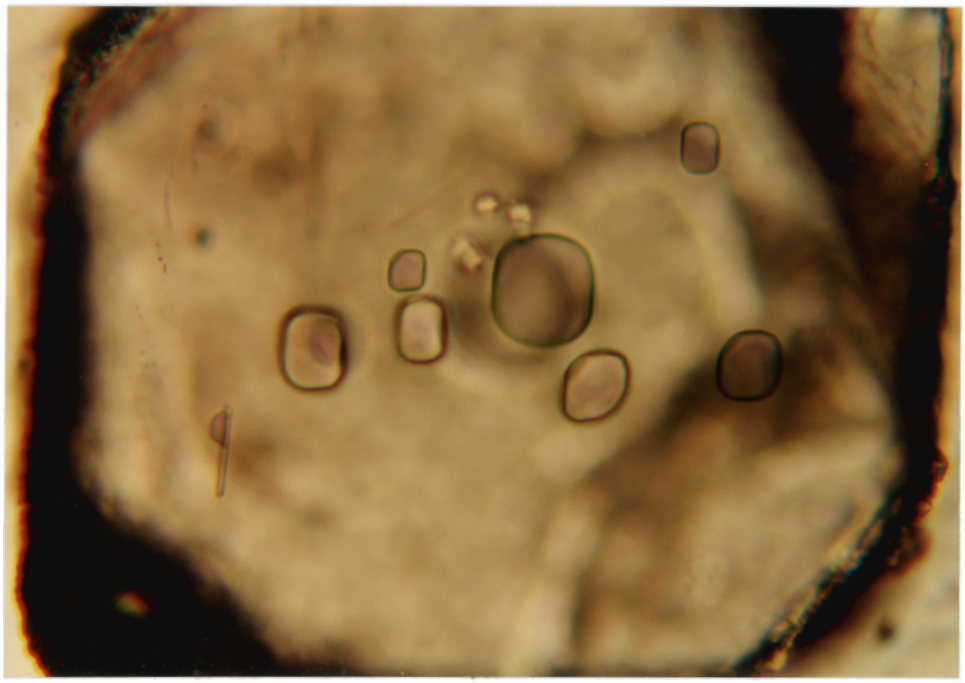

Figure 5.7 Photomicrograph of a quartz phenocryst from bentonite AX90-003. This crystal contains 12 individual glass inclusions, however, only eight appear in the focal plane of this picture. The elongate inclusion near the lower left corner may be an apatite or rutile crystal. Field of view = 0.5 mm.

inclusions during a sudden episode of crystal growth, in response to some perturbation of the magmatic system (Roedder 1984; Dunbar and Hervig 1992). Several devitrified inclusions, located close to the edges of the quartz host, include thin necks of glass attached to the outer edge of the crystal. Anderson (1991) described these "hourglass inclusions" as products of the unsuccessful capture of a gas bubble, followed by some loss of melt through the neck during magmatic decompression. The formation of hourglass inclusions requires saturation of the parent magma with gas; however, the proportion of gas could be large or small (Anderson 1991).

5.4.1 Major element compositions

Electron microprobe analyses of unaltered glass inclusions in quartz phenocrysts reveal the pre-eruptive major element compositions of the Kanguk bentonite parent magmas. All melt inclusions studied are internally homogeneous with respect to the major element oxides, and show no evidence of compositional zonation. Microprobe X-ray scans of Na, K, Al, and Fe show uniform distributions of each of these elements within the glass inclusions (Fig 5.8). However, these observations do not exclude possible changes in melt composition resulting from crystal growth at the time of trapping, or post-entrapment crystallization. Crystal growth selectively enriches or depletes melt at the crystal-melt interface, in elements which are incompatible or compatible, respectively, in the growing crystal (Dunbar and Hervig 1992). This process can generate "diffusive pile-up" of slow-diffusing elements at the crystal-melt interface, thus changing the local magma composition (Delano et al 1994). In addition, the rapid growth required for entrapment of melt inclusions increases the possibility of developing a concentration gradient. All elements analyzed within the glass inclusions of the present study have moderate to high diffusivities in peralkaline melts (Baker and Watson 1988; Bacon 1989); therefore, the concentrations of these elements remain relatively unaffected by quartz growth. No textural evidence exists for post-entrapment crystallization of quartz on the walls of the melt inclusion; however, this process could cause slight elevation of all major element concentrations, with the exception of SiO_2 (Roedder 1984).

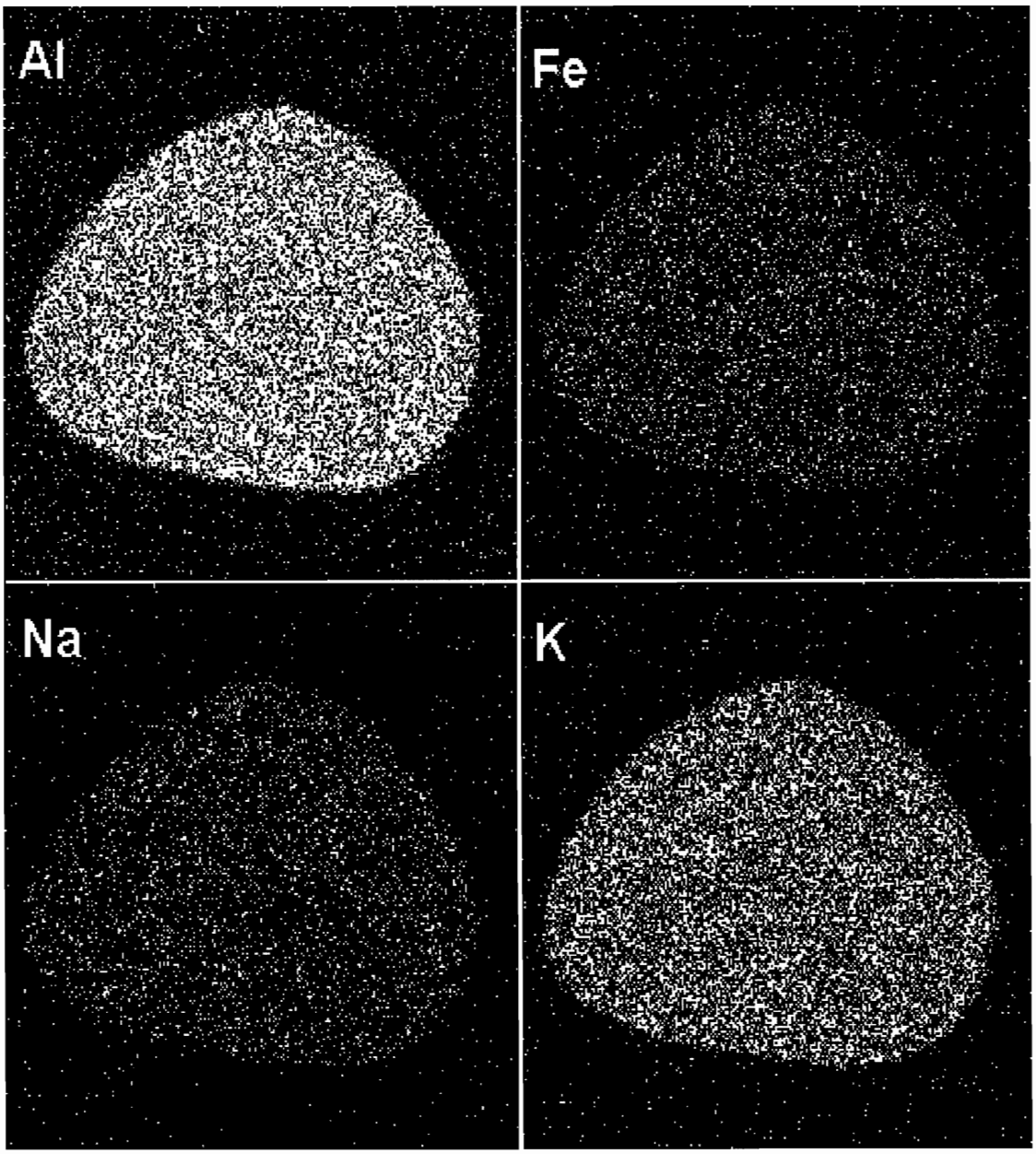

Figure 5.8 Electron microprobe X-ray scans of Al, Na, Fe, and K within a quartz-hosted glass inclusion from bentonite AX90-004. These scans reveal the compositional homogeneity of the melt inclusion with respect to each of these four elements. Spot densities indicate the concentration of each element, relative to the quartz host (approximate inclusion diameter: 70 μm).

Melt inclusions for the six Kanguk bentonites from western Axel Heiberg Island are alkaline to mildly peralkaline, with values of molecular $(Na_2O + K_2O)/Al_2O_3$ between 0.99 and 1.09. Table 5.2 illustrates the peralkalinity indices for each sample, calculated from dry analyses. Major

Sample	Peralkalinity Index
AX90-003	1.08
AX90-004	1.06
AX90-021	0.99
AX90-022	1.00
AX90-023	1.09
AX90-024	1.03

Table 5.2 Peralkalinity indices for six Kanguk Formation bentonites, calculated from volatile-free analyses of glass inclusions in quartz phenocrysts. Note that the index for AX90-023 is based on a single melt inclusion analysis.

elemet variations are generally similar to those found in peralkaline rhyolites (cf. Macdonald et al 1987), however, the narrow range of peralkalinity values precludes the development of strong compositional differences between samples. With increasing peralkalinity, an increase in FeO_t (total Fe as FeO) accompanies a decrease in Al_2O_3 (Figs. 5.9, 5.10). The relative amounts of Al_2O_3 versus FeO_t also distinguish between the two main classes of peralkaline rhyolites. According to Macdonald (1974a), comendites have $Al_2O_3 > (1.33 \times FeO_t + 0.44)$, whereas pantellerites have $Al_2O_3 < (1.33 \times FeO_t + 0.44)$. Based on this classification scheme, the parent magmas of the Kanguk Formation bentonites include both comendites and pantellerites (Fig 5.11).

In general, CaO also decreases slightly with increasing peralkalinity, and K_2O and SiO_2 remain relatively constant. Both MnO and MgO occur in minor amounts (usually less than 0.2 wt%), and ZrO_2 is above detection limits in many inclusions, with concentrations up to 0.31 wt% (3100 ppm). In all melt inclusions, K_2O is greater than Na_2O by weight; this potassic character is typical of continental comendites, in contrast to more sodic oceanic comendites (Macdonald et al 1987). Additional isotopic evidence, and trace element parameters (e.g., Th contents), may indicate the degree of crustal contamination within the Kanguk bentonite parent magmas.

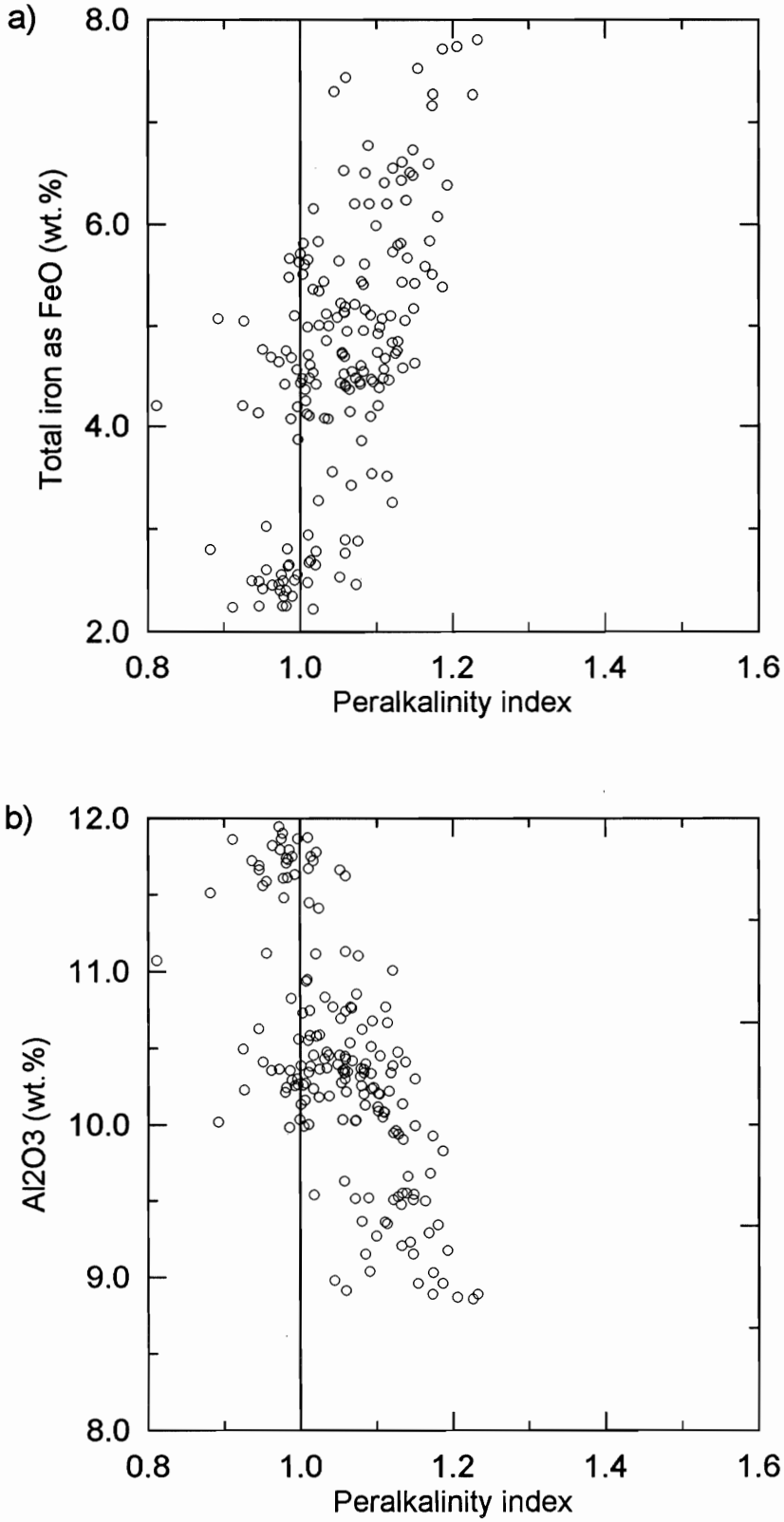

Figure 5.9 Plot of individual glass inclusion analyses from the Kanguk bentonites showing (a) increasing FeO_t and, (b) decreasing Al_2O_3, with increasing peralkalinity. The vertical line on each graph indicates the boundary between alkaline and peralkaline compositions (molecular $(Na_2O + K_2O)/Al_2O_3 = 1.0$)

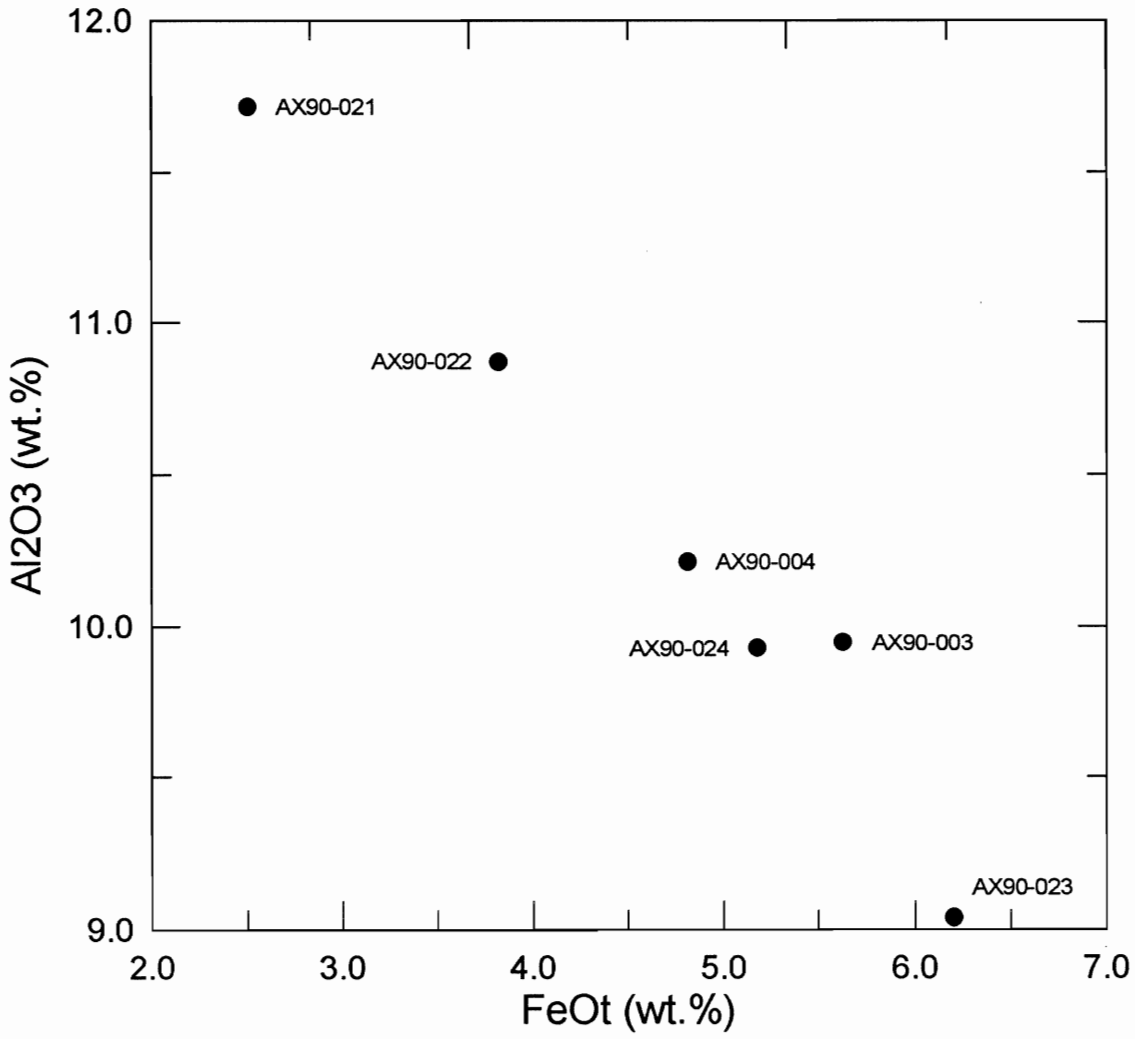

Figure 5.10 Plot of average glass inclusion analyses from six Kanguk bentonites, demonstrating the decrease in Al_2O_3 with increasing FeO_t. This trend roughly corresponds to an increase in sample peralkalinity from left to right.

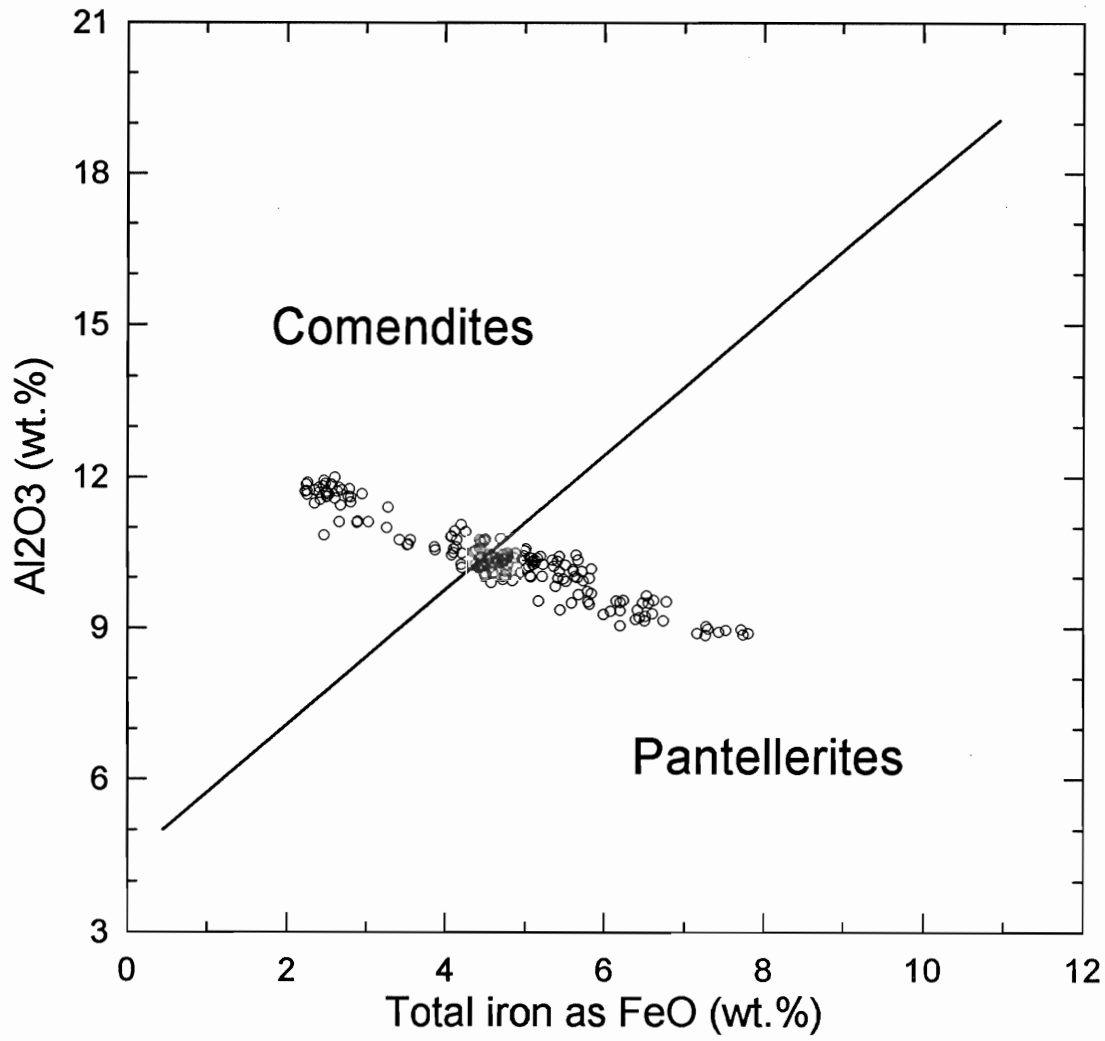

Figure 5.11 Classification plot showing the subdivision of peralkaline rhyolites into comendites and pantellerites, based on relative Al_2O_3 and FeO_t contents. Individual glass inclusion analyses indicate that the parent magmas of the Kanguk Formation bentonites include both comendites and pantellerites (after Macdonald 1974a).

A comparison of alkali ratios in the melt inclusions and sanidine phenocrysts for each sample provides further evidence of peralkaline rhyolitic parent magma compositions. In all bentonites, the ratio $CaO/(Na_2O + K_2O)$ is greater in the melt inclusions than in the coexisting sanidine phenocrysts. Additionally, K_2O in the feldspars always exceeds K_2O in glass inclusions from the same bentonite. Both of these situations are typical of most felsic rocks (including peralkaline rhyolites); therefore, the glass inclusions from each bentonite appear to represent the composition of the parent magma from which the coexisting feldspars crystallized (Noble et al 1971; Macdonald et al 1987).

However, no simple relationship exists between the molecular ratio $Na_2O/(Na_2O + K_2O)$ of the glass inclusions and the same ratio in the associated feldspars. If the Kanguk bentonites evolved from a single, cooling, pantelleritic parent magma, feldspar and melt compositions should show characteristic compositional changes over time. As the melt crystallizes, the feldspar compositions should become progressively more potassic, whereas the residual melt becomes more sodic and more peralkaline (provided there is no significant coprecipitation of a sodic ferromagnesian mineral, or removal of Na_2O as the proportion of liquid decreases) (Nicholls and Carmichael 1969). Figure 5.12 shows that, in general, the glass compositions become progressively less sodic over time in the Kanguk bentonites, while the feldspar compositions become slightly more albitic (note that feldspars from sample AX90-023 are much more albitic than feldspars from all other bentonites). These trends are opposite to those expected from a cooling pantellerite melt. The lack of simple progressive compositional relationships between the glass inclusions and feldspar phenocrysts may support the earlier conclusion that the Kanguk bentonites represent deposits from a series of discrete magma batches of slightly different bulk compositions.

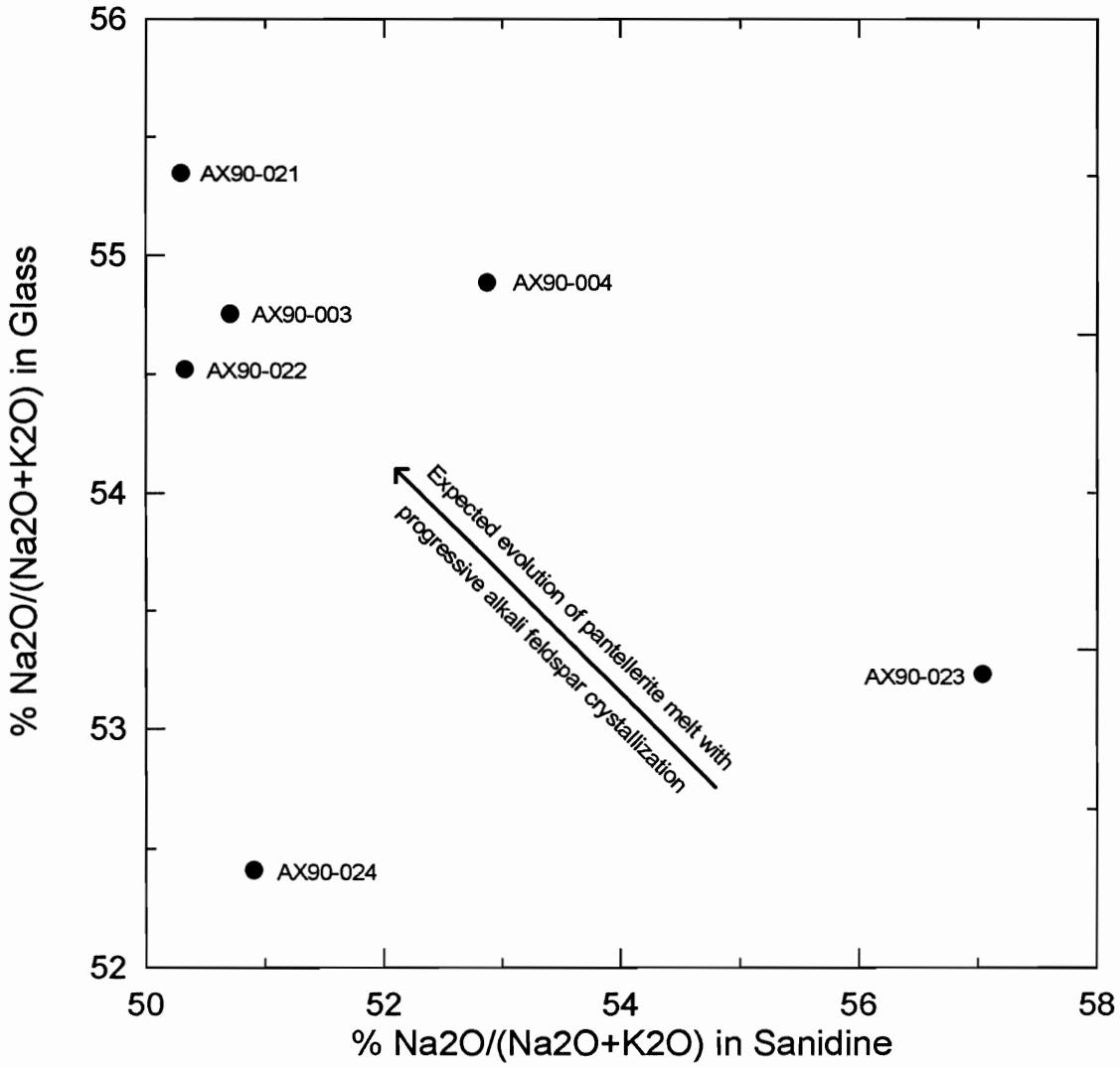

Figure 5.12 Plot of $\%Na_2O/(Na_2O + K_2O)$ in glass inclusions and sanidine phenocrysts from the Kanguk bentonites. Note that the Kanguk samples do not show a distinct compositional trend, such as that expected from the progressive cooling of a single pantellerite melt (after Nicholls and Carmichael 1969).

5.4.2 Magmatic volatile contents and eruptive dynamics

Microprobe analyses of glass inclusions also provide indirect evidence for pre-eruptive volatile contents in the parent magmas. Melt inclusions trapped within quartz phenocrysts form small pressure vessels that do not outgas during decompression and eruption and, therefore, may preserve the pre-eruptive water content of the original magma (Lowenstern and Mahood 1991). Most microprobe analyses of glass inclusions from the Kanguk bentonites show low totals relative to the quartz host, and the glass standard CAM66. The totals for most analyses range from 96-99 wt%, possibly indicating volatile contents of 1-4% within the melt inclusions. These volatile contents coincide with the results of recent electron microprobe, ion microprobe, and infrared spectroscopic studies of quartz-hosted glass inclusions from peralkaline rhyolites (e.g., Kovalenko et al 1988; Lowenstern and Mahood 1991; Wilding et al 1993). In addition to H_2O, F, Cl, and CO_2 may constitute a minor component of the volatile content. Microprobe analyses indicate Cl contents of 0.12-0.22 wt%.

Magmatic volatile contents strongly influence the style and volume of volcanic eruptions. The distribution and fragmentation of pyroclastic material comprising the Kanguk Formation bentonites indicate highly explosive, Plinian-style eruptions (Section 4.2.1). Theoretical considerations suggest that erupting magmas must contain at least 1 wt% H_2O to sustain a Plinian eruption column (Wilson et al 1980). However, "the eruptive style of a nonhydrovolcanic eruption is controlled by the volatile content of the magma at the time of magma fragmentation (not at the time of entrapment of melt inclusions) and is, therefore, a function of the magmatic degassing path. High pre-eruptive water content is neither a necessary nor a sufficient condition for an explosive eruption" (Lowenstern and Mahood 1991, p 82). Thus, pre-eruptive volatile contents preserved in glass inclusions do not constrain the dynamics of the eruptions that produced the Kanguk bentonites.

5.5 Element Mobility during Bentonite Formation

The major element compositions of pristine, quartz-hosted glass inclusions provide a means of evaluating element mobility during the formation of six Kanguk bentonites. However, modelling of elemental fluxes during bentonitization depends on a number of major assumptions.

Foremost, the major element compositions of the unaltered melt inclusions must represent the composition of the original volcanic ashes, prior to bentonite formation. This premise assumes eruption from a compositionally homogeneous magma chamber, trapping of melt relatively close to the time of eruption, and the absence of post-entrapment crystallization within the melt inclusions. The narrow range of glass inclusion compositions within each sample, and the lack of crystallization textures, support these assumptions.

Secondly, all quartz crystals containing glass inclusions must be of primary, volcanic origin (i.e., no detrital quartz crystals). Careful hand-picking of pristine, bipyramidal quartz phenocrysts preceded microprobe analysis whenever possible, however, not all bentonites contained euhedral quartz crystals. The relatively uniform compositions of most glass inclusions indicates that detrital contamination is probably not significant in the bentonites studied.

Finally, based on the low solubility of $Al(OH)_3$ at pH values between 6 and 8, this model assumes a constant mass of alumina (Al_2O_3) during chemical weathering, even though its concentration appears to have changed (Faure 1991). Assuming that the bulk bentonite compositions approximate the compositions of the parent magmas, the weight percent Al_2O_3 in the glass inclusions is equivalent to the weight percent Al_2O_3 in the bulk bentonites, based on volatile-free analyses. The low volume percentage of crystals in all Kanguk bentonites suggests that most of the original ash consisted of vitric material, therefore, the bulk compositions should represent the approximate melt compositions. This assumption may not be valid for trace elements (e.g., Zr) that occur in high concentrations within late-crystallizing, accessory phases

(e.g., zircon).

The constant Al_2O_3 assumption allows the calculation of a weight-loss factor, defined as the weight percent ratio of Al_2O_3 in the unaltered glass, to Al_2O_3 in the bentonite (the inverse of this ratio represents an "enrichment" factor). Provided that the volume of the original ash is equal to the volume of the resulting bentonite, multiplying the major element concentrations in the glass by this factor yields the weight lost during bentonitization. Huff and Turkmenoglu (1981) applied these calculations to Ordovician bentonites that plotted in the trachyandesitic field on a Zr/TiO_2 versus Nb/Y classification diagram (e.g., Fig. 5.1 of the present study). Based on tabulated analyses of trachyandesites, and assuming constant Al_2O_3, the results of these calculations indicate losses (between 1.39 and 6.43 g/100 g) of Fe_2O_{3t}, CaO, Na_2O, SiO_2, and TiO_2, and slight gains of MgO and K_2O.

However, these researchers disregarded the effects of changing volumes throughout their compositional modelling. Density comparisons between bentonite deposits and unaltered volcanic ash layers indicate the requirement for volume changes during the process of bentonite formation. Typical bentonite densities, measured using sonic velocities and gas pycnometry, range from 2.38-2.72 g/cm^3 (e.g., Brunton 1988; Bielders et al 1990). Volcanic glasses that commonly occur within ash deposits display a wide range of compositions and densities; typical densities for rhyolitic to trachytic glasses lie between 2.3 and 2.6 g/cm^3 (Carmichael 1989).

Gresens (1967) provides a model for calculating chemical fluxes during metasomatic processes, which accounts for volume changes during alteration. Application of this model to bentonite formation requires the compositions and densities of the original volcanic ash and resulting bentonitic clay. Based on this model, the following equations allow the calculation of element changes (in g/100 g) during bentonite formation, provided the absolute amount of Al_2O_3 remains unchanged:

$$\delta x = 100 \times \left[f_v \times x_b \times \left(\frac{\rho_b}{\rho_g} \right) - x_g \right] \qquad f_v = \frac{(x_{Al_2O_3})_g}{(x_{Al_2O_3})_b \times \left(\frac{\rho_b}{\rho_g} \right)} \qquad (5.1)$$

where, δx = element change between unaltered glass and bentonite,

x_g, x_b = array of weight fraction of elements in glass and bentonite, respectively,

ρ_g, ρ_b = density of glass and bentonite, respectively,

$(x_{Al2O3})_g$, $(x_{Al2O3})_b$ = weight fraction of Al_2O_3 in glass and bentonite, respectively, and

f_v = volume change factor.

This equation permits calculation of element fluxes during the formation of the Axel Heiberg bentonites, ultimately leading to the reconstruction of original bulk ash compositions. Figure 5.13 illustrates a typical calculation, using volatile-free, major element analyses of glass inclusions and the associated bulk bentonite. This model assumes a typical density for peralkaline rhyolites of 2.35 g/cm^3, based on density measurements of five aphyric glasses of differing degrees of peralkalinity (Wilding et al 1993). The bentonite density (2.46 g/cm^3) used in this model represents a typical value calculated from average sonic velocity measurements of bentonite particles suspended in water (Brunton 1988). Table D4 in Appendix D contains tabulated major element fluxes for six Kanguk bentonites, and the calculated volume change factors.

Figure 5.14 displays a graphical representation of these element fluxes for each sample, illustrating actual gains and losses of major elements, relative to constant Al_2O_3, during bentonite formation. The most prominent feature of these diagrams is the major loss of SiO_2 from all bentonites, ranging from 43 to 53 g/100 g. This SiO_2 loss reflects the high solubility of amorphous silica compared to crystalline forms (Faure 1991). Significant losses of Na_2O, K_2O, and FeO_t occur in all samples, except AX90-004, which shows a gain in FeO_t of 2.12 g/100g. Losses of these elements probably indicate the formation of soluble ions or complexes. Increases

Sample: AX90-003

Volatile-free microprobe and XRF data:

	Glass Inclusions g	xg := g/∑g xg	Bentonite b	xb := b/∑b xb
SiO_2	75.53	0.7554	63.47	0.6348
TiO_2	0.26	0.0026	0.62	0.0062
Al_2O_3	9.98	0.0998	21.72	0.2172
FeO_t	5.64	0.0564	6.10	0.061
MnO	0.11	0.0011	0.04	0.0004
MgO	0.04	0.0004	1.77	0.0177
CaO	0.23	0.0023	1.05	0.0105
Na_2O	3.58	0.0358	2.88	0.0288
K_2O	4.49	0.0449	2.18	0.0218
P_2O_5	0.13	0.0013	0.16	0.0016

$\sum g = 99.99$ $\sum b = 99.99$

$\rho g := 2.35$ $\rho b := 2.46$

Equations:

$$fv := \frac{xg_2}{xb_2 \cdot \left(\frac{\rho b}{\rho g}\right)} \qquad fv = 0.44 \qquad \delta x := 100 \cdot \left[fv \cdot xb \cdot \left(\frac{\rho b}{\rho g}\right) - xg \right]$$

Element changes (in g/100 g), relative to constant Al_2O_3:

−46.37	SiO_2
0.02	TiO_2
0.00	Al_2O_3
−2.84	FeO_t
−0.09	MnO
0.77	MgO
0.25	CaO
−2.26	Na_2O
−3.49	K_2O
−0.06	P_2O_5

Figure 5.13 Calculation of element changes (in g/100 g) for the formation of bentonite AX90-003. This calculation is based on the model of Gresens (1967), and yields element fluxes relative to constant Al_2O_3. All symbols defined in text; Table D4 in Appendix D contains fluxes for all Axel Heiberg samples. Note that the expressions for f_v and δx in this figure appear in Mathcad format (Mathsoft 1991), however, the equations are identical to Equation 5.1.

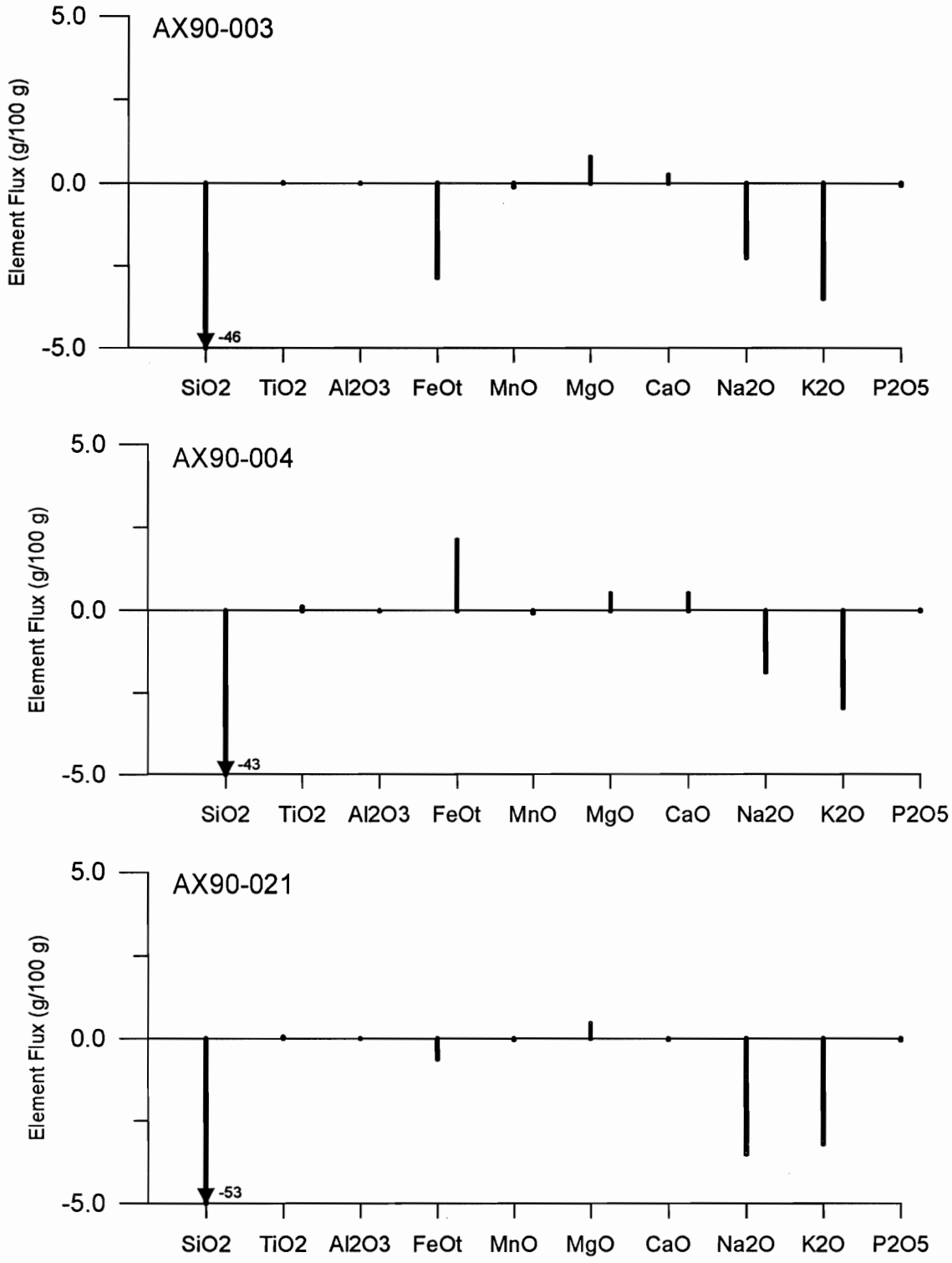

Figure 5.14 Plots of calculated major element changes (g/100 g) during bentonite formation, based on the calculations of Gresens (1967). Vertical bars indicate gains (+) or losses (-) of major element oxides, relative to constant Al_2O_3.

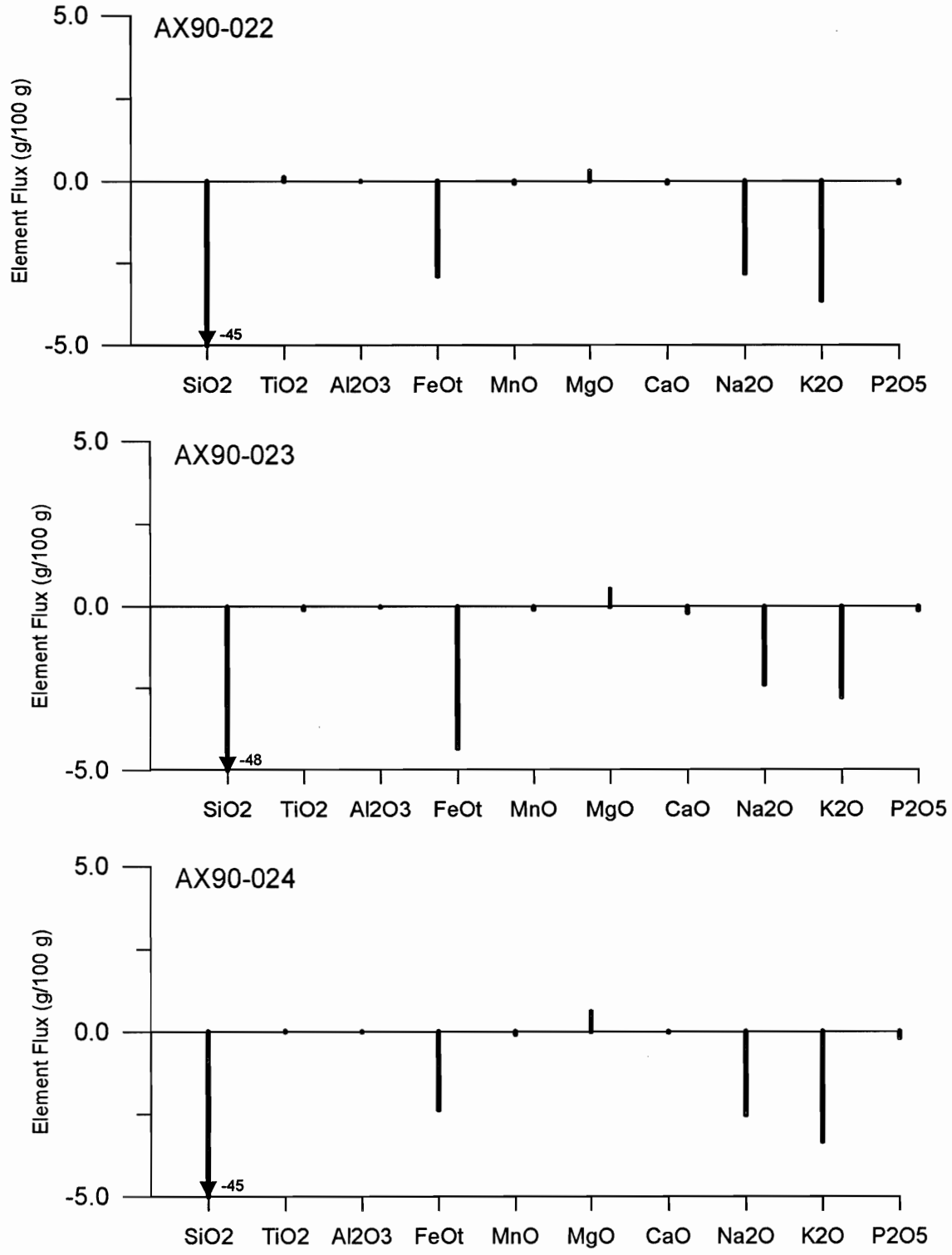

Figure 5.14 (continued)

in the MgO content of all bentonites coincide with the observations of Huff and Turkmenoglu (1981), however, CaO shows both increases and decreases. Enrichment of Mg, Ti, Ca, and Fe may result from structural incorporation in clay minerals, ion exchange, adsorption, or concentration in an insoluble residue (Zielinski 1982).

The calculated volume change factors, when multiplied by immobile element concentrations (volatile-free) in the bulk bentonites, yield the absolute amounts of these elements in the original volcanic ashes. Note that these calculations can only provide parent magma concentrations for those elements that remained immobile during bentonitization. In the following sections, the concentrations of Zr, Y, Nb, Ga, and the REE represent bulk bentonite geochemical data recalculated using the assumptions outlined above, unless otherwise stated in the text or figure captions.

5.5.1 Corrected trace elements

Corrected Zr, Y, and Ga concentrations in the bulk bentonites confirm the classification and compositional trends of the Axel Heiberg samples. Comparison of uncorrected and corrected Ga XRF data provides justification for the modelling of element mobility during bentonite formation. Ga is an incompatible, immobile element that increases in concentration with the progressive differentiation of alkaline rocks (Winchester and Floyd 1977). Uncorrected, volatile-free Ga concentrations in the bulk bentonites range from 63-92 ppm, compared with a range of 29-40 ppm for the corrected data. Plotted against the ratio Zr/TiO_2 (unchanged by alteration), the corrected Ga data all lie within the pantellerite field, with the exception of one sample (AX90-003), which lies in the phonolite/trachyte field (Fig. 5.15). In contrast, the uncorrected data plot far outside the limits of this classification diagram and, therefore, do not represent natural volcanic rock compositions. This observation attests to Ga enrichment in the bulk bentonites, relative to its concentration in the original volcanic ashes.

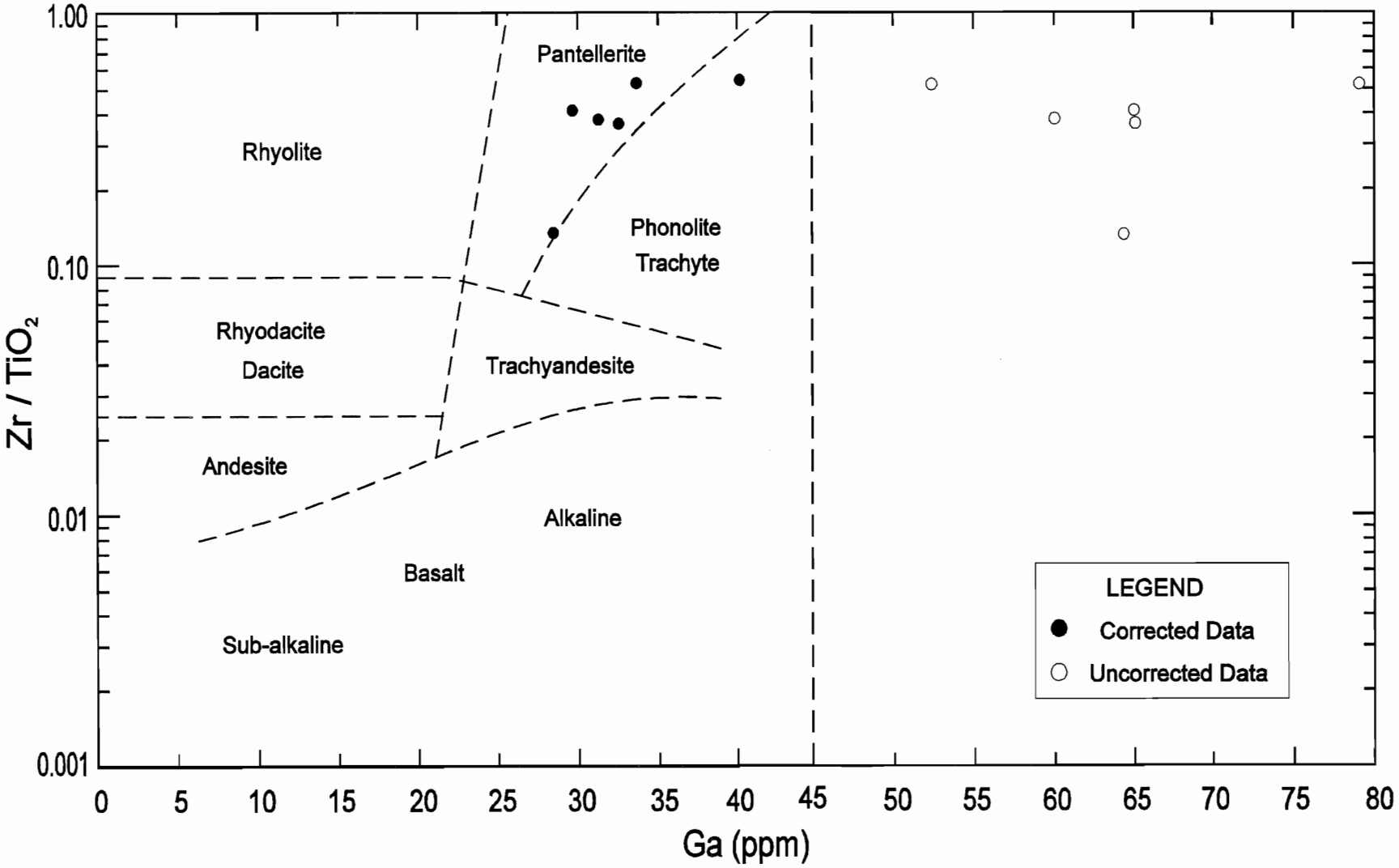

Figure 5.15 Zr/TiO_2-Ga discrimination diagram showing tentatively delimited fields for common volcanic rocks. The Kanguk Peninsula and Kanguk River bentonites show strongly differentiated compositions (corrected), with Ga enrichments typical of peralkaline suites. Note that the uncorrected bulk bentonite compositions plot far outside the limits of this classification diagram (after Winchester and Floyd 1977).

The Zr/TiO_2-Nb/Y (Fig. 5.1) and Zr/TiO_2-Ga (Fig. 5.15) plots yield different rock-type classifications for three of the Kanguk Formation bentonites. Sample AX90-003 plots in the comendite-pantellerite field of the Zr/TiO_2-Nb/Y plot, and in the phonolite-trachyte field of the Zr/TiO_2-Ga diagram. This feature probably does not reflect magmatic influences (assuming similar incompatibility of Nb, Y, and Ga in the parent magma); rather, it may be the result of over-enrichment of Ga relative to Al_2O_3 during bentonite formation (40 ppm - anomalous value), or assimilation of Ga from crustal rocks prior to eruption. Bentonite AX90-021, which plots as a rhyolite on the Zr/TiO_2-Nb/Y diagram, also plots as the least differentiated sample on the Zr/TiO_2-Ga plot, with an absolute Ga content of 29 ppm. This difference in classification could also result from a slightly high f_v value. Finally, bentonite AX90-024, classified as a trachyte on the Zr/TiO_2-Nb/Y plot, and a pantellerite on the Zr/TiO_2-Ga plot, is most likely a trachyte, because the f_v value for this sample comes from only four glass analyses.

Absolute concentrations of Zr and Y in the bulk bentonites confirm the mildly peralkaline nature of the original volcanic ashes. Zr contents range from 323-1861 ppm and, in general, show a linear increase with increasing melt peralkalinity (Fig. 5.16a). These high concentrations of Zr in the parent magma are typical of alkaline to mildly peralkaline rhyolites and trachytes (Section 4.5). Yttrium also demonstrates a linear increase with increasing melt peralkalinity (Fig 5.16b), and the absolute concentrations resemble those reported from Naivasha comendites (~100-250 ppm) by Macdonald et al (1987). The preservation of these magmatic differentiation trends within the bulk bentonites indicates that both Zr (in zircon and altered glass) and Y (in altered glass) remain immobile during the process of bentonite formation. Absolute concentrations of both Zr and Y fit well with inferred parent magma compositions, and reveal the applicability of Gresen's (1967) metasomatic model to the alteration of volcanic ash.

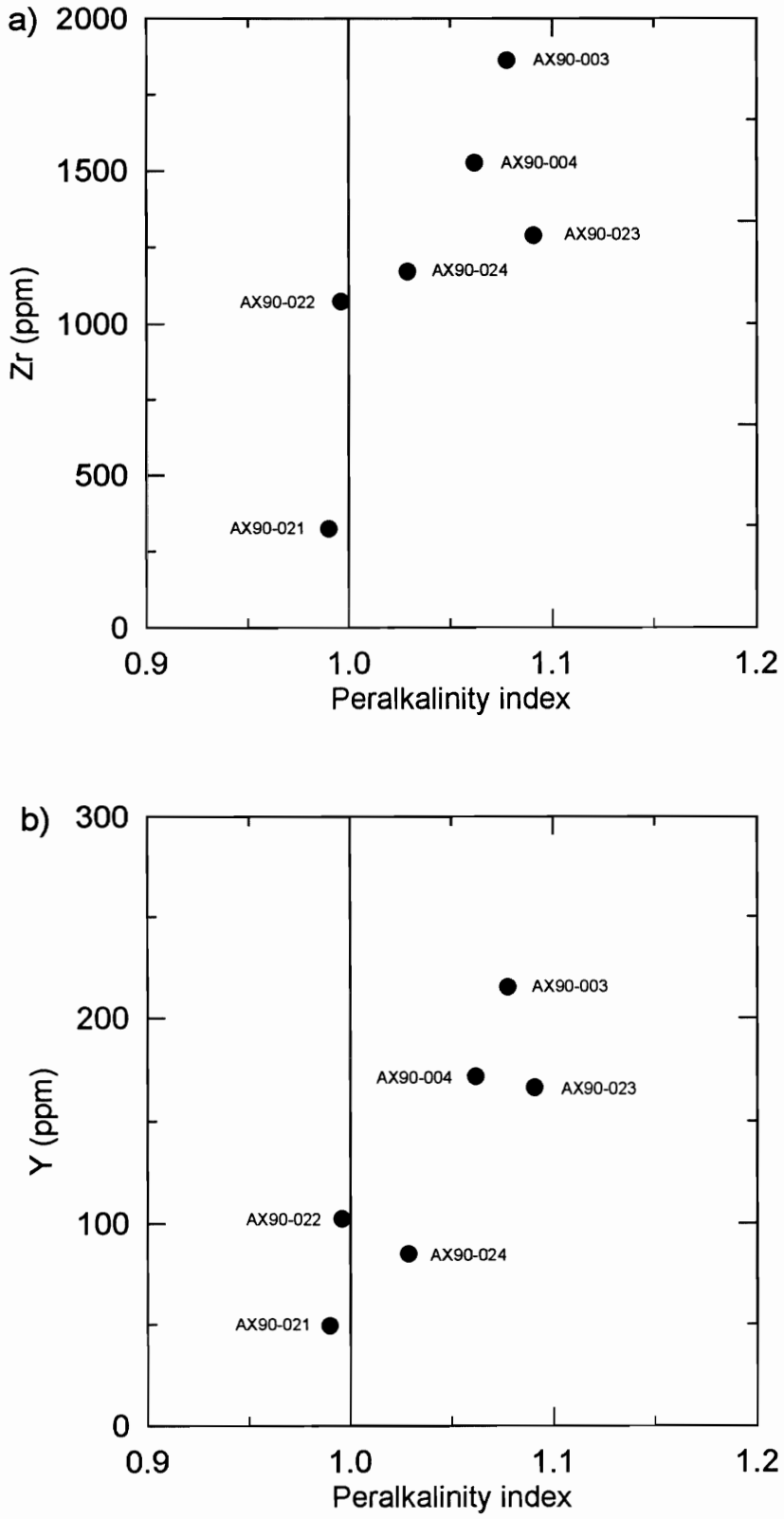

Figure 5.16 Plot of corrected bulk analyses of the Kanguk bentonites showing (a) increasing Zr and, (b) increasing Y with increasing peralkalinity. The vertical line on each diagram represents the boundary between alkaline and peralkaline compositions.

5.5.2 Corrected rare earth elements

The REE all have very similar geochemical properties, with valences of +3 (except for Eu and Ce, which may be +2 or +4, respectively), and large ionic radii that decrease from La to Lu. This "lanthanide contraction" causes the heavy REEs (HREE) to have larger crystal-liquid partition coefficients than the light REEs (LREE). Thus, in general, the LREE accumulate in late-stage felsic differentiates of magma, whereas the HREE remain in early-formed mafic products (McBirney 1984; Faure 1991).

Bentonites AX90-003, AX90-024, and EL92-001 all demonstrate enrichment in LREE, and show subparallel, chondrite-normalized REE patterns (Figs. 5.17, 5.18). This enrichment in LREE supports the premise that the Kanguk bentonites represent late-stage alkaline differentiates. Modest negative Eu anomalies in each sample suggest decreased Eu partitioning into alkali feldspar, consistent with mild peralkalinities. The REE concentrations also exceed those found in metaluminous rocks of similar silica content. As shown in Figures 15.7 and 15.8, sanidine phenocrysts associated with the bulk bentonites have modest positive Eu anomalies, and also display slight LREE enrichment.

Crystal-liquid partition coefficients vary with melt composition, temperature, and crystal composition. Table 5.3 contains crystal-melt partition coefficients for samples AX90-003 (peralkalinity index: 1.08) and AX90-024 (peralkalinity index: 1.03), calculated from the ratio of selected REEs and trace elements in the sanidine to those in the bulk bentonites (corrected). In general, most of the trivalent REEs have smaller partition coefficients in the more peralkaline sample (AX90-003). This decrease in partition coefficients may reflect decreasing anorthite content in the fractionating feldspar (Mahood and Stimac 1990); however, microprobe analyses of feldspar phenocrysts from both samples do not support this suggestion.

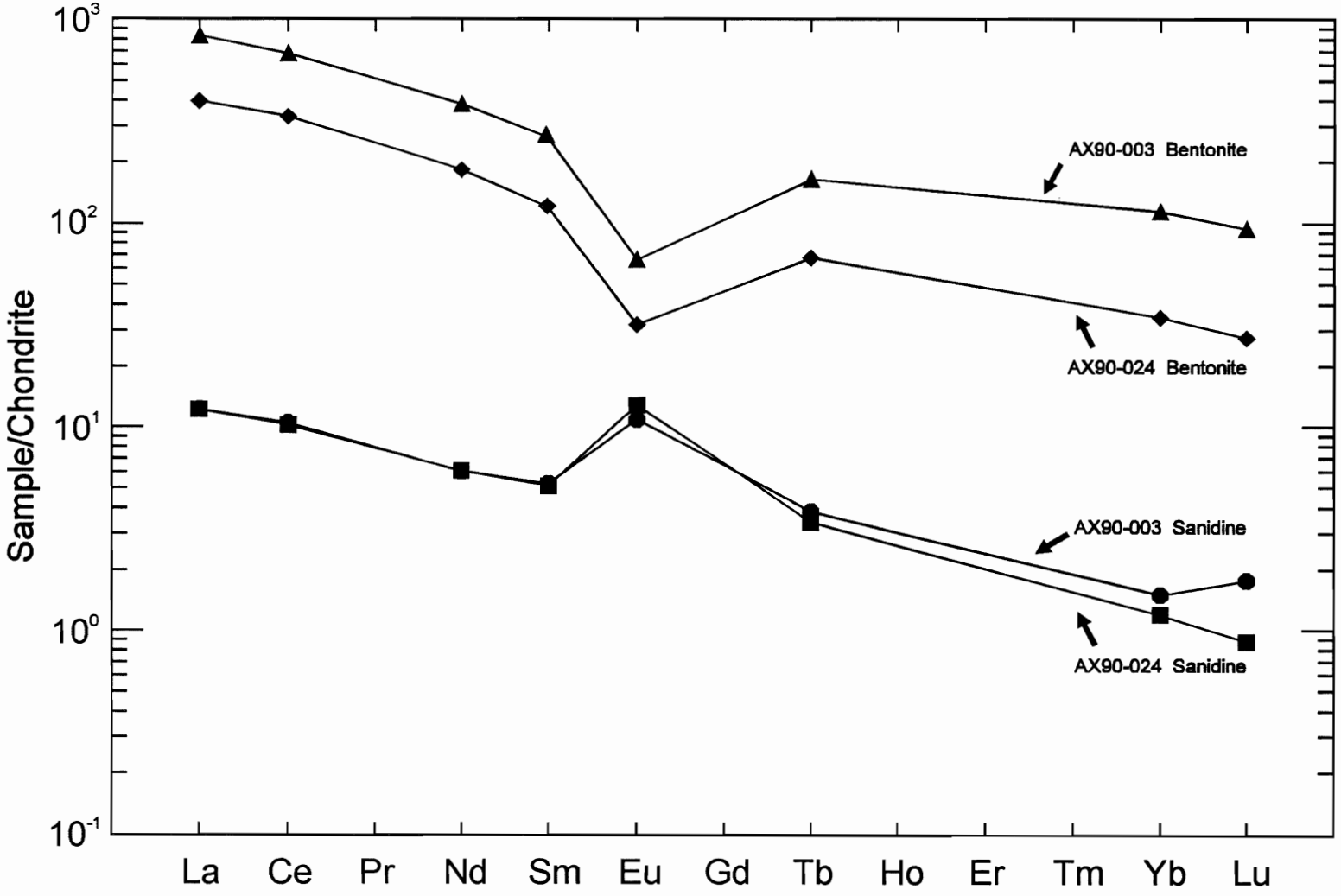

Figure 5.17 Chrondrite normalized REE patterns for two Kanguk bentonites (corrected data) and their associated sanidine phenocrysts. Note the enrichment in LREE, and modest Eu anomalies. Chondrite REE abundances from Haskin and Haskin (1968).

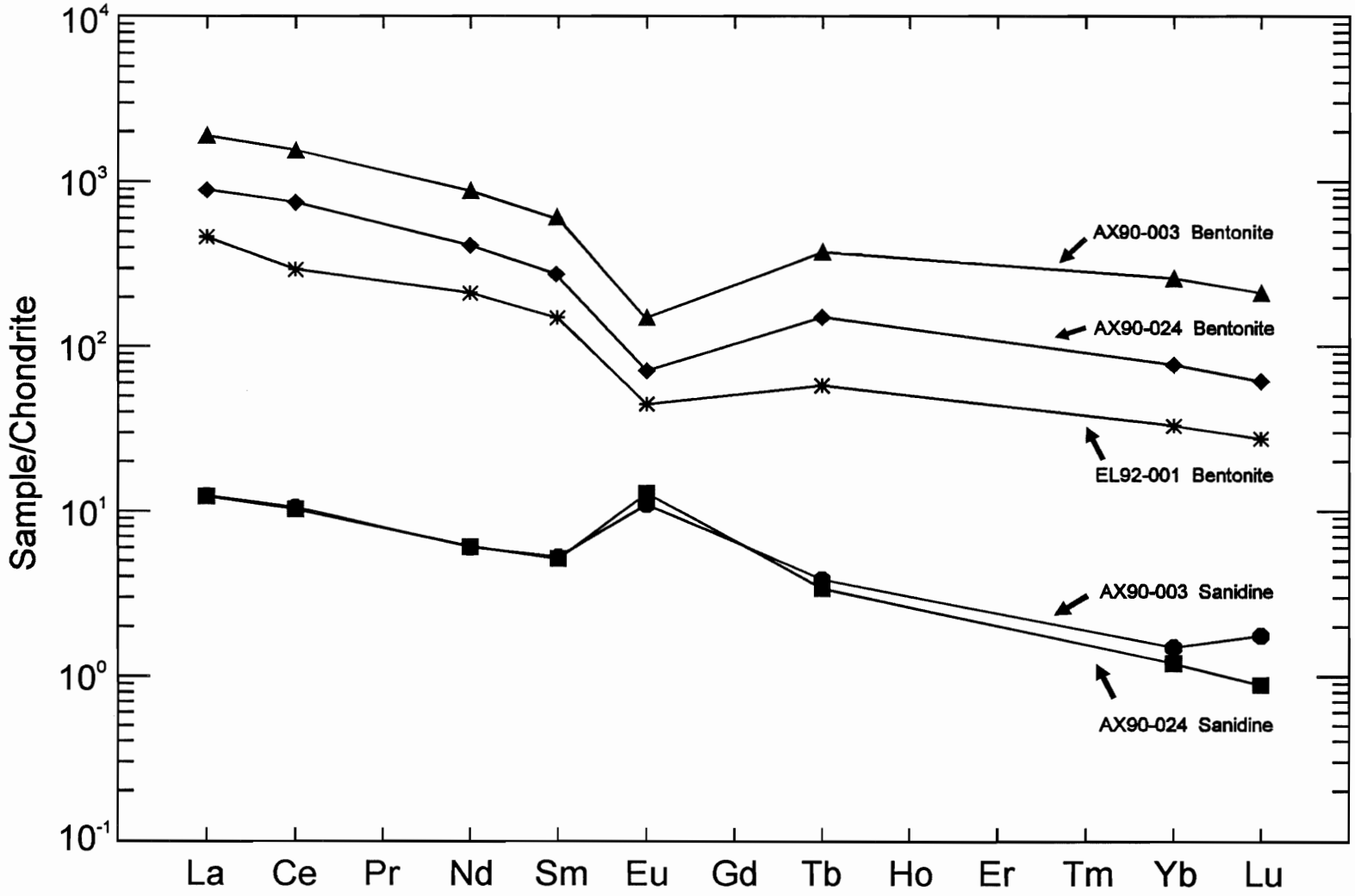

Figure 5.18 Chrondrite normalized REE patterns for three Kanguk bentonites (uncorrected data) and two sanidine separates. Note the enrichment in LREE, and modest Eu anomalies. Chondrite REE abundances from Haskin and Haskin (1968).

Element	Crystal-melt Partition Coefficient	
	AX90-003	AX90-024
Sc	0.062	0.070
Co	0.336	0.014
La	0.015	0.031
Ce	0.015	0.030
Nd	0.016	0.033
Sm	0.025	0.036
Eu	0.164	0.400
Tb	0.023	0.050
Yb	0.013	0.035
Lu	0.019	0.032
Hf	0.032	0.059
Ta	0.059	0.043
Th	0.031	0.045
U	0.028	0.090

Table 5.3 Crystal-melt partition coefficients for selected trace and rare earth elements between sanidine phenocrysts and bulk bentonites.

5.6 Summary

The geochemical characteristics of the Kanguk Formation bentonites support the petrographic classification presented in Chapter 4. Immobile element ratios within the bulk bentonites indicate several different parent magma compositions, including comendite-pantellerite, rhyolite, trachyte, and trachyandesite. Microprobe analyses of unaltered glass inclusions in quartz phenocrysts reveal the pre-eruptive volatile contents (1-4%) and major element compositions within the parent magmas. The relative proportions of Al_2O_3 and FeO_t in the melt inclusions indicate that the parent magmas include both comendites, and pantellerites. Calculated peralkalinity indices range from 0.99-1.09, revealing the mildly peralkaline nature of the parent magmas. Appropriate modelling of elemental fluxes during bentonite formation reveals distinct compositional trends within the parent melts, and confirms the classification of five samples as peralkaline rhyolites.

CHAPTER 6 : DISCUSSION

6.1 Introduction

The Kanguk Formation bentonites represent the diagenetically altered remains of highly differentiated, marginally peralkaline air-fall deposits, generated during Plinian volcanic eruptions. The compositions of these bentonites, combined with their widespread distribution and textural characteristics, provide many constraints on the nature of the parent volcanism. Incompatible trace element distributions in the Kanguk bentonites permit a tectonomagmatic classification of the volcanic sources, based on compositional affinities with fresh rocks of known tectonic setting. In addition, the dominantly peralkaline, silicic nature of these volcanic ashes suggests probable emplacement of the parent magmas in a narrow range of tectonic settings, where more than 90% of other peralkaline rhyolitic suites exist (Macdonald 1974b).

However, many factors complicate the exact location of the source volcanoes. All the bentonites studied probably represent distal air-fall deposits and, therefore, do not occur in close association with the original volcanic vents. Correlation of the Kanguk bentonites with similar pyroclastic deposits throughout the High Arctic depends on an accurate reconstruction of plate tectonic motions within the Arctic region since the Late Cretaceous. The Kanguk bentonites may represent late-stage magmatic activity within the Sverdrup Basin, or they may be the products of extra-basinal volcanism.

6.2 Nature of Parent Volcanism

Peralkaline silicic rocks occur in a wide range of tectonic settings. More than 90% of peralkaline rhyolites occur in continental rift environments related to continental extension. However, high-silica peralkaline rocks may also form on oceanic islands, during the later stages of

orogenic cycles as isolated occurrences in active mobile belts, and in areas of extensional tectonics near continental plate margins. Most peralkaline suites are typically bimodal, consisting of transitional basalts or alkali olivine basalts, in association with rhyolites, trachytes, and peralkaline rhyolites (Macdonald 1974b).

The general geochemical features of the Kanguk Formation bentonites closely resemble the compositions of marginally peralkaline rhyolites, trachytes, and comendites from the Quaternary to Recent volcanic complexes of the Kenya Rift Valley (Macdonald et al 1987). Within this volcanic province, distinct lava flows and pumice fall deposits (trachytes-pantellerites) erupted from different volcanic centres; however, adjacent volcanoes are sufficiently close for intercalation of the erupted products. Chemical variation diagrams show no continuous evolution of melts below the rift, and distinctive products from each eruptive centre (Baily and Macdonald 1987). The geochemical similarities between the Kanguk bentonites and the Kenyan volcanics (e.g., concentrations of majors, incompatible traces, REEs, differentiation trends) suggest that the tectonic setting of the Kenya Rift Valley may be analogous to the Late Cretaceous tectonics of the Kanguk bentonite source area. Therefore, the original volcanic source region for the Kanguk ashes may include closely-spaced bimodal suites of alkaline basalts, rhyolites, trachytes, and peralkaline rhyolites.

6.2.1 Tectonomagmatic discrimination

The corrected concentrations of certain incompatible elements within the Kanguk bentonites provide constraints on the tectonic setting of the parent volcanism. The tectonomagmatic discrimination diagrams of Pearce et al (1984) use the compositions of unaltered granitoid rocks, of known tectonic setting, to determine the character of ancient, and possibly altered granitoid rocks. The positions of the field boundaries which separate rocks from particular tectonic settings are strictly empirical; however, some of the discriminant boundaries have petrogenetic

significance. These diagrams can also discriminate between high-silica volcanic ashes (and their bentonitized equivalents) from various tectonic settings, following the correction of bulk compositions for the effects of element mobility during alteration. Appropriate modelling of chemical fluxes is essential in applying these discriminant diagrams to altered rocks, because all of the plots require absolute elemental concentrations. Several studies (e.g., Thomas et al 1990; Huff et al 1992) use uncorrected bentonite compositions to construct these discriminant diagrams, possibly leading to incorrect conclusions regarding the tectonomagmatic character of the source volcanoes.

Figure 6.1 shows a tectonomagmatic discrimination diagram using the incompatible, immobile elements Nb and Y to discriminate between ocean ridge granites (ORG), within-plate granites (WPG), volcanic-arc granites (VAG), and syn-collisional granites (syn-COLG). Corrected trace element compositions for the Kanguk bentonites plot inside the WPG field, indicating an intracontinental tectonic setting for the parent magmas. This classification coincides with the trace element compositions (e.g., relative REE and HFSE enrichment), and the peralkaline nature of the bentonites, both of which suggest a within-plate environment for the volcanic source.

Figure 6.2 displays a second tectonomagmatic discriminant diagram, which distinguishes between rocks from the above tectonic settings using Rb plotted against the sum of Y and Nb. Rubidium is an incompatible element that belongs to a group of large cations with low valences, known as the large-ion lithophile (LIL) elements. Most common igneous minerals cannot accommodate these large cations in their crystal structure; therefore, the LIL elements become enriched in the first products of partial melting, or in the residual liquid of crystal fractionation (McBirney 1984). However, the Rb contents of most bentonites probably do not represent the original magmatic concentrations, because Rb is extremely mobile (lost from the bentonites) during alteration processes (Faure 1991). As shown in Figure 6.2, most of the Kanguk bentonites plot within the ORG field of this discriminant diagram. Most ORG occur as small, localized bodies in oceanic crust, with no extrusive equivalents; therefore, this classification most likely

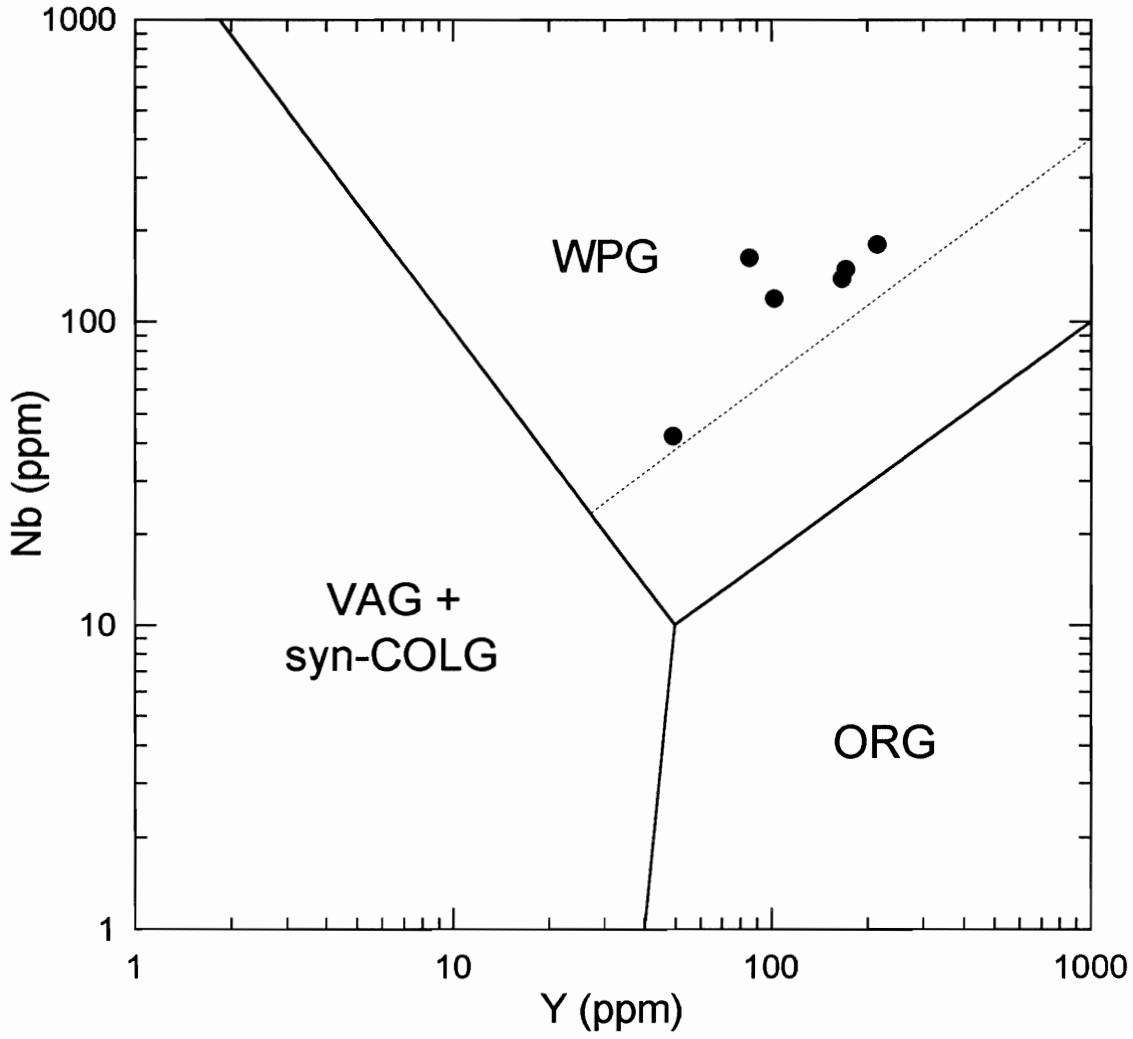

Figure 6.1 Nb-Y discriminant diagram for ocean ridge granites (ORG), within-plate granites (WPG), volcanic-arc granites (VAG), and syn-collisional granites (syn-COLG). The dashed line represents the upper compositional boundary for ORG from anomalous ridge segments. Note that all of the Kanguk bentonites plot inside the WPG field, indicating an intraplate tectonic setting for the parent volcanism (after Pearce et al 1984).

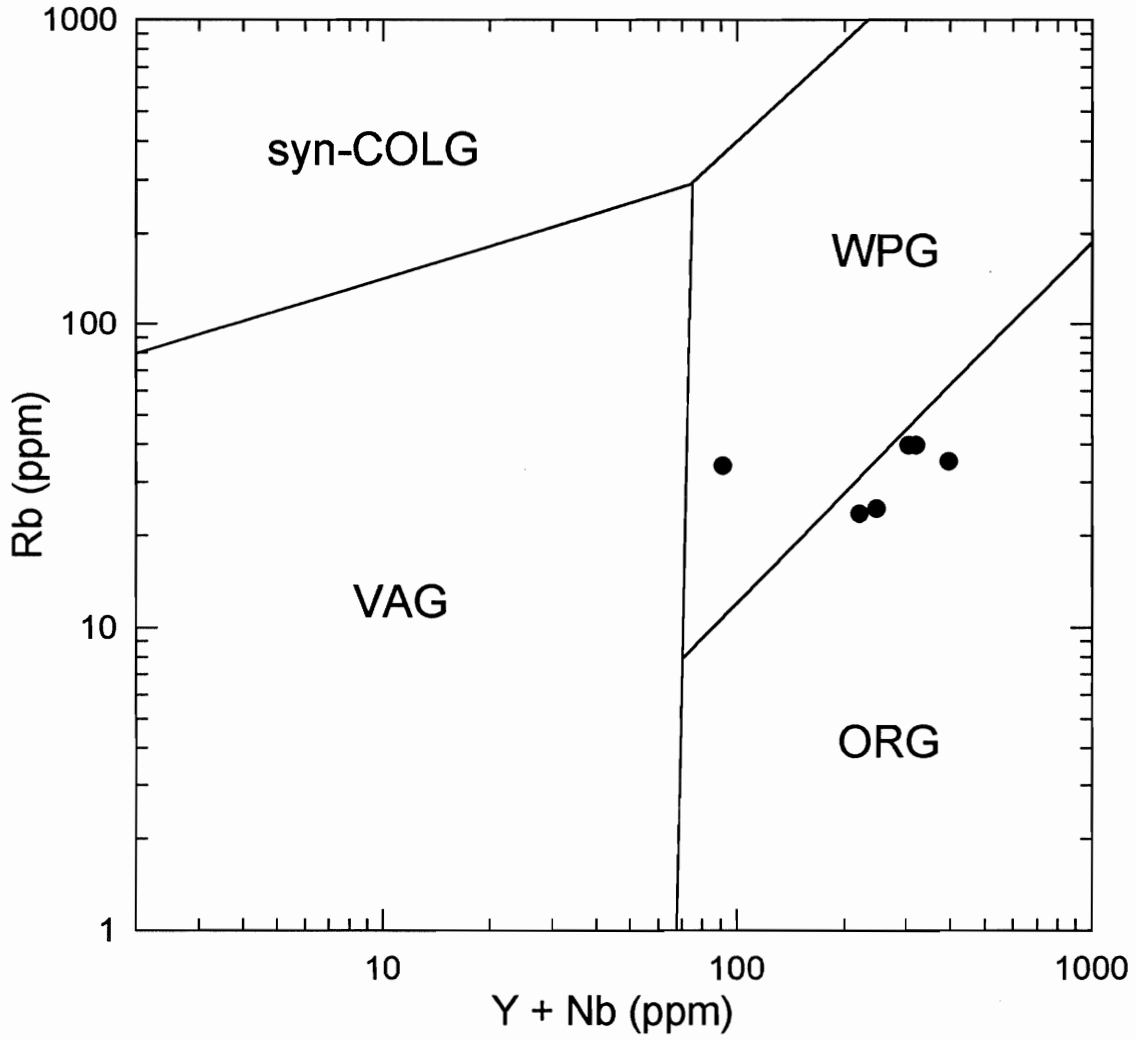

Figure 6.2 Rb-(Y+Nb) discriminant diagram for ocean ridge granites (ORG), within-plate granites (WPG), volcanic-arc granites (VAG), and syn-collisional granites (syn-COLG). The apparent compositional affinity of the Kanguk bentonites with ORG most likely reflects mobility of Rb during bentonite formation, and is not a reliable tectonomagmatic classification. The WPG tectonic setting indicated in Figure 6.1 is probably more accurate, because both Y and Nb remain relatively immobile during alteration processes (after Pearce et al 1984).

reflects mobility of Rb during bentonite formation (Pearce et al 1984). Loss of Rb during alteration of the original volcanic ashes has probably resulted in decreased Rb concentrations within the Kanguk bentonites, thereby lowering the plotted positions of the Kanguk samples from their true positions in the WPG field.

6.3 Late Cretaceous Arctic Volcanism and Provenance of Original Ashes

The highly explosive, mildly peralkaline volcanism represented by the Kanguk bentonites contrasts strongly with earlier Cretaceous, subalkaline to transitional basaltic magmatism within the Sverdrup Basin (Muecke 1990). Late Cretaceous to Early Tertiary volcanic rocks include the Kanguk Formation bentonites (Late Cenomanian to Middle Campanian; GK Muecke, personal communication 1994), and the Hansen Point volcanics on northwestern Ellesmere Island (Late Campanian to Danian). The stratigraphically lowest basalt flow within the Hansen Point volcanics near Phillips Inlet may overlie sediments of the upper Kanguk Formation on northwestern Ellesmere Island (Merrett and Muecke 1989), suggesting possible overlap in the ages of these stratigraphic units.

The Hansen Point volcanics occur at volcanic centres near Emma Fiord, Phillips Inlet, and Yelverton Inlet (Fig. 6.3). These volcanics erupted as a series of bimodal suites dominated by strongly alkaline basalts, rhyolites, trachytes, and peralkaline rhyolites (Muecke 1992). Thick, interbedded sequences of pyroclastics and volcanic ash layers indicate that extensive explosive volcanism accompanied the formation of these volcanic successions. Strongly contrasting magma compositions occur over short distances, and few intermediate compositions are present (Merrett and Muecke 1989). The composition, volcanic style, and spatial association of the bimodal Hansen Point volcanics closely resemble the Tertiary-Recent peralkaline silicic rocks of the Kenya Rift Valley (Bailey and Macdonald 1987). The peralkaline compositions of some of the Hansen Point volcanics, combined with the explosive nature of the volcanic activity, suggest that the

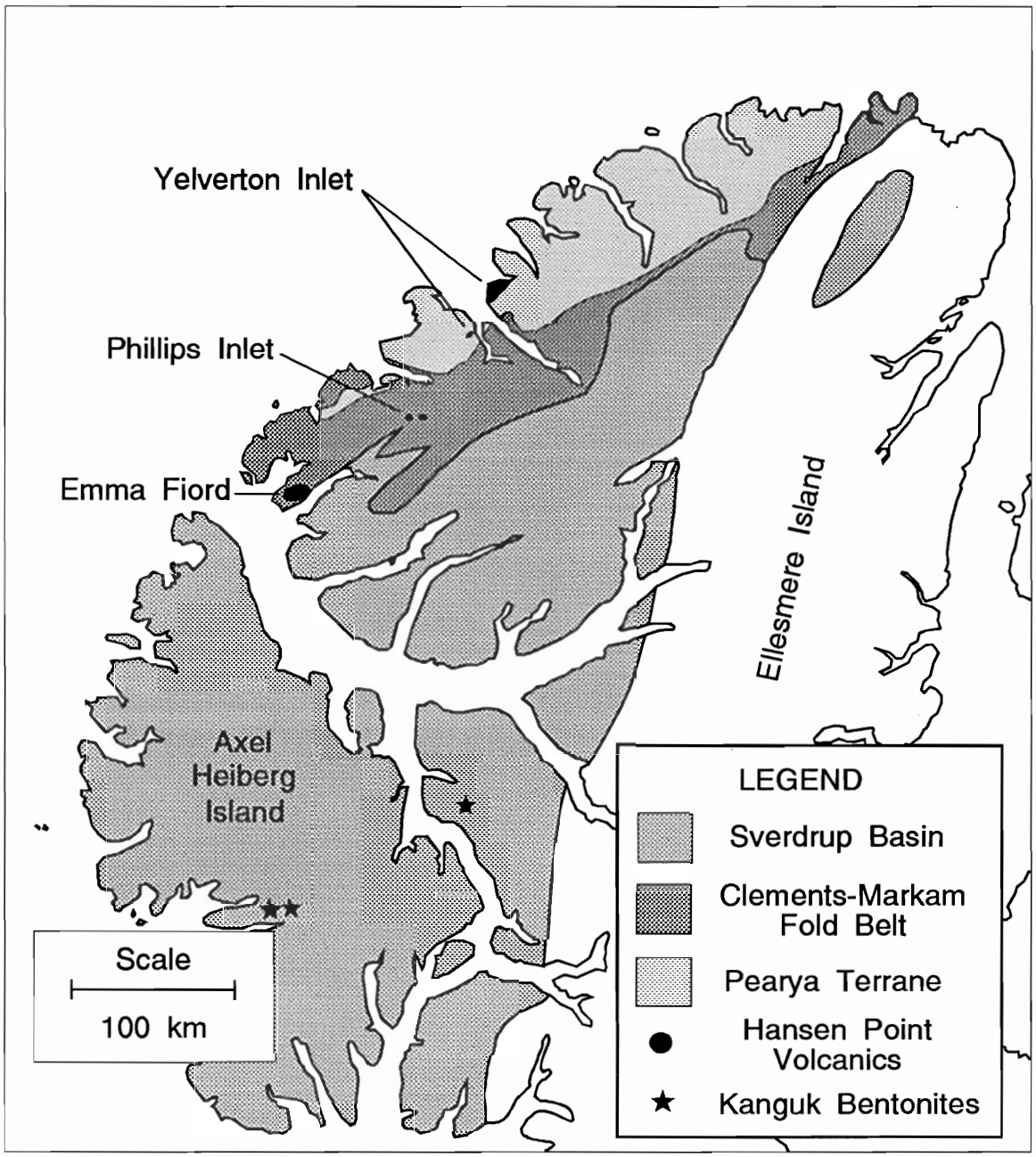

Figure 6.3 Map of Axel Heiberg and Ellesmere Islands showing the distribution of the Hansen Point volcanics, and their generalized geological setting. Note the positions of the exposed Kanguk Formation bentonites, relative to the Cretaceous volcanic centres on northwestern Ellesmere.

Kanguk bentonites may represent early stages of explosive volcanism during the evolution of this bimodal igneous province. The source volcanoes of the Hansen Point volcanics existed along the northeastern Sverdrup Rim, a large horst that separates the Sverdrup Basin from the Canada Basin to the northwest (Fig. 2.1). Plinian volcanic eruptions of mildly peralkaline, silicic magmas from this intracontinental tectonic setting may have generated the source ashes of the Kanguk Formation bentonites.

Extrusion of peralkaline volcanic rocks also occurred on the north coast of Greenland (Fig. 6.4) at, or just before, the Cretaceous-Tertiary boundary (approximately 65 Ma). The Kap Washington Group volcanics consist of a strongly bimodal suite of predominately transitional-alkaline basaltic lavas, rhyolites, comendites, and comenditic ash-flow tuffs (Brown et al 1987). Pyroclastic rocks and extensive ash-flow tuffs attest to the explosivity of the volcanic eruptions, however, no evidence of original volcanic form, vent, or caldera, remains. The comendites have peralkalinity indices ranging from 0.91 to 1.17, and demonstrate enrichments of LREE and HFSE typical of continental peralkaline suites. A swarm of northwest-trending alkali-dolerite dykes, intruded just before the extrusive activity, suggests a predominately extensional tectonic environment (Brown et al 1987).

Brown et al (1987) relate the extrusion of the Kap Washington volcanics to active sea-floor spreading within the Makarov Basin (Fig. 6.4), based on the peralkaline nature of the associated volcanism, and the parallel orientation of the North Greenland dyke swarm to the basin axis. Spreading within the Makarov Basin began during the Late Cretaceous (anomaly 34, about 80 Ma), and resulted in the development of an extensional graben-like trough near the Greenland continental shelf (Taylor et al 1981). The initial phases of rifting within the Makarov Basin (i.e., prior to the onset of sea-floor spreading) may also have generated tensional stresses within the continental crust underlying northern Ellesmere Island, resulting in the development of mildly peralkaline volcanic activity. Further isotopic studies of the Kanguk bentonites and the Hansen Point volcanics, combined with geophysical studies concerning the deep crustal structure of the

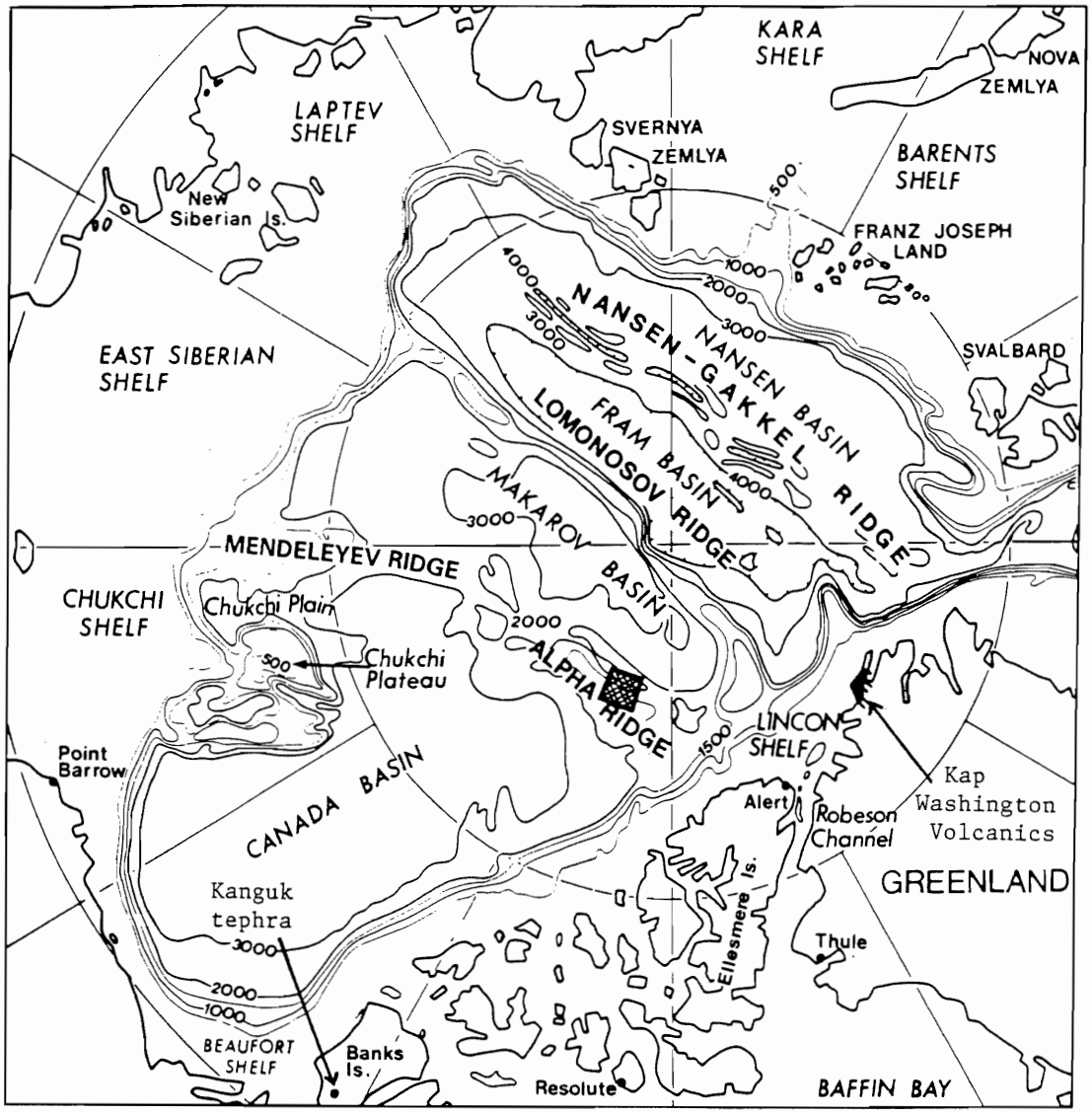

Figure 6.4 Major bathymetric features of the present-day Arctic Ocean. The cross-hatched area shows the location of the 1985 CESAR (Canadian Expedition to Study the Alpha Ridge) bathymetry survey. Note the location of the Kap Washington Volcanics, and the tephra layers within the Kanguk Formation on Banks Island (after Van Wagoner and Robinson 1985).

present-day polar continental shelf, may provide additional evidence for this tectonomagmatic interpretation.

6.4 Geochemical Correlation and Possible Lateral Equivalents

Future correlation of the Kanguk bentonites with similar pyroclastic deposits throughout the High Arctic may reveal the areal extent of ash deposition, and suggest additional volcanic source regions. Microprobe analyses of unaltered glass inclusions preserved within quartz phenocrysts permit the geochemical correlation of individual bentonites derived from compositionally distinct parent magmas (Delano et al 1994). Provided that melt inclusions exist within bentonites from each different location, this technique can distinguish between ashes generated during, for example, within-plate, and volcanic-arc magmatism. Appropriate modelling of element mobilities during bentonite formation (e.g., using the methods described in Section 5.5) permit the recalculation of original ash compositions, which may contain characteristic "geochemical fingerprints" for use in bentonite correlation. These techniques may resolve individual volcanic events without using complex multivariate statistical methods (e.g., Huff and Kolata 1989).

Two thin tephra beds occur within the Kanguk Formation at Duck Hawk Bluffs, southwestern Banks Island (Figs. 6.4, 2.1). One of these ash layers lies within a glacially-transported Pleistocene till, the other is intercalated with the Kanguk mudstones several meters below the contact with the overlying Tertiary and glacial Pleistocene deposits (Kemp and Westgate 1991). Each of these tephra beds is vitric and crystal-poor, in contrast to the Kanguk bentonites examined in the present study, which contain no preserved matrix glass. Isothermal plateau (ITP) fission-track dating of hydrated glass shards from these ash layers, combined with K-Ar radiometric dating, yields ages of 65.7 +/- 1.68 Ma for the glacially transported bed, and 67.8 +/- 3.1 Ma for the *in situ* tephra bed. These dates indicate that explosive volcanism within the High Arctic may have extended into the Tertiary. According to Kemp and Westgate (1991), both

tephra beds "are potassic, high-silica rhyolites but are chemically distinct, representing separate volcanic eruptions." These tephra compositions are similar to the compositions of the Kanguk bentonites analyzed in the present study. However, the ages of the Banks Island deposits are too young to be laterally equivalent to the Axel Heiberg and Ellesmere bentonites. The similarities in compositions may indicate that the volcanic source of the Kanguk ashes remained active into the Tertiary; however, changes in the sedimentary regime within the eastern Sverdrup Basin region (generating the sandstone-dominated Eureka Sound Group) prevented the preservation of these ash layers. If explosive volcanism on northwestern Ellesmere Island generated the Kanguk tephra beds on Bank's Island, the low abundance of free crystals may reflect density sorting during atmospheric transport (e.g., Sigurdsson and Carey 1989).

Numerous bentonites and welded tuff beds also occur within the Aptian to Maastrichtian (Paleocene?), organic rich, Hue Shale Member of the Seebee Formation in northern-central Alaska (Molenaar et al 1986). The Hue Shale consists mainly of fissile black shale, and contains abundant *Inoceramus* fossils. Bentonite beds comprise more than 30% of the formation at some localities, with thicknesses ranging from 6 mm to 150 cm. Phenocrysts within the welded tuff consist of silt or smaller size particles. Radiometric K-Ar and $^{40}Ar/^{39}Ar$ ages measured on biotite phenocrysts range from 91.5 +/- 0.9 Ma to 93.6 +/- 1.2 Ma for bentonites in the Seebee Formation (Lanphere and Tailleur 1983). These radiometric ages are similar to the maximum $^{40}Ar/^{39}Ar$ dates obtained from sanidine phenocrysts in the Kanguk bentonites (approximately 91.5 Ma; GK Muecke, personal communication 1994). In addition, the very fine grain-size in the welded tuff suggests that these ash layers may represent distal air-fall deposits. Apparently, no detailed geochemical studies of the Seebee bentonites exist; however, the presence of biotite phenocrysts probably indicates a different volcanic source for the Seebee and Kanguk bentonites. The Seebee bentonites may represent deposits from explosive, calc-alkaline volcanism along the western coast of Alaska, associated with Late Cretaceous subduction of the Farallon and Kula

Plates. Geochemical analyses of the Seebee bentonites may confirm a VAG tectonic setting for the parent volcanism.

Late Cretaceous-Tertiary volcanic ash layers also occur within laminated, deep-ocean sediments along the north edge of the Alpha Ridge graben (Fig. 6.3). Mudie and Blasco (1985) reported volcanic ash deposits within CESAR core 6, recovered from an erosional surface at the top of a fault block on the northern crest of Alpha Ridge (latitude: 85°49.8' N, longitude: 109°09.2' W). Preserved silicoflagellates, diatoms, and palynomorphs indicate a Late Cretaceous to Paleogene age for the surrounding sediments. Much of the sediment consists of fine silt- to clay-sized feldspar, quartz, hornblende, pyroxenes, opaque minerals, garnet, and brown volcanic glass. The presence of preserved glass shards, in addition to hornblende and pyroxene, may reflect different diagenetic conditions from those that formed the Kanguk bentonites. If these volcanic ashes erupted along northwestern Ellesmere Island, the garnet grains (angular?) within the CESAR core may represent xenocrysts from the Precambrian crystalline basement underlying the Sverdrup Rim (Pearya terrane (Fig. 6.3); Trettin 1987). Further geochemical work (e.g., analyses of glass shards, feldspar compositions, glass inclusions(?)) may reveal compositional affinities with the Kanguk bentonites.

Finally, Cretaceous-Tertiary sediments recovered from the east face of Northwind Ridge, Chukchi Borderland (Fig. 6.3), also contain dacitic or rhyolitic air-fall volcanic ash (Arctic Summer Scientific Party 1992). These ashes occur within piston cores obtained from a ridge-capping, seismic stratigraphic unit near 74°48' N. Detailed geochemical analyses of these ashes do not yet exist to date; however, the presence of these ashes indicates the wide areal extent of Late Cretaceous-Tertiary explosive volcanism throughout the Arctic region.

6.5 Summary

The peralkaline nature of the Kanguk Formation bentonites suggests that the parent volcanism occurred within a continental extensional environment. Trace element distributions, in conjunction with discriminant diagrams, indicate a within-plate tectonic setting for the parent magmas. The geochemical characteristics of the bentonites closely resemble the compositions of Quaternary to Recent, marginally peralkaline volcanics from the Kenya Rift Valley. The Hansen Point volcanics on northwestern Ellesmere Island consist of bimodal volcanic suites similar to the Kenyan rocks, suggesting a possible volcanic source for the Kanguk bentonites. Late Cretaceous explosive volcanism may relate to the initial phases of rifting in the Makarov Basin. The Kanguk bentonites may represent deposits from the same volcanic source as that which generated volcanic ashes on Banks Island, the Alpha Ridge, the Chukchi Borderland, and in Alaska. However, the absence of detailed compositional data for pyroclastic deposits from each of these locations precludes geochemical correlation with the Kanguk bentonites.

CHAPTER 7 : CONCLUSIONS

Late Cretaceous-Tertiary explosive volcanism deposited blankets of volcanic ash over much of the Arctic region. The Kanguk Formation on Axel Heiberg and Ellesmere Islands contains subaqueous fallout deposits, intercalated with organic-rich mudstones, shales, and minor sandstones. The Kanguk bentonites represent the diagenetically altered remains of vitric-crystal ashes deposited in shallow marine sedimentary basins from approximately the Late Cenomanian to the Middle Campanian (GK Muecke, personal communication 1994).

Free crystal grain-size distributions are similar for bentonites collected from each section; however, distributions are very different between the Axel Heiberg and Ellesmere sections. Maximum grain-size measurements suggest that the volcanic source of the original ashes was closer to Kanguk Peninsula than to Fosheim Peninsula. The widespread ash dispersal, and fine crystal-sizes in most bentonites, indicate high-energy eruptions typical of Plinian systems. However, complete replacement of vitric fragments within the Kanguk bentonites precludes estimates of size relationships between free crystals and vitric pyroclasts; therefore, grain size parameters provide few constraints on eruption dynamics and the position of the volcanic vents.

The diagenetically stable, primary mineral assemblage in the Kanguk bentonites includes quartz, sanidine, ilmenite, zircon, apatite and acmite. The presence of quartz and acmite indicates that the parent magmas have peralkaline rhyolitic compositions. However, the ubiquitous nature of ilmenite in all Kanguk bentonites, coupled with the coexistence of primary zircon phenocrysts in most samples, suggests that the parent magmas were only mildly peralkaline. The absence of primary plagioclase in all samples studied may indicate that fractionation of relatively anorthitic plagioclase was a controlling factor in generating peralkaline conditions. The restricted range of sanidine compositions (Or_{41-52}) within all bentonites coincides with reported feldspar compositions from other peralkaline suites (e.g., Macdonald et al 1987).

Classification of the bulk bentonites using the incompatible, immobile element ratios Zr/TiO_2 and Nb/Y indicates several different parent magma compositions, including comendite-pantellerite, rhyolite, trachyte, and trachyandesite. These results confirm the mildly peralkaline nature of the parent melts, and suggest that the Kanguk bentonites may represent ashes from several parent magmas within the same volcanic province, each in a different stage of evolution.

Microprobe analyses of glass inclusions preserved within quartz phenocrysts reveal the pre-eruptive volatile contents (1-4%) and major element compositions of the Kanguk bentonite parent magmas. The six bentonites from western Axel Heiberg Island are alkaline to mildly peralkaline, with peralkalinity indices ranging from 0.99 to 1.09. The relative concentrations of Al_2O_3 versus FeO_t within the melt inclusions indicate that the peralkaline rhyolitic parent magmas include both comendites and pantellerites. Comparison of melt inclusion compositions with phenocrysts from the same bentonite reveal no distinct compositional trends, supporting the premise that the bentonites represent deposits from a series of discrete magma batches.

Appropriate modelling of element mobilitites during bentonite formation permits recalculation of the original ash compositions from bulk bentonite analyses. Classification using corrected compositions indicates pantelleritic parent magma compositions for the Kanguk bentonites. In addition, corrected Zr, Y, and REE concentrations reveal distinct compositional trends within the parent melts, and the absolute concentrations of these elements fit well with the inferred parent compositions. These observations indicate the applicability of Gresen's (1967) metasomatic model to the process of bentonite formation.

The peralkaline nature of the Kanguk bentonites, combined with corrected trace-element compositions (Nb, Y), suggest that the parent volcanism occurred within a continental extensional environment. The bimodal Hansen Point volcanics on northwestern Ellesmere Island may represent the volcanic source of the original Kanguk ashes. This Late Cretaceous explosive volcanism may relate to early rifting within the Makarov Basin, and may also have resulted in the deposition of ashes on Banks Island, the Alpha Ridge, the Chukchi Borderland, and in Alaska.

REFERENCES

American Geological Institute (1987) Glossary of geology. Bates RL, Jackson JA (eds) 3rd edition, McGraw-Hill

Anderson AT (1991) Hourglass inclusions: theory and application to the Bishop Rhyolitic Tuff. Amer Miner 76:530-547

Arctic Summer West Scientific Party (1992) Cruise to the Chukchi Borderland, Arctic Ocean. EOS 74:249-254

Baadsgaard H, Lerbekmo JF (1982) The dating of bentonite beds. In: Numerical dating in stratigraphy. Odin GS (ed) John Wiley & Sons, New York, pp 423-440

Bacon CR (1989) Crystallization of accessory phases in magmas by local saturation adjacent to phenocrysts. Geochim Cosmochim Acta 53:1055-1066

Bailey DK, Macdonald R (1987) Dry peralkaline felsic liquids and carbon dioxide flux through the Kenya rift zone. In: Magmatic processes: physicochemical principles. Mysen BO (ed). Geochem Soc Spec Pub 1:91-105

Baker DR, Watson EB (1988) Diffusion of major and trace elements in compositionally complex Cl- and F-bearing silicate melts. J Noncryst Solids 102:63-70

Balkwill HR (1978) Evolution of the Sverdrup Basin, Arctic Canada. Amer Assoc Petrol Geol Bull 62:1004-1028

Bielders CL, De Backer LW, Delvaux B (1990) Particle density of volcanic soils as measured with a gas pycnometer. Soil Sci Soc Amer J 54:822-826

Brown PE, Parsons I, Becker SM (1987) Peralkaline volcanicity in the Arctic Basin - the Kap Washington Volcanics, petrology and paleotectonics. J Geol Soc Lond 144:707-715

Brunton GD (1988) Density and compressibility of Wyoming bentonite particles. Clays Clay Miner 36:94-95

Cameron BI (1989) Petrochemistry and origin of altered Permian basalts in the Sverdrup Basin, Arctic Canada. Unpublished MSc Thesis. Dalhousie University, Halifax, Nova Scotia

Carmichael ISE (1967) The iron-titanium oxides of salic volcanic rocks and their associated ferromagnesian silicates. Cont Miner Petrol 14:36-64

Carmichael RS (1989) Practical handbook of physical properties of rocks and minerals. CRC Press, Florida

Christidis G, Scott PW (1993) Laboratory evaluation of bentonites. Indust Min Mag 311:51-54

Christie RL, Dawes PR (1991) Geographic and geological exploration. In: Geology of the Innuitian Orogen and Arctic Platform of Canada and Greenland. Trettin HP (ed) Geol Surv Can, Geology of Canada, pp 7-25

Compton RR (1985) Geology in the field. John Wiley & Sons, New York.

Delano JW, Tice SJ, Mitchell CE, Goldman D (1994) Rhyolitic glass in Ordovician K-bentonites: a new stratigraphic tool. Geology 22:115-118

Drummond KJ (1973) Canadian Arctic Islands. In: Future petroleum provinces of Canada. Can Soc Petrol Geol Memoir 1:443-472

Dunbar NW, Hervig RL (1992) Petrogenesis and volatile stratigraphy of the Bishop Tuff: evidence from melt inclusion analysis. J Geophys Research 97:15,129-15,150

Embry AF (1991) Mesozoic history of the Arctic Islands. In: Geology of the Innuitian Orogen and Arctic Platform of Canada and Greenland. Trettin HP (ed) Geol Surv Can, Geology of Canada, pp 369-433

Embry AF, Osadetz KG (1988) Stratigraphy and tectonic significance of Cretaceous volcanism in the Queen Elizabeth Islands, Canadian Arctic Archipelago. Can J Earth Sci 25:1209-1219

Faure G (1991) Principles and applications of inorganic geochemistry. Macmillan Publishing Company, New York

Fisher RV, Schmincke HU (1984) Pyroclastic rocks. Springer-Verlag, Berlin

Fortier YO, Morley LW (1956) Geological unity of the Arctic Islands. Trans Royal Soc Can 50:3-12

Gibson IL, Jagam P (1980) Instrumental neutron activation analysis of rocks and minerals. In: Short course in neutron activation analysis in the geosciences. Muecke GK (ed). vol 5. Miner Assoc Can, pp 109-131

Gresens RL (1967) Composition-volume relationships of metasomatism. Chem Geol 2:47-65

Grim RE, Guven N (1978) Bentonites: geology, mineralogy, properties and uses. Developments in sedimentology, vol. 24. Elsevier Scientific Publishing Company, Amsterdam

Gwinn R, Hess PC (1989) Iron and titanium solution properties in peraluminous and peralkaline rhyolitic liquids. Cont Miner Petrol 101:326-338

Haskin LA, Haskin MA (1968) Origin and distribution of the elements. Ahrens LH (ed) pp 889-912

Huff WD, Bergstrom SM, Kolata DR (1992) Gigantic Ordovician volcanic ash fall in North America and Europe: biological, tectonomagmatic, and event-stratigraphic significance. Geol 20:875-878

Huff WD, Kolata DR (1989) Correlation of K-bentonite beds by chemical fingerprinting using multivariate statistics. In: Quantitative dynamic stratigraphy. Cross TA (ed). Prentice Hall. pp 567-577

Huff WD, Turkmenoglu AG (1981) Chemical characteristics and origin of Ordovician K-bentonites along the Cincinnati Arch. Clays Clay Miner 29:113-123

Kemp KM, Westgate JA (1991) Latest Maastrichtian age for the Kanguk Formation at Duck Hawk Bluffs, Banks Island, Arctic Canada. In: Geol Assoc Can, Annual Meeting, Program with Abstracts. 16:A64

Knight WC (1898) Bentonite. Eng Mining J 66:491

Kovalenko VI, Hervig RL, Sheridan MF (1988) Ion-microprobe analyses of trace elements in anorthoclase, hedenbergite, aenigmatite, quartz, apatite, and glass in pantellerite: evidence for high water contents in pantellerite melt. Amer Miner 73:1038-1045

Lanphere MA, Tailleur IL (1983) K-Ar ages of bentonites in the Seebee Formation, Northern Alaska: a Late Cretaceous (Turonian) time-scale point. Cret Res 4:361-370

Lowenstern JB, Mahood GA (1991) New data on magmatic H_2O contents of pantellerites, with implications for petrogenesis and eruptive dynamics at Pantelleria. Bull Volcanol 54:78-83

Macdonald R, Davies GR, Bliss CM, Leat PT, Bailey DK, Smith RL (1987) Geochemistry of high-silica peralkaline rhyolites, Naivasha, Kenya Rift Valley. J Petrol 28:979-1008

Macdonald R (1974a) Nomenclature and petrochemistry of the peralkaline oversaturated extrusive rocks. In: Oversaturated peralkaline rocks. Bailey DK, Barberi F, Macdonald R (eds) Bull Volcanol 38:498-516

Macdonald R (1974b) Tectonic settings and magma associations. In: Oversaturated peralkaline rocks. Bailey DK, Barberi F, Macdonald R (eds) Bull Volcanol 38:575-593

Mahood GA, Stimac JA (1990) Trace-element partitioning in pantellerites and trachytes. Geochim Cosmochim Acta 54:2257-2276

Mathsoft (1991) Mathcad 3.0 user's guide. Mathsoft Inc, Cambridge, Massachusetts

McBirney AR (1984) Igneous petrology. Freeman, Cooper & Company, San Francisco

McKenzie D (1978) Some remarks on the development of sedimentary basins. Earth Planet Sci Lett 40:25-32

Merrett DC, Muecke GK (1989) Preliminary observations on the volcanics of Phillips Inlet, Ellesmere Island: the last phase of Cretaceous volcanism in the Sverdrup Basin. The Muskox 37:28-38

Molenaar CM, Bird KJ, Kirk AR (1986) Cretaceous and Tertiary stratigraphy of northeastern Alaska. In: Alaskan North Slope geology. Tailleur IL, Weimer P (eds) U S Geol Surv Field Trip Guide, pp 513-528

Mudie PJ, Blasco SM (1985) Lithostratigraphy of the CESAR cores. In: Initial geological report on CESAR: the Canadian expedition to study the Alpha Ridge, Arctic Ocean. Jackson HR, Mudie PJ, Blasco SM (eds) Geol Surv Can Paper 84-22, pp 59-99

Muecke GK (1992) Tectonomagmatic history of the Sverdrup Basin, Canadian Arctic Islands: pertinence to circum-Arctic event correlation. In: Int Conf on Arctic Margins, Anchorage, Alaska, ICAM Abstracts. p 39

Muecke GK, Williamson M-C, MacRae RA (1991) Recognition and significance of invasive flows in the Strand Fiord Formation, Axel Heiberg Island, Canadian Arctic Archipelago. In: Geol Assoc Can, Annual Meeting, Program with Abstracts. 16:A95

Muecke GK (1990) Secular and spatial evolution of extensional basin magmatism: development of the Sverdrup Basin, Canadian Arctic Islands. In: Int Volcanological Congress, Mainz, FRG, Abstracts. p 74

Muecke GK, Reynolds PH, Avison HA (1990) $^{40}Ar/^{39}Ar$ geochronology of episodic magmatism during the late phases of Sverdrup Basin development, Canadian Arctic Islands. In: Geol Assoc Can, Annual Meeting, Program with Abstracts. 15:A93

Nicholls J, Carmichael ISE (1969) Peralkaline acid liquids: a petrological study. Cont Miner Petrol 20:268-294

Noble DC, Korringa MK, Haffty J (1971) Distribution of calcium between alkali feldspar and glass in some highly differentiated silicic volcanic rocks. Amer Miner 56:2088-2097

Nunez-Betelu LK, MacRae RA, Hills LV, Muecke GK (in press) Uppermost Albian-Campanian palynological biostratigraphy of Axel Heiberg and Ellesmere islands (Canadian Arctic). In: 1992 ICAM Proceedings Volume

Nunez-Betelu LK (1991) Palynology of the Kanguk Formation (Late Cretaceous), Remus Creek, Ellesmere Island, Canadian Arctic Archipelago. Unpublished MSc Thesis. The University of Calgary, Calgary, Alberta

Pearce JA, Harris NBW, Tindle AG (1984) Trace element discrimination diagrams for the tectonic interpretation of granitic rocks. J Petrol 25:956-983

Person A (1982) The genesis of bentonites. In: Numerical dating in stratigraphy. Odin GS (ed) John Wiley & Sons, New York, pp 407-421

Pettijohn FJ, Potter PE, Siever R (1972) Sand and sandstone. Springer-Verlag, New York

Ricketts BD (1991) Delta evolution in the Eureka Sound Group, western Axel Heiberg Island: the transition from wave-dominated to fluvial-dominated deltas. Geol Surv Can Bull 402

Ricketts BD, Osadetz KG, Embry AF (1985) Volcanic style in the Strand Fiord Formation (Upper Cretaceous), Axel Heiberg Island, Canadian Arctic Archipelago. Polar Research. 3:107-122

Ritcey DH (1989) A geochemical study of the Carboniferous Audhild Volcanics, northwestern Ellesmere Island, Arctic Canada: Initial volcanism in the Sverdrup Basin. Unpublished BA Thesis. Dalhousie University, Halifax, Nova Scotia

Roedder E (1984) Fluid inclusions. In: Reviews in mineralogy. Ribbe PH (ed) Vol 12. Miner Soc Amer, Washington

Roux J, Varet J (1975) Alkali feldspar liquid equilibrium relationships in peralkaline oversaturated systems and volcanic rocks. Cont Miner Petrol 49:67-81

Schmid R (1981) Descriptive nomenclature and classification of pyroclastic deposits and fragments: Recommendations of the IUGS Subcommission on the Systematics of Igneous Rocks. Geology 9:41-43

Sigurdsson H, Carey S (1989) Plinian and co-ignimbrite tephra fall from the 1815 eruption of Tambora Volcano. Bull Volcan 51:243-270

Sobczak LW, Mayr U, Sweeney JF (1986) Crustal section across the polar continent-ocean transition in Canada. Can J Earth Sci 23:608-621

Stephenson RA, Embry AF, Nakiboglu SM, Hastaoglu MA (1987) Rift-initiated Permian to early Cretaceous subsidence of the Sverdrup Basin. In: Sedimentary basins and basin-forming mechanisms. Beaumont C, Tankard AJ (eds) Can Soc Petrol Geol Memoir 12:213-231

Streckeisen A (1979) Classification and nomenclature of volcanic rocks, lamprophyres, carbonatites, and melilitic rocks: recommendations and suggestions of the IUGS Subcommission on the Systematics of Igneous Rocks. Geology 7:331-335

Taylor PT, Kovacs LC, Vogt PR, Johnson GL (1981) Detailed aeromagnetic investigation of the Arctic Basin, 2. J Geophys Res 86:6323-6333

Thomas RG, Eberth DA, Deino AL, Robinson, D (1990) Composition, radioisotopic ages, and potential significance of an altered volcanic ash (bentonite) from the Upper Cretaceous Judith River Formation, Dinosaur Provincial Park, southern Alberta, Canada. Cret Res 11:125-162

Thorsteinsson R, Tozer ET (1970) Geology of the Arctic Archipelago. In: Geology and economic minerals of Canada. Douglas RJW (ed) Geol Surv Can Econ Geol Report 1:547-590

Trettin HP (1989) The Arctic Islands. In: The Geology of North America, Vol A The Geology of North America - An Overview. Bally AW, Palmer RS (eds) Geol Soc Amer pp 349-370

Trettin HP (1987) Pearya: a composite terrane with Caledonian affinities in northern Ellesmere Island. Can J Earth Sci 24:224-245

Walker GPL (1981) Plinian eruptions and their products. Bull Volcanol 44:223-240

Watson EB (1979) Zircon saturation in felsic liquids: experimental results and applications to trace element geochemistry. Cont Miner Petrol 70:407-419

Wilding MC, Macdonald R, Davies JE, Fallick AE (1993) Volatile characteristics of peralkaline rhyolites from Kenya: an ion microprobe, infrared spectroscopic and hydrogen isotope study. Cont Miner Petrol 114:264-275

Williamson M-C (1988) The Cretaceous Igneous Province of the Sverdrup Basin, Canadian Arctic: field relations and petrochemical studies. Unpublished PhD Thesis. Dalhousie University, Halifax, Nova Scotia

Wilson L, Sparks RSJ, Walker GPL (1980) Explosive volcanic eruptions - IV. The control of magma properties and conduit geometry on eruption column behavior. Geophys J R Astr Soc 63:117-148

Winchester JA, Floyd PA (1977) Geochemical discrimination of different magma series and their differentiation products using immobile elements. Chem Geol 20:325-343

Zhang Y, Huff WD (1992) Grain size as an indicator of ash source and distribution in Middle Ordovician K-bentonites of eastern North America. Geol Soc Amer Abstr Prog. 24:A267

Zielinski RA (1982) The mobility of uranium and other elements during alteration of rhyolite ash to montmorillonite: a case study in the Troublesome Formation, Colorado, U.S.A. Chem Geol 35:185-204

APPENDIX A : FIELD DESCRIPTIONS

Fosheim Anticline, Fosheim Peninsula, Ellesmere Island (79°43' N, 84°47' W):

EL92-001
Section: 92-01 Stratigraphic position: Unit A1, 2.0 m Rock type: Bentonite
Physical description: 30 - 50 cm thick, light greenish grey, uniform color, strongly deformed and slumped, visible only on upper slope, thickness varies 30 - 50 cm possibly as a result of slumping (base of section taken at last sandstone bearing plant remains); bentonite A2 (5.0 cm thick) at 19.0 m not collected because of shale contamination

EL92-002
Section: 92-01 Stratigraphic position: Unit A3, 35.0 m Rock type: Bentonite
Physical description: 75 cm thick, sharp contact against black shale at base (contact is locally highly deformed from slumping/compaction), basal 1 cm slightly rusty, darkening upward, top contact somewhat gradational into black shale (bioturbated ?)

EL92-003
Section: 92-01 Stratigraphic position: Unit A4, 36.1 m Rock type: Bentonite
Physical description: 80 cm thick, layered bentonite, sample interval 10 - 20 cm, slightly lighter color than lower 10 cm, not blocky, gritty

EL92-004
Section: 92-01 Stratigraphic position: Unit A4, 36.2 m Rock type: Bentonite
Physical description: 80 cm thick, layered bentonite, sampling interval 20 - 30 cm, bluish grey, blocky

EL92-005
Section: 92-01 Stratigraphic position: Unit A4, 36.3 m Rock type: Bentonite
Physical description: 80 cm thick, layered bentonite, sampling interval 30 - 60 cm, khaki green with lighter and darker color tones (light central band)

EL92-006
Section: 92-01 Stratigraphic position: Unit A4, 36.0 m Rock type: Bentonite
Physical description: 80 cm thick, layered bentonite, sampling interval 0 - 10 cm, blocky, greenish grey, very fine-grained, no grit, in sharp contact with black fissile shale typical of Kanguk

EL92-007
Section: 92-01 Stratigraphic position: Unit A4, 36.6 m Rock type: Bentonite
Physical description: 80 cm thick, layered bentonite, sampling interval 60 - 80 cm, grey plastic clay transitional to overlying black shale (bioturbated?)

EL92-008
Section: 92-01 Stratigraphic position: Unit A5, 45.1 m Rock type: Bentonite
Physical description: 35 cm thick, knife-sharp contact with underlying black shale, slightly rusty weathering in lowest 2 cm, sampling interval (0 - 20 cm) is homogeneous light greenish grey with rusty streaks, upper 15 cm is slightly darker and gradational into grey plastic clay, after 20 cm of grey plastic clay: black shale of typical Kanguk

EL92-009
Section: 92-01 Stratigraphic position: Unit A6, 46.1 m Rock type: Bentonite
Physical description: 60 cm thick, basal contact sharp against 1 cm of black plastic shale, below plastic layer is black fissile shale, basal 1 cm highly oxidized, uniform light greenish grey with abundant rusty streaks, sampling interval 10 - 20 cm, upper 5 cm highly oxidized (orange and red) followed by 5 cm of plastic grey clay before black fissile shale of typical Kanguk

EL92-010
Section: 92-01 Stratigraphic position: Unit A7, 49.55 m Rock type: Bentonite
Physical description: 70 cm thick, layered bentonite, basal contact against 1 cm of crumbly black shale, black fissile shale below, lower 15 cm of unit consists of medium grey plastic clay, internal contacts somewhat diffuse, sampling interval 5 - 15 cm

EL92-011
Section: 92-01 Stratigraphic position: Unit A7, 49.7 m Rock type: Bentonite
Physical description: 70 cm thick, layered bentonite, middle interval of unit (15 - 35 cm) consists of blocky, lithified light greenish grey bentonite, sampling interval 20 - 30 cm

EL92-012
Section: 92-01 Stratigraphic position: Unit A7, 49.95 m Rock type: Bentonite (?)
Physical description: 70 cm thick, layered bentonite, upper interval of unit (35 - 70 cm) consists of plastic medium grey clay, sampling interval 45 - 55 cm

EL92-013
Section: 92-01 Stratigraphic position: Unit A8, 51.2 m Rock type: Bentonite
Physical description: 15 cm thick, sharp lower contact against black fissile shale, basal 3 cm highly oxidized, sampling interval (3 - 10 cm) light to medium greenish grey, slightly lithified, overlain by 5 cm of medium grey plastic clay, followed by black fissile shale of typical Kanguk

EL92-014
Section: 92-01 Stratigraphic position: 49.4 m Rock type: Shale
Physical description: Typical black, organic-rich shale of Kanguk, just below Unit A7

EL92-015
Section: 92-01 Stratigraphic position: 35.9 m Rock type: Shale
Physical description: Typical black organic-rich, fissile shale of Kanguk below bentonite A4

EL92-016
Section: 92-01 Stratigraphic position: Unit A9, 54.5 m Rock type: Sandstone
Physical description: 45 cm thick, layered bentonite (?), basal contact against black fissile shale, then 3 - 6 cm of light greenish grey coarse sandstone, grains angular (grit), sandstone unit split by 1 cm of soft dark grey shale

EL92-017
Section: 92-01 Stratigraphic position: Unit A9, 54.56 m Rock type: Bentonite
Physical description: 45 cm thick, layered bentonite (?), homogeneous layer, very fine-grained, light greenish grey, appears to be impure bentonite with high proportion of clastic sand, possibly reworked or redeposited, sampling interval 6 -12 cm

EL92-018
Section: 92-01 Stratigraphic position: Unit A9, 54.66 m Rock type: Sandstone
Physical description: 45 cm thick, layered bentonite (?), blocky and much more lithified than lower portion, highly indurated and rich in fine-grained sand in a clay-dominated matrix, light greenish grey, upper contact against dark grey blocky shale

EL92-019
Section: 92-01 Stratigraphic position: 54.4 m Rock type: Shale
Physical description: Typical black organic-rich, fissile shale of Kanguk just below Unit A9

EL92-020
Section: 92-01 Stratigraphic position: Unit A10, 57.9 m Rock type: Bentonite
Physical description: Variable thickness 4 - 8 cm (pinches and swells along strike), sharp base against black fissile shale, friable, light greenish grey, rafts of black shale incorporated into bentonite, upper 1 cm highly oxidized

EL92-021
Section: 92-01 Stratigraphic position: 62.4 m Rock type: Shale
Physical description: Typical black organic shale of Kanguk below A11, sampling interval 20 - 30 cm below contact with bentonite

EL92-022
Section: 92-01 Stratigraphic position: Unit A11, 62.6 m Rock type: Bentonite
Physical description: 20 cm thick, pinches and swells along strike, lower contact against 1 cm of plastic black shale, underlain by indurated black shale, lower 3 -5 cm oxidized, remainder is uniform greenish grey color with streaks of oxidation throughout, sharp contact with overlying plastic dark grey clay

EL92-023
Section: 92-01 Stratigraphic position: Unit A11, 62.8 m Rock type: Bentonite (?)
Physical description: 30 cm thick, dark grey plastic clay layer in sharp contact with underlying bentonite, basal portion blocky, then homogeneous, sampling interval 3 - 15 cm above bentonite

EL92-024
Section: 92-01 Stratigraphic position: Unit A12, 66.3 m Rock type: Bentonite
Physical description: 25 cm thick, basal contact sharp against fissile black shale, basal ~1 cm highly oxidized, uniformly light greenish grey with irregular oxidation streaks and patches, sharp upper contact with indurated fine siltstone, light grey in color, sampling interval 5-20 cm

EL92-025
Section: 92-01 Stratigraphic position: Unit A13, 75.1 m Rock type: Bentonite
Physical description: 75 cm thick, pinches and swells along strike, sharp basal contact with fissile black shale, olive color with abundant oxidation on partings, very blocky and somewhat indurated, lower 50 cm uniform in color and texture, sampling interval 10 - 25 cm, upper 25 cm same texture but becomes more grey, upper contact somewhat gradational into overlying black shale

EL92-026
Section: 92-01 Stratigraphic position: Unit A14, 81.0 m Rock type: Bentonite
Physical description: 8 cm thick, first unit of the lower bentonite triplet, sharp base against fissile black shale, poorly preserved and commonly mixed with shale chips, light greenish grey, sample taken from core but may contain some shale contamination

EL92-027
Section: 92-01 Stratigraphic position: Unit A15, 81.7 m Rock type: Bentonite
Physical description: 15 cm thick, sharp base against black fissile shale, light greenish and yellowish grey with irregular orange oxidation streaks, gradational upper contact into greenish mudstone, then greyish mudstone, and finally black shale over 20 cm interval

EL92-028
Section: 92-01 Stratigraphic position: Unit A16, 82.0 m Rock type: Bentonite
Physical description: 6 cm thick, basal contact against dark grey shale, light greenish grey with some oxidation, blocky and in part well indurated, very difficult to sample, small sample only

EL92-029
Section: 92-01 Stratigraphic position: Unit A17, 88.5 m Rock type: Bentonite
Physical description: 15 cm thick, pinches and swells, first unit of the upper bentonite triplet, some shale infolded along strike, basal contact sharp against blocky black shale, uniform yellowish green color with minor oxidation

EL92-030
Section: 92-01 Stratigraphic position: Unit A18, 88.9 m Rock type: Bentonite
Physical description: 10 cm thick, same as A17, scattered patches of oxidation

EL92-031
Section: 92-01 Stratigraphic position: Unit A19, 89.2 m Rock type: Bentonite
Physical description: 2 - 4 cm thick, pinches and swells along strike, considerable intermixing with shale; bentonite A20 (2 - 5 cm thick, yellowish) at 108.0 m not collected because of shale contamination

EL92-032
Section: 92-01 Stratigraphic position: Unit A21, 111.25 m Rock type: Bentonite
Physical description: 55 cm thick, sharp basal contact against blocky black shale, slight oxidation at base, slightly blocky with uniform olive yellowish color, diffuse upper contact with greyish shale, sampling interval 25 - 35 cm

EL92-033
Section: 92-01 Stratigraphic position: 116.2 m Rock type: Shale
Physical description: Black shale or mudstone directly below unit A22

EL92-034
Section: 92-01 Stratigraphic position: Unit A22, 116.3 m Rock type: Bentonite
Physical description: 100 cm thick, layered bentonite, sharp basal contact with black shale, lowest 1 cm slightly oxidized, blocky, light greenish grey, and uniform for the lower 70 cm, sampling interval 30 - 45 cm

EL92-035
Section: 92-01 Stratigraphic position: Unit A22, 117.0 m Rock type: Bentonite (?)
Physical description: 100 cm thick, layered bentonite, 20 cm thick, brownish-grey plastic clay layer in diffuse contact with the greenish bentonite beneath (very similar to upper contacts of other thick bentonites), brownish-grey layer is overlain by, and grades into distinctly rusty and oxide-rich layer ~10 cm thick; this weathering horizon is in sharp contact with dark grey mudstone

EL92-036
Section: 92-01 Stratigraphic position: Unit A23, 120.0 m Rock type: Bentonite
Physical description: 20 cm thick, mixing with black mudstone along basal contact, discontinuous dark grey mudstone layer projects ~3 cm into the bentonite; may be mechanically incorporated due to movement, uniform yellowish green color with little oxidation, very plastic, sharp upper contact, sampling interval 8 - 18 cm

EL92-037
Section: 92-01 Stratigraphic position: Unit A24, 207.0 m Rock type: Bentonite
Physical description: 20 cm thick, pinches and swells along strike, faulted along middle of slope, strongly deformed due to solifluction, sharp upper and lower contacts against mudstones containing giant (up to 1 m) *Inoceramus* shells, uniformly greenish grey, blocky and well indurated in part

EL92-038
Section: 92-01 Stratigraphic position: Unit A25, 215.0 m Rock type: Bentonite
Physical description: 70 cm thick, sharp lower contact against dark grey mudstone, homogeneous in texture and greenish color, patchy oxidation, blocky and quite indurated, shale intermixing near top possibly as a result of slumping

EL92-039
Section: 92-01 Stratigraphic position: Unit A26, 219.0 m Rock type: Bentonite
Physical description: 15 cm thick, sharp basal contact against blocky black mudstone, basal 5 mm highly oxidized, remainder uniform yellowish green color, upper contact somewhat diffuse

EL92-040
Section: 92-01 Stratigraphic position: Unit A27, 223.0 m Rock type: Bentonite
Physical description: 5 cm thick, sharp basal contact against blocky mudstone, oxidized at basal margin, buff to light brown color differs from other bentonites in the section, strongly intermixed with dark grey mudstone fragments throughout, upper contact against black mudstone somewhat diffuse, only possible to obtain small sample

Kanguk River, Axel Heiberg Island (79°18' N, 90°37' W):

AX90-003
Section: 90-01 Stratigraphic position: 118.4 m Rock type: Bentonite
Physical description: ~ 20 cm thick, overlies ~ 40 cm of black highly bituminous shale with sharp contact, shales below this more greenish to greyish in color, overlain by ~ 15 cm sandy bed, greenish yellow with common light colored siliceous (?) concretions, sampling interval 0 -10 cm

AX90-004
Section: 90-01 Stratigraphic position: 56.6 m Rock type: Bentonite
Physical description: ~ 15 cm thick, not well exposed, appears to be affected by slumping (particularly near top), sharp base against dark grey to black shale, yellowish green to yellow with variable oxidation to rusty colors, increasingly orange to rusty at top, top poorly defined, contains veinlets of pure white clay material

Kanguk Peninsula, Axel Heiberg Island (79°15' N, 91°31' W):

AX90-020
Section: 90-05 Stratigraphic position: 48.2 m Rock type: Bentonite
Physical description: 2 - 3 cm thick, over ~ 10 m interval below the sample at least 6 thin bentonite horizons occur, usually < 1 cm thick, which could not be sampled because of poor outcrop and thickness of units, yellowish green color, no mixing with surrounding black shale observed

AX90-021

Section: 90-01 Stratigraphic position: 99.7 m Rock type: Bentonite

Physical description: ~ 2 - 4 cm thick, but up to 20 cm due to slumping, at least one more bentonite horizon < 2 cm thick observed between this unit and AX90-020, overlies ~ 10 cm thick ironstone bed, yellowish green, small crystals visible, overlain by black shale, highly contorted by slumping

AX90-022A

Section: 90-05 Stratigraphic position: 141.0 m Rock type: Bentonite

Physical description: 20 cm thick, sharp basal contact with black shale is contorted because of slumping, lower half is light grey becoming rusty brown in its upper portion, common pockets of pure white clay mineral (sample AX90-022B)

AX90-022B

Section: 90-05 Stratigraphic position: 141.0 m Rock type: Bentonite

Physical description: Pure white clay pockets in light grey bentonite bed

AX90-023

Section: 90-05 Stratigraphic position: 151.0 m Rock type: Bentonite

Physical description: 20 cm thick, underlain by an ~8 cm highly fractured irregular ironstone bed, and then black, deeply-weathered shale, yellowish rusty brown near surface, changes to light grey at depth in hillside, overlain by <20 cm siltstone bed; note that this section is associated with some of the more indurated horizons (silica release by glass alteration ?)

AX90-024

Section: 90-05 Stratigraphic position: 233.0 m Rock type: Bentonite

Physical description: 10 cm thick, poorly exposed and slumped, sample free of contamination by surrounding black shale, greenish-yellow to grey at depth in hillside, rusty greenish-brown when weathered, no more bentonites observed before first sandstone unit of Eureka Sound Group

APPENDIX B : MINERAL SEPARATION AND PURIFICATION

The preparation of pure mineral separates from the Kanguk Formation bentonites required extensive laboratory processing. In each sample chosen for geochemical and geochronological work, primary phenocryst minerals constituted less than 5% of the bulk bentonite volume. The following sections describe the general procedure for isolating phenocryst minerals from the bulk bentonite samples.

Step 1: Removal of clay matrix

Approximately 500 cm^3 of the bentonite field sample are added to 3-4 L of water plus 50-75 mL of 10% calgon dispersant solution. The resulting slurry is strongly mixed, and the coarse fraction is allowed to settle for two to three minutes. The suspended clay is decanted from the coarse material, and the coarse fraction is diluted with water again. This process is repeated up to 15 times to remove as much clay as possible. The coarse material is then added to a series of four metal sieves (1.0 mm, 425 μm, 250 μm, 63 μm), and disaggregated using a soft brush, and a steady flow of water. The resulting clay-free fractions are dried in air, then collected and bottled.

Step 2: Separation of magnetic minerals

A Franz Isodynamic separator allows the removal of magnetic minerals from the clay-free fraction. Ilmenite is removed by orienting the Franz with a 90° forward slope, and a 0° side tilt. A sheet of paper is taped to the front of the electromagnet, the sample is poured along the central axis (vertical) of the separator, and the ilmenite collects on the paper (current: 1.8A; vibrator: off). Removal of micas, siderite, and Fe-stained grains is accomplished by pouring the sample down the separator slide using a 15° forward slope and a 10° side tilt (current: 1.8A; vibrator: 9). A final separation using a 10° forward slope and a 5° side tilt (current: 1.8A; vibrator: 8) removes most altered feldspar grains, and additional authigenic material.

Step 3: Heavy liquid density separations

(i) Sanidine separation: The non-magnetic fraction from each sample is placed in a separatory funnel approximately two-thirds full of sodium polytungstate (SPT) solution. The density of the SPT is adjusted to sink quartz (ρ = 2.65 g/cm^3), and float sanidine (ρ = 2.56-2.62 g/cm^3). The sample is then mixed with the SPT, and additional SPT is added to cover all of the grains. Once a satisfactory separation is achieved, the heavy fraction (including quartz) is drained out the bottom of the separatory funnel, and the light fraction is rinsed off the sides of the funnel using distilled water. Each fraction is then rinsed four to five times with distilled water, and air-dried.

(ii) Zircon and apatite separation: The magnetic fractions and heavy SPT fraction are combined, and placed in a separatory funnel two-thirds full of 1,1,2,2-tetrabromoethane (TBE; ρ = 2.967 g/cm^3). The sample is mixed with the TBE, and additional liquid is added to cover all the grains. Following separation, the heavy fraction ($\rho > 2.967$) contains both zircon and apatite, and quartz remains in the light fraction. Methanol is used to clean the TBE from each separate. Magnetic separation of the heavy fraction (using the method outlined in step 2) concentrates the apatite and zircon in the non-magnetic separate.

Step 4: Hand-picking

Hand-picking of the concentrated mineral separates is required to produce pure samples for geochemical and geochronological work. The concentrated density or magnetic separates are placed in a series of dry 8 cm diameter sieves (180 μm, 150 μm, 125 μm, pan (63-125 μm)), and the coarsest grains are hand-picked under a binocular microscope using a wetted paintbrush.

APPENDIX C : MINERAL CHEMISTRY DATA

Table C1 : Mean Sanidine Analyses - Major Element Oxides (wt%)
(Bracketed number indicates total grains analysed)

	AX90-003 (18)		AX90-004 (16)		AX90-021 (10)	
	Mean	SD	Mean	SD	Mean	SD
SiO2	67.82	0.21	67.81	0.39	66.88	0.24
TiO2	0.01	0.02	0.02	0.02	0.02	0.02
Al2O3	18.32	0.19	18.44	0.11	18.74	0.20
FeO	0.44	0.10	0.33	0.06	0.36	0.19
MnO	0.01	0.01	0.01	0.02	0.01	0.02
MgO	0.01	0.01	0.01	0.02	0.01	0.02
CaO	0.03	0.05	0.07	0.04	0.11	0.08
Na2O	5.09	0.13	5.19	0.15	5.12	0.24
K2O	7.53	0.45	7.04	0.41	7.70	0.50
BaO	0.03	0.04	0.02	0.02	0.06	0.04
Total	99.28	0.22	98.95	0.58	99.02	0.16
An	0.00	0.00	0.00	0.00	0.01	0.00
Or	0.49	0.02	0.47	0.02	0.49	0.03
Ab	0.51	0.02	0.53	0.02	0.50	0.03

	AX90-022 (2)		AX90-023 (20)		AX90-024 (12)	
	Mean	SD	Mean	SD	Mean	SD
SiO2	68.05	0.29	67.13	0.35	67.71	0.27
TiO2	0.00	0.00	0.02	0.02	0.03	0.02
Al2O3	18.74	0.00	18.61	0.16	18.58	0.23
FeO	0.33	0.07	0.51	0.13	0.43	0.10
MnO	0.01	0.00	0.01	0.02	0.01	0.01
MgO	0.02	0.02	0.01	0.01	0.01	0.01
CaO	0.07	0.05	0.02	0.02	0.04	0.07
Na2O	5.06	0.01	5.58	0.12	5.20	0.10
K2O	7.59	0.05	6.39	0.20	7.64	0.55
BaO	0.08	0.03	0.13	0.07	0.04	0.03
Total	99.96	0.27	98.43	0.41	99.70	0.29
An	0.00	0.00	0.00	0.00	0.00	0.00
Or	0.49	0.00	0.43	0.01	0.49	0.02
Ab	0.50	0.00	0.57	0.01	0.51	0.02

Table C2 : Mean Ilmenite Analyses - Major Element Oxides (wt%)
(Bracketed number indicates total grains analysed)

	AX90-003 (7)		AX90-004 (9)		AX90-024 (11)	
	Mean	SD	Mean	SD	Mean	SD
SiO2	0.14	0.06	0.19	0.37	0.18	0.16
TiO2	51.77	0.31	51.06	2.41	51.29	2.27
Al2O3	0.01	0.02	0.03	0.11	0.03	0.07
Cr2O3	0.02	0.04	0.02	0.04	0.04	0.04
FeO	45.83	0.55	46.04	3.08	45.13	3.60
MnO	1.98	0.39	1.73	0.29	1.93	0.64
MgO	0.03	0.05	0.03	0.05	0.05	0.06
CaO	0.00	0.00	0.00	0.00	0.00	0.00
Total	99.78	0.45	99.11	1.11	98.63	1.86

Table C3 : Mean Rutile Analyses - Major Element Oxides (wt%)
(Bracketed number indicates total grains analysed)

	AX90-003 (1)		AX90-004 (2)		AX90-024 (2)	
	Mean	SD	Mean	SD	Mean	SD
SiO2	0.50	0.24	0.39	0.15	0.79	0.35
TiO2	96.42	0.57	97.27	0.85	95.99	0.38
Al2O3	0.12	0.09	0.05	0.05	0.26	0.12
Cr2O3	0.05	0.08	0.04	0.06	0.11	0.08
FeO	1.28	0.45	0.66	0.22	1.00	0.27
MnO	0.00	0.00	0.00	0.00	0.00	0.00
MgO	0.00	0.00	0.00	0.00	0.00	0.00
CaO	0.00	0.00	0.00	0.00	0.00	0.00
Total	98.37	0.20	98.41	0.72	98.14	0.39

APPENDIX D : BULK BENTONITE GEOCHEMICAL DATA

Table D1 : XRF Analyses - Major and Minor Element Oxides (wt %), Loss on Ignition (wt %), and Trace Elements (ppm)

	AX90-003	AX90-004	AX90-021	AX90-022	AX90-023	AX90-024
SiO2	54.40	48.68	49.46	59.81	59.72	55.38
Al2O3	18.62	15.04	24.96	20.69	18.86	17.85
Fe2O3t	5.81	11.34	4.47	1.96	4.33	5.60
MgO	1.52	0.78	1.02	0.60	1.06	1.13
CaO	0.90	1.06	0.80	0.48	0.24	0.42
Na2O	2.47	2.61	0.82	1.48	1.64	1.28
K2O	1.87	2.30	3.36	1.71	3.06	2.06
TiO2	0.53	0.40	0.46	0.49	0.56	0.49
MnO	0.03	0.02	0.02	0.02	0.04	0.04
P2O5	0.14	0.28	0.24	0.11	0.15	0.09
LOI	14.50	19.00	14.20	13.00	9.30	16.80
Total	100.79	101.51	99.78	100.35	98.96	101.14
Ba	109	158	255	170	275	131
Rb	80	75	89	54	97	55
Sr	156	227	77	46	63	37
Y	423	268	110	204	364	161
Zr	3659	2380	722	2143	2817	2215
Nb	355	233	94	238	303	307
Th	76	59	59	76	62	46
Pb	38	39	35	<10	<10	33
Ga	79	52	64	65	65	60
Zn	590	168	112	127	473	305
Cu	13	15	30	22	<5	13
Ni	12	7	6	10	20	38
V	<5	16	31	8	8	<5
Cr	<5	<5	8	14	<5	7

Table D1 (continued)

	EL92-001	EL92-002	EL92-032	EL92-034	EL92-038	EL92-039
SiO2	50.09	59.22	57.25	56.78	70.16	60.86
Al2O3	19.06	18.97	18.75	18.05	12.00	17.50
Fe2O3t	5.01	5.79	5.61	6.27	5.40	7.90
MgO	2.39	1.94	1.17	1.32	0.79	1.35
CaO	0.23	0.22	0.27	0.28	0.13	0.30
Na2O	2.21	2.43	2.69	2.52	2.29	2.50
K2O	0.57	0.72	1.30	1.17	0.97	0.74
TiO2	0.59	0.32	0.46	0.52	0.39	0.44
MnO	0.07	0.02	0.01	0.01	0.01	0.03
P2O5	0.28	0.09	0.14	0.14	0.05	0.08
LOI	18.90	11.00	10.80	11.40	8.80	9.60
Total	99.40	100.72	98.45	98.47	100.98	101.30
Ba	87	233	174	184	86	26
Rb	17	13	34	25	29	24
Sr	52	62	156	153	118	86
Y	83	146	216	213	90	115
Zr	491	912	2044	2050	913	1342
Nb	83	137	205	242	175	215
Th	29	44	50	41	25	32
Pb	20	49	30	32	13	<10
Ga	37	51	66	66	36	47
Zn	198	208	424	530	182	152
Cu	13	<5	<5	<5	<5	<5
Ni	31	<5	<5	<5	<5	18
V	32	<5	8	<5	<5	6
Cr	7	<5	<5	<5	<5	<5

Table D2 : INAA Analyses - Selected Minor and Rare Earth Elements in Bulk Bentonites and Sanidine Separates (ppm)

Bulk Bentonites

	AX90-003	AX90-024	EL90-001
Sc	3.9	3.0	4.4
Co	1.6	20.0	11.4
La	392.8	248.4	122.4
Ce	858.3	558.1	208.3
Nd	331.4	207.8	101.7
Sm	73.9	49.3	23.6
Eu	6.5	4.2	2.5
Tb	11.0	6.0	2.2
Yb	32.8	13.1	5.3
Lu	4.6	1.8	0.8
Hf	84.4	51.7	16.5
Ta	32.1	20.5	6.4
Th	61.3	37.5	20.0
U	14.4	10.1	9.8

Sanidine Separates

	AX90-003	AX90-024
Sc	0.2	0.1
Co	0.4	0.2
La	4.1	4.0
Ce	9.2	9.0
Nd	3.6	3.6
Sm	1.0	0.9
Eu	0.8	0.9
Tb	0.2	0.2
Yb	0.3	0.2
Lu	0.1	<0.1
Hf	1.9	1.6
Ta	1.3	0.5
Th	1.3	0.9
U	0.3	0.5

Table D3 : Mean Glass Inclusion Analyses - Major Element Oxides (wt%)
(Bracketed number indicates total inclusions analysed)
(P.I. = Peralkalinity Index = Molecular (Na2O + K2O)/Al2O3)

	AX90-003 (58)		AX90-004 (67)		AX90-021 (23)	
	Mean	SD	Mean	SD	Mean	SD
SiO2	73.28	0.68	73.52	1.05	74.66	0.35
TiO2	0.25	0.07	0.17	0.06	0.16	0.05
Al2O3	9.68	0.46	9.89	0.58	11.49	0.15
FeOt	5.47	0.52	4.66	1.17	2.46	0.19
MnO	0.11	0.06	0.08	0.06	0.03	0.03
MgO	0.04	0.04	0.03	0.03	0.02	0.03
CaO	0.22	0.06	0.20	0.06	0.39	0.06
Na2O	3.47	0.35	3.51	0.38	3.83	0.19
K2O	4.36	0.22	4.38	0.19	4.69	0.10
P2O5	0.13	0.07	0.16	0.08	0.16	0.09
Cl	0.18	0.05	0.21	0.05	0.15	0.03
ZrO2	0.07	0.09	0.06	0.08	0.01	0.02
Total	97.26	0.99	96.87	1.37	98.05	0.68
P.I.	1.08	0.15	1.06	0.08	0.99	0.02

	AX90-022 (27)		AX90-023 (1)		AX90-024 (4)	
	Mean	SD	Mean	SD	Mean	SD
SiO2	74.12	0.96	72.80	0.00	72.67	0.77
TiO2	0.14	0.08	0.34	0.00	0.25	0.04
Al2O3	10.56	0.69	8.64	0.00	9.50	0.52
FeOt	3.70	1.05	5.93	0.00	4.95	0.78
MnO	0.07	0.05	0.10	0.00	0.10	0.06
MgO	0.03	0.03	0.00	0.00	0.03	0.02
CaO	0.31	0.12	0.30	0.00	0.24	0.08
Na2O	3.49	0.38	3.05	0.00	3.11	0.41
K2O	4.42	0.22	4.07	0.00	4.30	0.25
P2O5	0.13	0.07	0.18	0.00	0.22	0.06
Cl	0.12	0.04	0.19	0.00	0.22	0.09
ZrO2	0.04	0.06	0.03	0.00	0.05	0.06
Total	97.14	0.99	95.64	0.00	95.64	1.24
P.I.	1.00	0.08	1.09	0.00	1.03	0.09

Table D4 : Calculated Major Element Changes (g/100 g) during Bentonite Formation, based on Constant Alumina (Fv = Volume Change Factor)

	AX90-003	AX90-004	AX90-021
SiO2	-46.38	-42.97	-53.01
TiO2	0.02	0.10	0.06
Al2O3	0.00	0.00	0.00
FeOt	-2.84	2.12	-0.62
MnO	-0.10	-0.07	-0.02
MgO	0.77	0.50	0.46
CaO	0.25	0.51	-0.02
Na2O	-2.26	-1.85	-3.52
K2O	-3.49	-2.97	-3.22
P2O5	-0.06	0.02	-0.05
Fv	0.44	0.53	0.38

	AX90-022	AX90-023	AX90-024
SiO2	-44.96	-47.61	-45.31
TiO2	0.12	-0.08	0.01
Al2O3	0.00	0.00	0.00
FeOt	-2.90	-4.34	-2.39
MnO	-0.06	-0.08	-0.08
MgO	0.29	0.51	0.60
CaO	-0.07	-0.20	-0.02
Na2O	-2.82	-2.41	-2.54
K2O	-3.66	-2.80	-3.35
P2O5	-0.07	-0.12	-0.19
Fv	0.44	0.41	0.45